Theoretical model for the realization of quantum gates using interacting endohedral fullerene molecules

Theoretical Model for the Realization of Quantum Gates Using Interacting Endohedral Fullerene Molecules

by
M. S. Garelli

A Doctoral Thesis submitted
for the award of the degree
Doctor of Philosophy
of
Loughborough University

Supervisor: Prof. F. Kusmartsev

September 2006

Abstract

We have studied a physical system composed of two interacting endohedral fullerene molecules for quantum computational purposes. The mutual interaction between these two molecules is determined by their spin dipolar interaction. The action of static magnetic fields on the whole system allows us to encode the qubit in the electron spin of the encased atom.

We present a theoretical model which enables us to realize single-qubit and two-qubit gates through the system under consideration. Single-qubit operations can be achieved by applying to the system time-dependent microwave fields. Since the dipolar spin interaction couples the two qubit-encoding spins, two-qubit gates are naturally performed by allowing the system to evolve freely. This theoretical model is applied to two realistic architectures of two interacting endohedrals. In the first realistic system the two molecules are placed at a distance of $1.14nm$. In the second design the two molecules are separated by a distance of $7nm$. In the latter case the condition $\Delta\omega_p >> g(r)$ is satisfied, i.e. the difference between the precession frequencies of the two spins is much greater than the dipolar coupling strength. This allows us to adopt a simplified theoretical model for the realization of quantum gates.

The realization of quantum gates for these realistic systems is provided by studying the dynamics of the system. In this extent we have solved sets of Schrödinger equations needed for reproducing the respective gates, i.e. phase-gate, π-gate and CNOT-gate. For each quantum gate reproduced through the realistic system, we have estimated their reliability by calculating the related fidelity. The presented two-qubit gates are characterized by very high values of fidelity. The value of minimum fidelity related to the realization of a CNOT-gate is $\mathcal{F} = 0.9995$, which differs from the ideal value $\mathcal{F} = 1$ by of the order of $10^{-2}\%$.

We also present suggestions regarding the improvements on systems composed of endohedral fullerenes in order to enable the experimental realization of quantum gates. This would allow these systems to become reliable building blocks of a quantum computer.

Acknowledgments

I am very pleased to thank Prof. Feodor Kusmartsev as the supervisor of my Ph.D. thesis for his helpful guidance throughout the course of my research. I would also like to thank Dr. John H. Samson for regular useful discussions and suggestions. Finally, I gratefully acknowledge my parents for their much valuable support, my best friend Chiara for her never-ending friendship and Pino for dedicating to me his patience and part of his life.

M. S. Garelli

September 2006

Contents

Introduction

In recent years there has been strong progress in modeling physical realizations of a quantum computer. Many quantum physical systems have been investigated for the realization of quantum gates. The most remarkable studies were related to systems associated with Quantum Optics Ion Traps, to Quantum Electrodynamics in Optical Cavities, and to Nuclear Magnetic Resonance. All these experiments are aimed at realizing a quantum gate. The first type of experiments is based on trapping ions in electromagnetic traps, where the ions, which encode the qubit in the charge degrees of freedom are subjected to the mutual electrostatic interaction and to a state selective displacement generated by an external state dependent force [1, 2, 3, 4]. Cavity quantum electrodynamics (QED) techniques are based on the coherent interaction of a qubit, generally represented by an atom or semiconductor dot system, with a single mode or a few modes of the electromagnetic field inside a cavity. Depending on the particular system, the qubit can be represented by the polarization states of a single photon or by two excited states of an atom. Although cavity QED experiments are very promising, they have only been accomplished for few qubits [5, 6, 7, 8]. In the third experiment, nuclear spins represent qubits. These spins can be manipulated using nuclear magnetic resonance techniques. Through the study of the quantum behavior of spins, quantum operations are realized. However, the number of spins which can be collected in a system is very limited, and this forbids the building up of a scalable quantum computer [9, 10, 11, 12]. From the study of such systems, we learn that the decoherence phenomenon is the main issue which prevents the realization of quantum gates.

We herein focus on physical systems which are promising candidates for producing realistic quantum gates. The basic elements of our system are fullerene molecules with encapsulated atoms or ions, which are called *buckyballs* or *endohedral fullerenes*. Each of the trapped atoms carries a spin. By applying static magnetic fields, we can encode a qubit in this spin, which is associated with electronic degrees of freedom, see Sec. 3.1. The mutual interaction between two buckyballs is determined by the dipolar spin

interaction, see Refs. [43, 44, 45]. It has been shown experimentally [43] that these endohedral systems provide a long lifetime for the trapped spins, and that the fullerene cages represent a good shielding environment for the very sensitive spins trapped inside.

These endohedral systems are typically characterized by two relaxation times (see Sec. 2.2.2). These are described as T_1, which is due to the interactions between a spin and the surrounding environment, and T_2 which is due to the dipolar interaction between the qubit encoding spin and the surrounding endohedral spins randomly distributed in the sample. It has been experimentally proven that both the relaxation time, T_1, and the coherence time, T_2, are temperature dependent [55], and that there is a correlation between them, $T_2 \simeq \frac{2}{3}T_1$, which is constant over a broad range of temperature. This relationship suggests that both relaxation times are determined by the same physical process, which is well described by an Orbach relaxation mechanism. The outstanding result of this research is the observation of a coherence time T_2 up to $0.25ms$.

Another remarkable feature of systems composed of buckyballs is that they can be easily maneuvered (see Sec. 2.2.1). It is experimentally allowed to assemble many-buckyballs systems such as dimers or arrays [46], which can open a new road for building up scalable systems for the realization of quantum computers [46].

In this study we present a physical system composed of two endohedral fullerene molecules for the realization of single-qubit and two-qubit gates. Single qubit-gates are performed by applying to the system time-dependent microwave fields, which allow the rotation of the spin of the encoded particle. Two-qubit gates are naturally realized through the mutual dipolar spin interaction by allowing the system to evolve freely (Chap. 4, Chap. 5, Chap. 6). We also provide the study of the fidelity related to each quantum gate (Secs. 5.4, 5.5). The fidelity determines the reliability of the produced realistic gates in comparison with the theoretical predictions.

In Chapter 1, we present an overview on the basic concepts of Quantum Computation.

In Chapter 2, we present some technical and physical properties of fullerenes endohedral fullerene molecules. The most important features which characterize these molecules are their easy maneuverability (see Sec. 2.2.1) and their long relaxation times (see Sec. 2.2.2).

In Chapter 3, we introduce theoretical tools needed to perform quantum computations on our two-buckyball system. We show how to encode a qubit (Sec. 3.1) and how to single address each qubit (Sec. 3.2). We also introduce the concept of *concurrence* (Sec. 3.3) which measures the degree of entanglement of a two-qubit state. We calcu-

late the concurrence for two realistic systems. The first described by a time-independent Hamiltonian (Sec. 3.4.1) and the second described by a time-dependent Hamiltonian (Sec. 3.4.2).

In Chapter 4, we present a theoretical model for the realization of quantum gates with a system composed of two particles interacting via dipolar spin interactions. We present a theory for realizing a two-qubit π-gate (Sec. 4.3) and a CNOT-gate (Sec. 4.4).

In Chapter 5, we apply the theoretical model presented in Chapter 4 to a realistic system composed of two endohedral fullerene molecules. Both single-qubit (Sec. 5.1), and two-qubit gates such as phase-gate (Sec. 5.3.1), π-gate (Sec. 5.3.2) and CNOT-gate can be realized by studying the time-evolution of the system, i.e. by solving sets of Schrödinger equations which define each transformation. To check the reliability of each gate operation, we have calculated the *quantum gate fidelity* (Sec. 5.4) and the *quantum state fidelity* (Sec. 5.5).

In Chapter 6, we present a different design of a realistic system composed of two endohedral molecules. We consider a two-distant-buckyball system which allows to simplify the theory involved in the study for the realization of quantum gates presented in Chap. 5. For this system we perform quantum gates and calculate their related fidelity.

In Chapter 7, we present the conclusions and suggestions on the future directions which could be followed in order to enable the experimental realization of quantum gates and allow two-buckyball systems to be reliable components of quantum computers.

Chapter 1

Introduction to Quantum Computation

Quantum computers operate with the use of *Quantum Gates*. Quantum gates are defined as quantum computer elements that act on the computational basis states and may be presented as unitary transformations. In our system, each spin represents one qubit and the two computational basis states for each qubit are represented by the two orthogonal spin $z-$component states. We will present the single-qubit gates and analyze the two-qubits gates which we want to realize with our realistic systems in Chap. 5 and Chap 6. We will describe examples of quantum operations which involve complex sets of quantum gates such as multiple-qubit quantum gates, no-cloning theorem, quantum teleportation and Deutsch algorithm. We will present DiVincenzo criteria, which is a set of conditions to be satisfied by a quantum system in order to efficiently implement a quantum computer.

1.1 Qubits and Quantum Circuits

The model of quantum computation which best fits the design of algorithms and a concrete physical realization is based on quantum logic circuits. In this chapter, we present the basic elements of quantum logic circuits: qubits, quantum logic gates and other simple components [12, 13, 14, 15].

A *quantum bit*, called for simplicity *qubit* [16], is a two-level quantum system, whose states are called $|\ 0\rangle$ and $|\ 1\rangle$. Unlike a classical bit, which can acquire only the discrete values 0 or 1, due to the superposition principle, a qubit can exist in an arbitrary

superposition of state $|0\rangle$ and $|1\rangle$. The state describing a qubit can be written as follows

$$|\psi\rangle = \alpha|0\rangle + \beta|1\rangle, \quad \alpha, \beta \text{ complex numbers.} \tag{1.1}$$

In matrix form, states $|0\rangle$ and $|1\rangle$ are represented by

$$|0\rangle = \begin{pmatrix} 1 \\ 0 \end{pmatrix}, \quad |1\rangle = \begin{pmatrix} 0 \\ 1 \end{pmatrix}, \tag{1.2}$$

and the general state $|\psi\rangle$ is given by

$$|\psi\rangle = \begin{pmatrix} \alpha \\ \beta \end{pmatrix}, \quad |\alpha|^2 + |\beta|^2 = 1. \tag{1.3}$$

A qubit can be conveniently described in the so called *Bloch sphere*, a sphere of unit radius in a tri-dimensional space, see Fig 1.1. An arbitrary qubit can be parametrized as

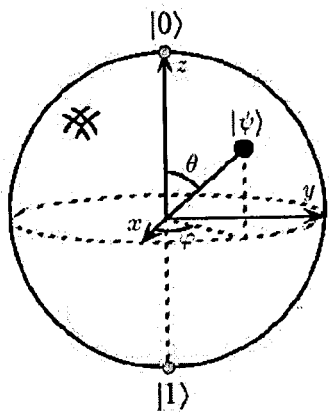

Figure 1.1: Bloch's sphere. θ is the polar angle and φ is the azimuthal angle.

follows

$$|\psi\rangle = \cos\frac{\theta}{2}|0\rangle + e^{i\varphi}\sin\frac{\theta}{2}|1\rangle, \tag{1.4}$$

where θ and φ are real numbers which describe a point on the Bloch sphere.

A *quantum register* is given by the tensor product of qubits. A natural number $x = x_{n-1}2^{n-1} + ... + x_1 2^1 + x_0 2^0$, with $x_i \in \{0, 1\}$ is represented by state $|x_{n-1}, ..., x_1, x_0\rangle$.

An important property of a quantum register is that it can simultaneously store more than one number. For example, the following register

$$\begin{aligned} &\tfrac{1}{\sqrt{2}}(|\,0\rangle + |\,1\rangle)\otimes|\,0\rangle \otimes \tfrac{1}{\sqrt{2}}(|\,0\rangle - |\,1\rangle)\otimes|\,1\rangle \\ &= \tfrac{1}{2}(|\,0001\rangle - |\,0011\rangle + |\,1001\rangle - |\,1011\rangle) \\ &= \tfrac{1}{2}(|\,1\rangle - |\,3\rangle + |\,9\rangle - |\,11\rangle), \end{aligned} \tag{1.5}$$

simultaneously represents numbers 1, 3, 9 and 11.

Considering a system composed of two qubits, the computational basis of the space containing the two qubits is represented by the following states

$$|\,00\rangle, |\,01\rangle, |\,10\rangle, |\,11\rangle, \tag{1.6}$$

whose vector form is

(1.7)

$$|\,00\rangle = \begin{pmatrix} 1 \\ 0 \\ 0 \\ 0 \end{pmatrix}, \quad |\,01\rangle = \begin{pmatrix} 0 \\ 1 \\ 0 \\ 0 \end{pmatrix}, \quad |\,10\rangle = \begin{pmatrix} 0 \\ 0 \\ 1 \\ 0 \end{pmatrix}, \quad |\,11\rangle = \begin{pmatrix} 0 \\ 0 \\ 0 \\ 1 \end{pmatrix}.$$

An arbitrary two-qubit state can be written as follows

$$|\,\psi\rangle = a_{00}\,|\,00\rangle + a_{01}\,|\,01\rangle + a_{10}\,|\,10\rangle + a_{11}\,|\,11\rangle, \tag{1.8}$$

whose vector form is

$$|\,\psi\rangle = \begin{pmatrix} a_{00} \\ a_{01} \\ a_{10} \\ a_{11} \end{pmatrix}, \tag{1.9}$$

where the normalization condition implies $|\,a_{00}\,|^2 + |\,a_{10}\,|^2 + |\,a_{01}\,|^2 + |\,a_{11}\,|^2 = 1$.

A very important example of two-qubit state is the so called *EPR pair*, where EPR stands for Einstein-Podolsky-Rosen, also known as the *Bell state*

$$|\,\psi_{EPR}\rangle = \frac{1}{\sqrt{2}}(|\,00\rangle + |\,11\rangle). \tag{1.10}$$

An EPR pair cannot be written as a tensor product of two single qubit states. A quantum state which cannot be written as a product of the states which compose the system is called

an *entangled state*. The *entanglement* is a very important feature of quantum states, as it demonstrates if the state is a good candidate for carrying quantum information. The results of a measurement on the first and second qubit of an EPR pair are correlated. The degree of entanglement of the two-qubit state is described by the extent of correlation of the measured results. A detailed discussion about entanglement is presented in Sec. 3.3.

1.2 Single-Qubit Gates

A single-qubit quantum gate is, in general, a linear unitary operator U, represented by a two by two matrix which acts on a qubit $|\psi\rangle$ and transforms it into another qubit $|\psi'\rangle$. In the classical case, only one single-qubit gate known as the NOT-gate exists. Its action is the swapping of bits, i.e. $0 \rightarrow 1$ and $1 \rightarrow 0$. However, in the quantum case there are many non-trivial single-qubit gates. Since the unitarity is the only constraint on quantum gates, any unitary matrix can represent a reliable quantum gate. Single-qubit rotations are the most general unitary transformations which can represent a quantum gate. The definition of a single-qubit rotation of an angle θ about $\vec{n}$ axis is expressed by the following

$$R_{\vec{n}}(\theta) = \exp[-\frac{\imath\theta\vec{n}\cdot\vec{\sigma}}{2}], \tag{1.11}$$

where $\vec{\sigma}$ is the vector of Pauli matrices

$$\vec{\sigma} = (\sigma_x, \sigma_y, \sigma_z), \tag{1.12}$$

where

$$\sigma_x = \begin{pmatrix} 0 & 1 \\ 1 & 0 \end{pmatrix}, \quad \sigma_y = \begin{pmatrix} 0 & -\imath \\ \imath & 0 \end{pmatrix}, \quad \sigma_z = \begin{pmatrix} 1 & 0 \\ 0 & -1 \end{pmatrix}. \tag{1.13}$$

Among the several single-qubit rotations which define a quantum gate, we show the most useful. The quantum counterpart of a classical NOT is a gate represented by the following transformation

$$|0\rangle \rightarrow |1\rangle, \qquad |1\rangle \rightarrow |0\rangle. \tag{1.14}$$

The operator corresponding to the previous transformation is

$$X = |0\rangle\langle 1| + |1\rangle\langle 0| = \begin{pmatrix} 0 & 1 \\ 1 & 0 \end{pmatrix}, \tag{1.15}$$

which is the σ_x Pauli matrix.

If we consider Pauli matrix σ_z, which is given by

$$Z \equiv \sigma_z = |\,0\rangle\langle 0\,| - |\,1\rangle\langle 1\,| = \begin{pmatrix} 1 & 0 \\ 0 & -1 \end{pmatrix}, \tag{1.16}$$

we can see that it leaves unaltered state $|\,0\rangle$ and it changes the sign of state $|\,1\rangle$,

$$Z: \ |\,0\rangle \rightarrow |\,0\rangle, \qquad |\,1\rangle \rightarrow -|\,1\rangle. \tag{1.17}$$

A very useful single-qubit quantum gate is the so called *Hadamard Gate*. Its unitary matrix is given by

$$H = \frac{1}{\sqrt{2}} \begin{pmatrix} 1 & 1 \\ 1 & -1 \end{pmatrix} \tag{1.18}$$

and its action over the qubit states is given by

$$H: \ |\,0\rangle \rightarrow \frac{(|\,0\rangle + |\,1\rangle)}{\sqrt{2}}, \qquad |\,1\rangle \rightarrow \frac{(|\,0\rangle - |\,1\rangle)}{\sqrt{2}}, \tag{1.19}$$

which can be generally written as

$$H: \ |\,x\rangle \rightarrow \frac{1}{\sqrt{2}}(|\,0\rangle + (-1)^x\,|\,1\rangle) = \frac{1}{\sqrt{2}}(|\,0\rangle + e^{i\pi x}\,|\,1\rangle), \quad x \in \{0,1\} \tag{1.20}$$

Since the Hadamard gate is a unitary transformation on a qubit, it can be represented as the composition of rotations, see Eq. (1.26).

Another important single-qubit gate is the phase-gate S, given by

$$S = \begin{pmatrix} 1 & 0 \\ 0 & e^{i\phi} \end{pmatrix}, \quad |\,0\rangle \rightarrow |\,0\rangle, \qquad |\,1\rangle \rightarrow e^{i\phi}\,|\,1\rangle, \tag{1.21}$$

whose action can be synthesized as follows

$$S: \ |\,x\rangle \rightarrow e^{ix\phi}\,|\,x\rangle, \quad x \in \{0,1\}. \tag{1.22}$$

A particular case of a S-gate is the so called $\frac{\pi}{8}$-gate, T, described by the following matrix

$$T = \begin{pmatrix} 1 & 0 \\ 0 & e^{i\pi/4} \end{pmatrix}. \tag{1.23}$$

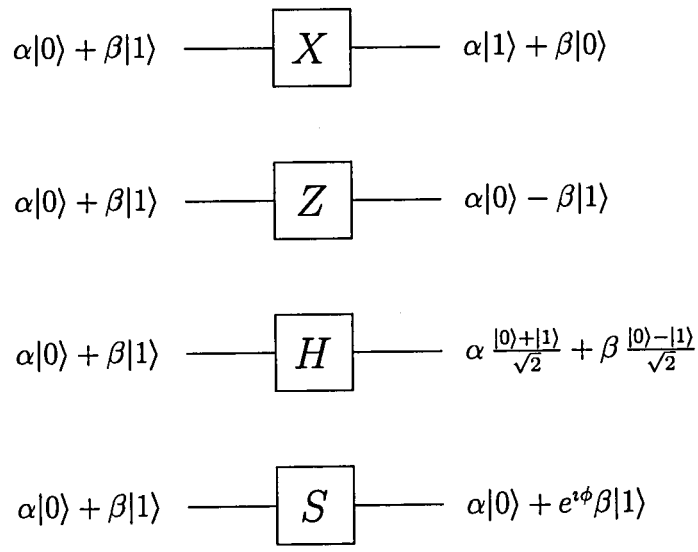

Figure 1.2: Examples of single-qubit quantum gates.

Fig. 1.2 presents the most important single-qubit gates.

There are many two by two unitary matrices, each of which defines a single-qubit quantum gate. However, it is possible to understand the properties of the complete set through the analysis of the properties of a much smaller set. It is possible to prove, see Ref. [12], that an arbitrary single-qubit unitary gate can be decomposed as a product of rotations

$$\begin{pmatrix} \cos\frac{\gamma}{2} & -\sin\frac{\gamma}{2} \\ \sin\frac{\gamma}{2} & \cos\frac{\gamma}{2} \end{pmatrix} \tag{1.24}$$

and of the z-axis rotation gate

$$\begin{pmatrix} e^{-i\beta/2} & 0 \\ 0 & e^{i\beta/2} \end{pmatrix} \tag{1.25}$$

together with a global phase shift of the form $e^{i\alpha}$, where α, β and γ are real numbers. Finally, an arbitrary two by two unitary matrix, and thus an arbitrary single-qubit quantum logic gate can be decomposed as follows

$$U = e^{i\alpha} \begin{pmatrix} e^{-i\beta/2} & 0 \\ 0 & e^{i\beta/2} \end{pmatrix} \begin{pmatrix} \cos\frac{\gamma}{2} & -\sin\frac{\gamma}{2} \\ \sin\frac{\gamma}{2} & \cos\frac{\gamma}{2} \end{pmatrix} \begin{pmatrix} e^{-i\delta/2} & 0 \\ 0 & e^{i\delta/2} \end{pmatrix} \tag{1.26}$$

The previous statement is generalized through *Bloch's theorem.* For any single qubit transformation U, there exist real numbers α, β, γ and δ such that

$$U = e^{i\alpha} R_x(\beta) R_y(\gamma) R_x(\delta) \tag{1.27}$$

which shows that any single-qubit transformation can be realized using a sequence of rotations about just two axes.

We conclude this section by showing how a quantum register can be built starting from only one element of the computational basis of n elements. For simplicity, we consider only three qubits and apply in parallel three Hadamard gates to the state $\mid 000\rangle$

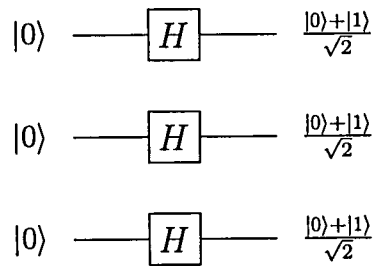

The final state is

$$\begin{aligned} &\tfrac{|0\rangle+|1\rangle}{\sqrt{2}} \otimes \tfrac{|0\rangle+|1\rangle}{\sqrt{2}} \otimes \tfrac{|0\rangle+|1\rangle}{\sqrt{2}} \\ &= \tfrac{1}{2^{3/2}}(\mid 000\rangle + \mid 001\rangle + \mid 010\rangle + \mid 011\rangle) \\ &+ \mid 100\rangle + \mid 101\rangle + \mid 110\rangle + \mid 111\rangle) \\ &= \tfrac{1}{2^{3/2}}(\mid 0\rangle + \mid 1\rangle + \mid 2\rangle + \mid 3\rangle + \mid 4\rangle + \mid 5\rangle + \mid 6\rangle + \mid 7\rangle). \end{aligned} \tag{1.28}$$

In general, by applying in parallel n Hadamard gates (we call this transformation as *Hadamard transform*), to the state $\mid x\rangle$, with $x \in \{0,1\}^n$, we obtain

$$H^{\otimes n} : \mid x\rangle \rightarrow \frac{1}{2^{n/2}} \sum_{y \in \{0,1\}^n} (-1)^{xy} \mid y\rangle, \tag{1.29}$$

where, if $x = x_{n-1}2^{n-1} + ... + x_1 2^1 + x_0 2^0$ and $y = y_{n-1}2^{n-1} + ... + y_1 2^1 + y_0 2^0$, product xy is

$$xy = x_{n-1}y_{n-1} + ... + x_1 y_1 + x_0 y_0. \tag{1.30}$$

1.3 Two-qubit Gates

Two-qubit quantum gates are unitary transformations which act on a two qubit state. They are described by four by four unitary matrices, and they do not have a direct classical counterpart. Indeed, in the classical case, two-bit gates are *non-invertible* operations, i.e. by knowing the output of the gate it is not possible to infer the input bits. For this reason, we cannot have a parallel correspondence between classical and quantum gates with more than one input element. To realize the quantum counterpart of a AND, $NAND$, OR or XOR classical gate, we need to introduce a *control* qubit, whose value conditions the action of the gate.

1.3.1 $CNOT$-gate

The most important two-qubit quantum gate is the *Universal Two-Qubit Quantum Gate* called *controlled-NOT* ($CNOT$), which corresponds to the classical XOR. Fig. 1.3 shows the scheme of a $CNOT$-gate; qubit $|\ x\rangle$ is the *control qubit* and qubit $|\ y\rangle$ is the *target qubit*. The CNOT operation is defined by the following four by four unitary matrix

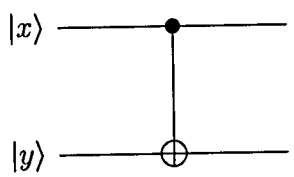

Figure 1.3: Circuit which describes a $CNOT$-gate.

$$U_{CNOT} = \begin{pmatrix} 1 & 0 & 0 & 0 \\ 0 & 1 & 0 & 0 \\ 0 & 0 & 0 & 1 \\ 0 & 0 & 1 & 0 \end{pmatrix}. \tag{1.31}$$

Its action over the computational basis states reads

$$|00\rangle \rightarrow |00\rangle \tag{1.32}$$

$$|01\rangle \rightarrow |01\rangle \tag{1.33}$$

$$|10\rangle \rightarrow |11\rangle \tag{1.34}$$

$$|11\rangle \rightarrow |10\rangle \tag{1.35}$$

(1.36)

that is, if the control qubit is in the state $|1\rangle$, then the target qubit is swapped. The synthetic expression which describes the action of a $CNOT$ over the computational basis is given by the following

$$CNOT: \ |x\rangle\,|y\rangle \rightarrow |x\rangle\,|y \oplus x\rangle, \tag{1.37}$$

where $x, y \in \{0, 1\}$ and $\oplus$ represents the addition modulo 2. It is clear that the target qubit realizes an XOR: $yXORx = y \oplus x$.

$CNOT$ is the prototype of controlled gates. A general controlled gate is represented by the following circuit

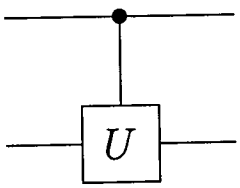

whose action is

$$|0\rangle\,|y\rangle \rightarrow |0\rangle\,|y\rangle; \qquad |1\rangle\,|y\rangle \rightarrow |1\rangle(U\,|y\rangle). \tag{1.38}$$

Another very useful quantum gate is the *phase-gate*, see Fig. 1.4, whose action is given by the following

$$cS = \ |x\rangle\,|y\rangle \rightarrow e^{ixy\phi}\,|x\rangle\,|y\rangle, \quad x, y \in \{0, 1\}, \tag{1.39}$$

and its matrix form is

$$S = \begin{pmatrix} 1 & 0 & 0 & 0 \\ 0 & 1 & 0 & 0 \\ 0 & 0 & 1 & 0 \\ 0 & 0 & 0 & e^{i\phi} \end{pmatrix}. \tag{1.40}$$

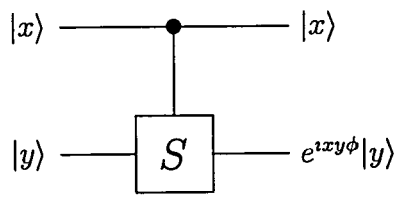

Figure 1.4: Circuit representing a two-qubit phase-gate

A particular case of the two-qubit phase-gate is the so called π-*gate*, G_π. Its action can be summarized as follows

$$G_\pi : \ |x\rangle\,|y\rangle \rightarrow (-1)^{xy}\,|x\rangle\,|y\rangle, \quad x, y \in \{0,1\}, \tag{1.41}$$

and its matrix form is given by

$$G_\pi = \begin{pmatrix} 1 & 0 & 0 & 0 \\ 0 & 1 & 0 & 0 \\ 0 & 0 & 1 & 0 \\ 0 & 0 & 0 & -1 \end{pmatrix}. \tag{1.42}$$

Following [12], we are able to give a very important universality result about the CNOT-gate, which explains its property as a universal quantum gate:
Any multiple qubit logic gate may be composed from CNOT and single-qubit gates. Since an arbitrary unitary operator U on a single qubit can be decomposed as $U = e^{i\phi}AXBXC$, with $ABC = I$ (I is the identity matrix) [12], it is trivial to prove that circuit in Fig 1.5 realizes a controlled-U.

The aim of our study is to evaluate a $CNOT$-gate through the analysis of the dynamics of our two-qubit system. In order to achieve our goal, it is easier to write the $CNOT$- gate in its factored form

$$CNOT = \frac{1}{\sqrt{2}} \begin{pmatrix} 1 & 1 & 0 & 0 \\ 1 & -1 & 0 & 0 \\ 0 & 0 & 1 & 1 \\ 0 & 0 & 1 & -1 \end{pmatrix} \begin{pmatrix} 1 & 0 & 0 & 0 \\ 0 & 1 & 0 & 0 \\ 0 & 0 & 1 & 0 \\ 0 & 0 & 0 & -1 \end{pmatrix} \frac{1}{\sqrt{2}} \begin{pmatrix} 1 & 1 & 0 & 0 \\ 1 & -1 & 0 & 0 \\ 0 & 0 & 1 & 1 \\ 0 & 0 & 1 & -1 \end{pmatrix} \tag{1.43}$$

where it can be seen that the $CNOT$-gate is given by an Hadamard gate on the second

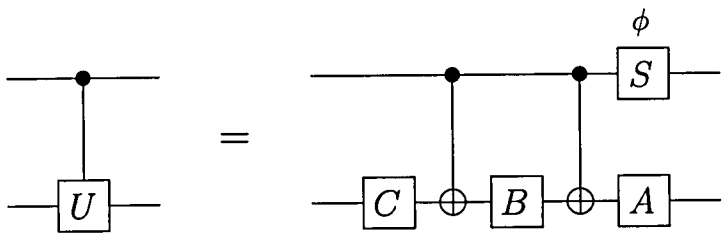

Figure 1.5: An arbitrary controlled-U realized via the combination of $CNOT$ and single-qubit gates.

qubit, whose matrix is given by

$$I \otimes H = \frac{1}{\sqrt{2}} \begin{pmatrix} 1 & 1 & 0 & 0 \\ 1 & -1 & 0 & 0 \\ 0 & 0 & 1 & 1 \\ 0 & 0 & 1 & -1 \end{pmatrix} \tag{1.44}$$

followed by a π-phase gate, which is in turn followed again by an Hadamard gate on the second qubit, $I \otimes H$. In order to realize the universal two-qubit $CNOT$-gate, we therefore need to realize two single qubit Hadamard gates and the two qubits $\pi-$phase gate. Fig. 1.6 illustrates the circuit which represents a $CNOT$ through the combination of a π-gate and two Hadamard gates.

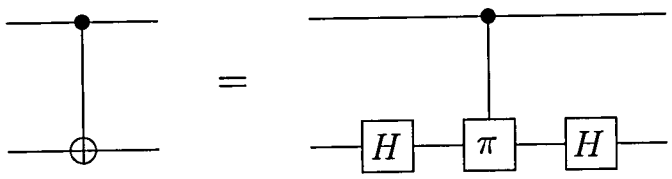

Figure 1.6: Realization of a $CNOT$ though the combination of a π-gate and two Hadamard gates.

In the following section we will explain in detail the very useful two-qubit π-gate.

1.3.2 Quantum Phase Gate

This section gives a more detailed account for the phase-gate, see Eq. (1.40).

As shown in the previous section, the $\pi-$gate, a particular case of the phase-gate, is very important. This is because by combining it with single qubit gates, it is possible to realize a $CNOT$-gate. Considering decomposition (1.43), the π-gate is the only two-qubit gate involved in the realization of a $CNOT$. In Chap. 4, we will show that a two-qubit gate is naturally realized through the mutual interaction between the two particles which encode the qubit. Therefore, a π-gate can be accomplished through the study of the time evolution of the two-particle system.

The explicit action of a phase-gate on the computational basis states is given by

$$\begin{aligned} |00\rangle &\rightarrow |00\rangle \\ |01\rangle &\rightarrow |01\rangle \\ |10\rangle &\rightarrow |10\rangle \\ |11\rangle &\rightarrow e^{i\vartheta}|11\rangle, \end{aligned} \tag{1.45}$$

where only state $|\ 11\rangle$ acquires a phase ϑ. When $\vartheta = \pi$, the resulting quantum gate is called a $\pi-$*gate.*

If the computational basis states $|\ ij\rangle, i, j = 0, 1$ are all energy eigenstates, the action of the time evolution on the four states belonging to the computational basis is the following

$$\begin{aligned} |00\rangle &\rightarrow e^{i\phi_{00}}|00\rangle \\ |01\rangle &\rightarrow e^{i\phi_{01}}|01\rangle \\ |10\rangle &\rightarrow e^{i\phi_{10}}|10\rangle \\ |11\rangle &\rightarrow e^{i\phi_{11}}\ |\ 11\rangle. \end{aligned} \tag{1.46}$$

In order to obtain the the action of the ideal quantum phase gate, Eqs. (1.45), following [4] we have to apply to the set of states in Eq. (1.46) the following local operator

$$\hat{S} = \hat{S}_1 \otimes \hat{S}_2, \tag{1.47}$$

where

$$\hat{S}_1 = |\ 0\rangle_1\langle 0\ |\ e^{is_1^0}+\ |\ 1\rangle_1\langle 1\ |\ e^{is_1^1} \tag{1.48}$$

$$\hat{S}_2 = |\ 0\rangle_2\langle 0\ |\ e^{is_2^0}+\ |\ 1\rangle_2\langle 1\ |\ e^{is_2^1} \tag{1.49}$$

and the phases s_i^j are defined as follows

$$
\begin{aligned}
s_1^0 &= -\phi_{00}/2 \\
s_1^1 &= -\phi_{10} + \phi_{00}/2 \\
s_2^0 &= -\phi_{00}/2 \\
s_2^1 &= -\phi_{01} + \phi_{00}/2,
\end{aligned}
\tag{1.50}
$$

After a straightforward calculation we obtain the desirable phase

$$\vartheta = \phi_{11} - \phi_{10} - \phi_{01} + \phi_{00}. \tag{1.51}$$

When phase $\vartheta = \pm\pi$ the resulting phase-gate is the π-gate, and its action on the computational basis states is the following

$$
\begin{aligned}
|00\rangle &\rightarrow |00\rangle \\
|01\rangle &\rightarrow |01\rangle \\
|10\rangle &\rightarrow |10\rangle \\
|11\rangle &\rightarrow -|11\rangle.
\end{aligned}
\tag{1.52}
$$

This is the two-qubit gate we are performing through the study of the time evolution of the physical system under consideration. In Chap.4 we will present a theoretical model which describes the procedure to follow for the realization of this two-qubit gate.

1.4 Multiple-qubit gates

A controlled gate may have more than one control qubit. The most important example of a multiple-controlled gate is the *Toffoli gate*, see Fig. 1.7, which is a $CNOT$ with two control qubits. The target qubit $|\ z\rangle$ is swapped only if control qubits $|\ x\rangle$ and $|\ y\rangle$ are both equal to $|\ 1\rangle$, otherwise $|\ z\rangle$ is left unaltered. Therefore, the action of a Toffoli gate can be summarized as follows

$$|\ x,y\rangle\ |\ z\rangle \rightarrow |\ x,y\rangle\ |\ z \oplus xy\rangle, \quad x,y,z \in \{0,1\}. \tag{1.53}$$

In particular, it gives

$$|\ x,y\rangle\ |\ 0\rangle \rightarrow |\ x,y\rangle\ |\ xy\rangle, \tag{1.54}$$

$$|\ x,y\rangle\ |\ 1\rangle \rightarrow |\ x,y\rangle\ |\ \overline{xy}\rangle. \tag{1.55}$$

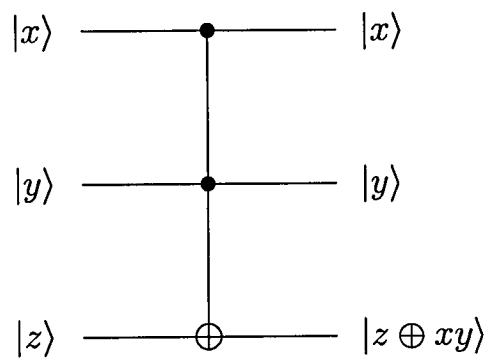

Figure 1.7: Toffoli gate.

From this, we can see that if the input target qubit is $|\ 0\rangle$, in output it becomes $|\ xy\rangle$ and the Toffoli gate realizes an AND, see Fig. 1.8. If the input target qubit is $|\ 1\rangle$, the Toffoli gate realizes a $NAND$. If one of the two control qubits (for example, $|\ x\rangle$) is equal to $|\ 1\rangle$ and the input target qubit is $|\ 0\rangle$, in output it will be equal to the other control qubit, i.e. $|\ y\rangle$. This scheme describes the so called $FANOUT$, see Fig. 1.9 We observe that unlike the classical AND, $NAND$ and $FANOUT$, which are *non-invertible*, the *quantum* $NAND$ and $FANOUT$, realized with Toffoli gates are reversible and invertible. This is due to the introduction of extra qubits called *ancillas*, with a fixed value equal to $|\ 0\rangle$ or $|\ 1\rangle$.

Classical $NAND$ and $FANOUT$ gates are universal classical gates. Circuits containing a combination of these two gates can reproduce all the classical gates. The fact that a Toffoli gate allows the reversible reproduction of these two elements shows that a quantum computer can perform any operation which can be computed on a classical computer.

1.5 No-Cloning Theorem

The *no-cloning* theorem, due to Dieks [17] and Wooters and Zurek [18], states that *a quantum state cannot be copied.*

Consider a system, an ideal copying machine, composed of two components A and B. A is in the state $|\ \psi\rangle$ (the state which has to be copied), and B is in its starting state

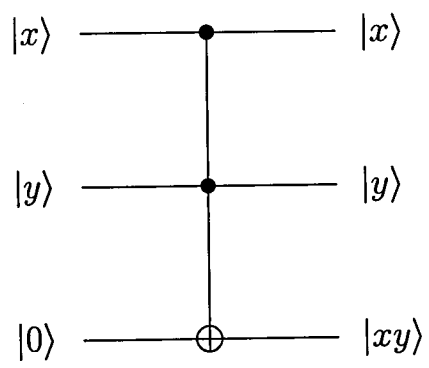

Figure 1.8: A reversible AND gate realized with a Toffoli gate.

$|\ s\rangle$. The initial state of the system is described by

$$|\ \psi\rangle\ |\ s\rangle. \tag{1.56}$$

Suppose that there exists an unitary operator U, which copies $|\ \psi\rangle$ on B, i.e.

$$U(|\ \psi\rangle\ |\ s\rangle) = |\ \psi\rangle\ |\ \psi\rangle, \quad \forall\ |\ \psi\rangle. \tag{1.57}$$

Since this operation must be valid for all $|\ \psi\rangle$, for another arbitrary state $|\ \phi\rangle$ it has to be satisfied, i.e.

$$U(|\ \phi\rangle\ |\ s\rangle) = |\ \phi\rangle\ |\ \phi\rangle. \tag{1.58}$$

If we multiply Eq. (1.57) and Eq. (1.58), for the unitarity of U, we obtain

$$\langle\psi\ |\ \phi\rangle = (\langle\psi\ |\ \phi\rangle)^2. \tag{1.59}$$

This equation implies that states $|\ \psi\rangle$ have to be equal or orthogonal to each other. Therefore, the unitary transformation for copying quantum states defined in Eq. (1.57) does not hold for all possible quantum states. This allows us to conclude that there is no universal device able to copy an arbitrary quantum state.

1.6 Quantum Teleportation

Quantum teleportation is a technique for transferring quantum states, or more appropriately for transferring the information needed to reproduce such states [19]. Consider two

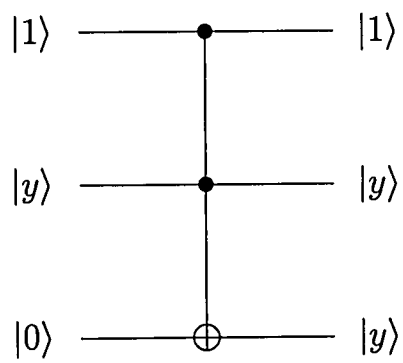

Figure 1.9: Reversible $FANOUT$ realized with a Toffoli gate.

parties, traditionally called *Alice* and *Bob*. Suppose that Alice wants to send Bob a qubit $|\psi_A\rangle$. As it is shown in Sec. 1.5, state $|\psi_A\rangle$ cannot be copied. Furthermore, since state $|\psi_A\rangle$ is a superposition

$$|\psi_A\rangle = \alpha|0\rangle + \beta|1\rangle, \tag{1.60}$$

where α and β are complex numbers, an infinite amount of classical information would be necessary to describe the state.

To transfer a quantum state, each of the two parties needs to posses a qubit in a Bell state

$$|B\rangle = \frac{|0\rangle|0\rangle + |1\rangle|1\rangle}{\sqrt{2}}. \tag{1.61}$$

The first qubit in $|B\rangle$ belongs to Alice and the second belongs to Bob.

The starting state is $|\Psi_0\rangle = |\psi_A\rangle|B\rangle$, i.e.

$$|\Psi_0\rangle = \frac{1}{\sqrt{2}}[\alpha|0\rangle(|0\rangle|0\rangle + |1\rangle|1\rangle) + \beta|1\rangle(|0\rangle|0\rangle + |1\rangle|1\rangle)]. \tag{1.62}$$

The first two qubits belong to Alice and the third belongs to Bob. Alice applies a $CNOT$ to her two qubits, using the first as control qubit. Therefore, the state of the system becomes

$$|\Psi_1\rangle = \frac{1}{\sqrt{2}}[\alpha|0\rangle(|0\rangle|0\rangle + |1\rangle|1\rangle) + \beta|1\rangle(|1\rangle|0\rangle + |0\rangle|1\rangle)]. \tag{1.63}$$

At this stage, Alice applies a Hadamard gate to her first qubit, consequently obtaining

(1.64)
$$| \Psi_2\rangle = \frac{1}{2}[\alpha(| 0\rangle + | 1\rangle)(| 0\rangle | 0\rangle + | 1\rangle | 1\rangle) + \beta(| 0\rangle - | 1\rangle)(| 1\rangle | 0\rangle + | 0\rangle | 1\rangle)].$$

Rearranging $| \Psi_2\rangle$ to put in evidence Bob's qubit, we obtain:

(1.65)
$$\begin{aligned} | \Psi_2\rangle = \; & \tfrac{1}{2}[| 0\rangle | 0\rangle(\alpha | 0\rangle + \beta | 1\rangle) + | 0\rangle | 1\rangle(\alpha | 1\rangle + \beta | 0\rangle) \\ & + | 1\rangle | 0\rangle(\alpha | 0\rangle - \beta | 1\rangle) + | 1\rangle | 1\rangle(\alpha | 1\rangle - \beta | 0\rangle)]. \end{aligned}$$

After these operations, if Alice measures the first two qubits, Bob's qubit (which we call $| \psi_B\rangle$) collapses in a state which depends on the results of the measurement performed by Alice. The four possible results are the following:

(1.66) measured 00 $\rightarrow$ $| \psi_B\rangle = \alpha | 0\rangle + \beta | 1\rangle$,

(1.67) measured 01 $\rightarrow$ $| \psi_B\rangle = \alpha | 1\rangle + \beta | 0\rangle$,

(1.68) measured 10 $\rightarrow$ $| \psi_B\rangle = \alpha | 0\rangle - \beta | 1\rangle$,

(1.69) measured 11 $\rightarrow$ $| \psi_B\rangle = \alpha | 1\rangle - \beta | 0\rangle$.

In the next step Alice needs to classically communicate to Bob the result of her measurement. Finally, Bob applies a quantum gate (X or Z), which allows him to transform state $| \psi_B\rangle$ into $| \psi_A\rangle$. For example, if Alice sends Bob the classical information 01, Bob may obtain $| \psi_A\rangle = \alpha | 0\rangle + \beta | 1\rangle$ through the action of an X-gate on its qubit $| \psi_B\rangle = \alpha | 0\rangle + \beta | 0\rangle$. This is the way to realize the teleportation of state $| \psi_A\rangle$ from Alice to Bob. It is important to observe that quantum teleportation includes a *classical communication* of the results of measures: this forbids the superluminal transmission of signals. A final remark is that quantum teleportation does not violate the no-cloning theorem. Since at the beginning of the process, the first qubit is in state $| \psi_A\rangle$, after the teleportation it collapses into $| 0\rangle$ or $| 1\rangle$, therefore state $| \psi_A\rangle$ is *not copied.*

1.7 Deutsch Algorithm

In 1985 Deutsch showed that there are problems which can be solved more rapidly with a quantum algorithm, rather than a classical one [20]. The scheme considered by Deutsch is the following. Consider a boolean function f of the form $f : \{0,1\} \rightarrow \{0,1\}$. Consider

four functions of this type:

$$f(0) = f(1) = 0, \tag{1.70}$$

$$f(0) = f(1) = 1, \tag{1.71}$$

$$f(0) = 0, \quad f(1) = 1, \tag{1.72}$$

$$f(0) = 1, \quad f(1) = 0. \tag{1.73}$$

The first two functions are *constant*, and the other two are *balanced*, i.e. half of the values are equal to 0 and the other half is equal to 1. The problem consists in finding out whether f is constant or balanced, through the minimum number of evaluations.

From a classical point of view, we can have a certain answer only through two evaluations of $f(x)$, i.e. computing both $f(0)$ and $f(1)$. However, quantum Deutsch algorithm allows us to instead solve the problem with only *one* evaluation of $f(x)$. The circuit which describes Deutsch algorithm is presented in Fig. 1.10. The input state is

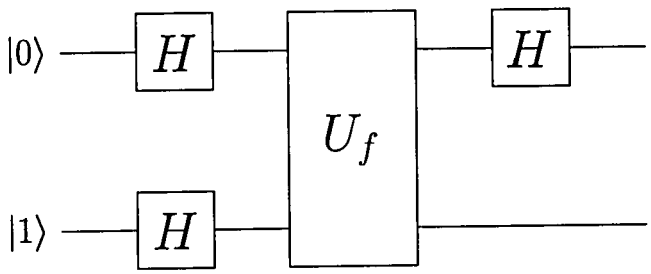

Figure 1.10: Circuit representing Deutsch algorithm.

$$|\psi_0\rangle = |0\rangle\,|1\rangle. \tag{1.74}$$

The Hadamard transform produces

$$|\psi_1\rangle = \frac{1}{2}(|0\rangle + |1\rangle)(|0\rangle - |1\rangle). \tag{1.75}$$

The effect of U_f leaves unaltered the target qubit if $f(x) = 0$ and swaps its sign if $f(x) = 1$. Its action can be summarized as follows

$$U_f: \ |x\rangle(|0\rangle - |1\rangle) \rightarrow (-1)^{f(x)}\,|x\rangle(|0\rangle - |1\rangle). \tag{1.76}$$

In the present case, the effect of U_f is to generate the following state

$$|\psi_2\rangle = \frac{1}{2}[(-1)^{f(0)}|0\rangle + (-1)^{f(1)}|1\rangle](|0\rangle - |1\rangle). \tag{1.77}$$

Acting with an Hadamard gate on the first qubit, the output state is (up to a global sign)

$$|\psi_3\rangle = |0\rangle \left(\frac{|0\rangle - |1\rangle}{\sqrt{2}}\right) \quad \text{if} \quad f(0) = f(1), \tag{1.78}$$

$$|\psi_3\rangle = |1\rangle \left(\frac{|0\rangle - |1\rangle}{\sqrt{2}}\right) \quad \text{if} \quad f(0) \neq f(1). \tag{1.79}$$

Therefore, a measurement of the first qubit allows us to know if the function $f(x)$ is constant or balanced. Unlike the classical case, this result has been obtained through *only one* evaluation of $f(x)$ with the use of U_f.

The shown algorithm is a recent version [21] of Deutsch algorithm [20]. This algorithm can be easily generalized for the case of constant or balanced functions of the type $f : \{0,1\}^n \rightarrow \{0,1\}$. This generalized algorithm is known as the Deutsch-Jozsa algorithm. Fig. 1.11 presents the circuit which describes the quantum algorithm which allows to know if $f(x)$ is constant or balanced through only one evaluation (i.e. through only one operation of U_f). The action of the algorithm is the following. The starting state,

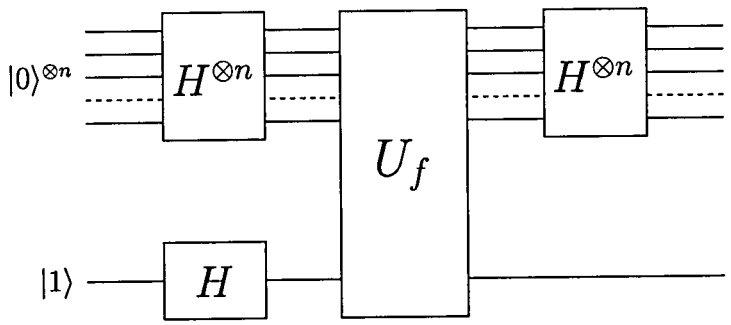

Figure 1.11: Circuit representing Deutsch algorithm for functions $f : \{0,1\}^n \rightarrow \{0,1\}$.

composed by $n+1$ qubit, is

$$|\psi_0\rangle = |0\rangle \ldots |0\rangle |1\rangle, \tag{1.80}$$

where the first n qubits (all equal to $|0\rangle$) form the control register of oracle U_f. The n Hadamard gates in parallel transform $|\psi_0\rangle$ in the following state

$$|\psi_1\rangle = \frac{1}{\sqrt{2^n}} \sum_x |x\rangle \left(\frac{|0\rangle - |1\rangle}{\sqrt{2}}\right). \tag{1.81}$$

As prescribed by Eq. (1.76), the action of U_f produces a phase dependent on $f(x)$, giving the following state

$$| \psi_2\rangle = \frac{1}{\sqrt{2^n}} \sum_x (-1)^{f(x)} | x\rangle \left(\frac{| 0\rangle - | 1\rangle}{\sqrt{2}} \right). \tag{1.82}$$

Using Eq. (1.29), the final set of Hadamard transformations of the control register gives

$$| \psi_3\rangle = \frac{1}{2^n} \sum_x \sum_y (-1)^{f(x)+xy} | y\rangle \left(\frac{| 0\rangle - | 1\rangle}{\sqrt{2}} \right). \tag{1.83}$$

The amplitude of state $| 0\rangle^{\otimes n}$ is

$$\frac{1}{2^n} \sum_x (-1)^{f(x)} = \begin{cases} \pm 1 & \text{if} f(x) \text{ is constant} \\ 0 & \text{if} f(x) \text{ is balanced} \end{cases} \tag{1.84}$$

Therefore, a measure of the first n qubits allows us to know if f is constant or balanced. It is important to observe that the oracle U_f is applied only once. On the other hand, a classical algorithm requires in the worst case a number of evaluations of $f(x)$ equal to $2^n/2 + 1$. It is clear that the quantum algorithm is much faster and more efficient than its classical counterpart.

1.8 Physical Realization of Quantum gates

In previous sections, we showed quantum gates by a theoretical point of view. If we want to experimentally implement a quantum gate, we have to face many obstacles. In the following sections we will show the main features which arise when we experimentally manipulate quantum systems. We will introduce the *decoherence* phenomenon, which is one of the most important problems which appears in quantum experiments. We will also show the well-known DiVincenzo criteria, which have to be satisfied by a quantum system when we want to perform quantum gates.

1.9 Decoherence

A quantum gate can be interpreted as the result of the time evolution of a qubit system. By definition, the time evolution of a quantum state has to be *unitary*. Therefore, the

superposition principle and the possibility of interference between quantum states have to be preserved. When a quantum computation is performed, the qubit is not isolated by the surrounding environment, and we have to take into account the coupling between qubits and the environment. This coupling generates deviations from the unitarity of the time evolution of qubits. This phenomenon is known as *decoherence*. Following [27], we will show the decoherence process through a simple example. Suppose that the qubit-environment joint system induces a time evolution of the form

$$|\alpha\rangle \otimes |E\rangle \xrightarrow[U(t)]{} |\alpha\rangle \otimes |E_\alpha(t)\rangle\,, \tag{1.85}$$

where $|\alpha\rangle$ is the qubit state, $|E\rangle$ is the initial state of the environment and $U(t)$ is the time evolution operator of the qubit-environment joint system. If the initial state of the qubit is a superposition of the basis state $|\ 0\rangle$ and $|\ 1\rangle$, the time evolution generates an entanglement between the qubit and the environment,

$$(a_0|0\rangle + a_1|1\rangle) \otimes |E\rangle \xrightarrow[U(t)]{} a_0|0\rangle \otimes |E_0(t)\rangle + a_1|1\rangle \otimes |E_1(t)\rangle\,. \tag{1.86}$$

Decoherence arises from the qubit-environment entanglement. To show the non unitarity of the time evolution of the qubit, we need to consider the reduced density matrix related to the qubit. The density matrix of the qubit-environment joint system can be written as

$$\sum_{\alpha,\beta} a_\alpha a_\beta^* |\alpha\rangle\langle\beta| \otimes |E\rangle\langle E| \xrightarrow[U(t)]{} \sum_{\alpha,\beta} (a_\alpha|\alpha\rangle|E_\alpha(t)\rangle)(\langle E_\beta(t)|\langle\beta|a_\beta^*)\,. \tag{1.87}$$

Performing the trace over the environment degrees of freedom, we obtain the qubit reduced density matrix

$$\rho_q(t) = \mathrm{tr}_E\, \rho_{q+E} = \begin{bmatrix} |a_0|^2 & a_0 a_1^* \langle E_1|E_0\rangle \\ a_1 a_0^* \langle E_0|E_1\rangle & |a_1|^2 \end{bmatrix}. \tag{1.88}$$

The off-diagonal terms in matrix (1.88) are the so called *coherences*. Therefore, we need to check the effect of the environment on these terms. The product between $|\ E_0(t)\rangle$ and $|\ E_1(t)\rangle$ describe the loss of information of the qubit state into the environment. In general, these states become increasingly more orthogonal with time as described by the following equation

$$\langle E_0(t)|E_1(t)\rangle = e^{-\Gamma(t)} \tag{1.89}$$

where $\Gamma(t)$ is a time dependent function whose specific form depends on the specific coupling between the qubit and the environment. The typical decoherence time varies from

10^4 for nuclear spins in a paramagnetic atom to 10^{-12} for electron-hole excitations in the bulk of a semiconductor. Therefore, due to the entanglement, the off-diagonal terms in Eq. (1.88) tend to vanish, but the diagonal terms remain unaffected. The decoherence phenomenon is the main problem to overcome in the realization of quantum gates. Preferable systems are characterized by long decoherence times in comparison to the operational time required to perform a quantum gate.

1.10 DiVincenzo Criteria

In order to manipulate the quantum information encoded in a quantum system certain criteria have to be fulfilled. Following DiVincenzo [28], at least five conditions have to be satisfied by a quantum system to efficiently implement quantum computation. These criteria are:

(1) The quantum system must be scalable with well defined qubits and offer the opportunity to perform a quantum register (which is a collection of qubits).

(2) We need to initialize the state of the qubits in a desirable state.

(3) The operational time t needed to perform a quantum operation has to be much smaller than the decoherence time T, which is determined by the interaction between the qubit and the environment. The ratio $n_{op} = T/t$ is the maximum number of operations that can be implemented by the quantum gate.

(4) A *universal* set of quantum gates is needed, which allows us to perform all the possible unitary operations on a qubit register. This set can be composed of $CNOT$ and of single-qubit quantum gates.

(5) There should be the capability of measuring the output qubits.

During the development of the study of realistic systems for the realization of quantum gates, we will discuss the fulfillment of DiVincenzo criteria.

Chapter 2

Fullerene and Endohedral Fullerene Molecules

After their discovery in 1985 by a joint research between Sussex and Rice Universities, fullerenes opened up an amazing new branch of chemistry. The experimental group was headed by Harry Kroto, Richard Smalley and Bob Curl, who, for their discovery, shared the 1996 Nobel prize in chemistry [29]. Many relevant applications of fullerenes have been suggested. They show promising applications in medicine and they can be used as lithographic films, lubricants, catalysts and in solar cells or batteries. Moreover, relevant to our interest, is their recent application for quantum computation.

In this chapter we present an overview on fullerene molecules and endohedral fullerenes. We will talk about their discovery and introduce their general features.

2.1 Fullerene Molecules

The path which led to the discovery of fullerenes started in the early seventies with studies on the chemistry of unsaturated carbon configurations. This research was led by Harry Kroto and David Walton at the University of Sussex. They developed methods for synthesizing long chain polyynes and they studied their dynamics by microwave spectroscopy. Their results found an application in molecular radioastronomy, which led to the detection of these molecules in the cloud material of the interstellar medium.

A decade later, Richard Smalley and Bob Curl at Rice University were performing

experiments on the production of atom clusters. Their experiments were based on the laser vaporisation of several different targets in order to produce clusters of atoms. Kroto suggested the use of a graphite target which subsequently resulted a collaboration between Sussex and Rice University research groups.

Following Ref. [30], we will describe the fullerene discovery experiment and their general properties. While performing mass-spectroscopy analysis of carbon vapor, were observed the presence of even-numbered clusters of carbon atoms in the range $C_{30} - C_{100}$ [29, 31, 32]. The experiment is carried out by directing a pulsed laser beam onto the surface of a rotating-translating graphite disk. The released vapor of carbon atoms is then mixed with a stream of helium gas. Therefore, clusters of fullerenes are spontaneously generated. The gas is then led into a vacuum chamber where it expands and is cooled to some degrees above absolute zero. The carbon clusters can then be analyzed by mass spectrometry, which subsequently reveals their molecular structure. The practical synthesis of fullerenes in larger quantities is due to the astrophysicists D. R. Huffman and W. Krätschmer in 1990 [33]. Their experiment was simply based on the evaporation of a graphite electrode. Two graphite rods are heated to a high temperature by an electric arc discharge in an atmosphere of helium at a pressure of $13kPa$. The resulting carbon cluster vapor is composed mainly of C_{60} and C_{70} fullerenes.

Fullerenes are a family of molecular, geodesic structures in the form of cage-like spheroids. The carbon atoms are bonded together in highly symmetrical hexagons and pentagons. Each fullerene contains $2(10 + M)$ carbon atoms corresponding to exactly 12 pentagons and M hexagons, therefore the smallest fullerene which can exist is the C_{20}. Fullerenes are edgeless, charge-less, and have no dangling bonds and no unpaired electrons. A remarkable property of C_{60} is their wave-particle duality which has been discovered in outstanding experiments by Arndt *et al* [34].

C_{60} is the first stable and the most abundant fullerene to be discovered, see Fig 2.1. The C_{60} is also known as *Buckminsterfullerene*, or *buckyball*, after the engineer and architect Richard Buckminster Fuller, as the molecule shares the architecture of his geodesic domes. A buckyball resembles a sphere and it is composed of twenty hexagons, in addition to the usual twelve pentagons. Each hexagon is connected to alternating hexagons and pentagons, and each carbon atom is shared by one pentagon and two hexagons. It was the discovery of the C_{60} fullerene which led the Sussex-Rice group being awarded the Nobel Prize in 1996.

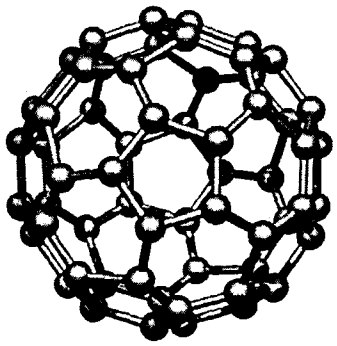

Figure 2.1: The C_{60} buckyball.

2.2 Endohedral Fullerene Molecules

The great interest in fullerene molecules allowed the investigation into new structures composed of these molecules. Experiments based on the ion bombardment of fullerene molecules led to the discovery of more complex structures known as *endohedral fullerene molecules*. An endohedral fullerene molecule is a composite molecule given by a fullerene cage which hosts an atom. Examples of endohedral molecules are Alkali fullerenes [35], noble gas fullerenes [36]. We herein focus our attention on $N@C_{60}$ endohedrals, see Fig. 2.2.

$N@C_{60}$ was discovered by Almeida Murphy *et al.* [37], and successively investigated by other groups [38, 39, 40, 41, 42]. Endohedral $N@C_{60}$ is produced by ion implantation procedures. Ion implantation is a very powerful technique, which in principle allows the encasement of any element inside the fullerene, but the main concern is the stability of the produced molecule. A remarkable property of $N@C_{60}$ is that the encased nitrogen atom retains all of its characteristics as a free atom along with a greater stability toward its outside environment. The experimental set-up is shown schematically in Fig. 2.3. C_{60} fullerenes are evaporated from an effusion cell onto a copper substrate and simultaneously irradiated with nitrogen ions from an ion source. In a five hour run, 2 to $4\mu m$ thick films are produced [40]. Subsequently, the irradiated material is removed from the copper substrate and is dissolved in toulene and filtered. This material is then investigated by Electron Paramagnetic Resonance (EPR). The inset of Fig. 2.3 shows the three sharp ^{14}N EPR lines of the sample irradiated with ^{14}N ions (nuclear spin $I = 1$). The line splitting is due to the hyperfine interaction with the nuclear spin. For more technical

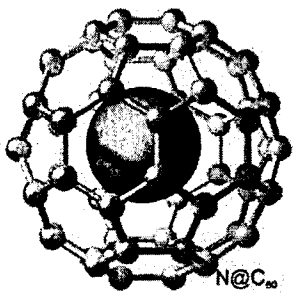

Figure 2.2: $N@C_{60}$ endohedral fullerene molecule.

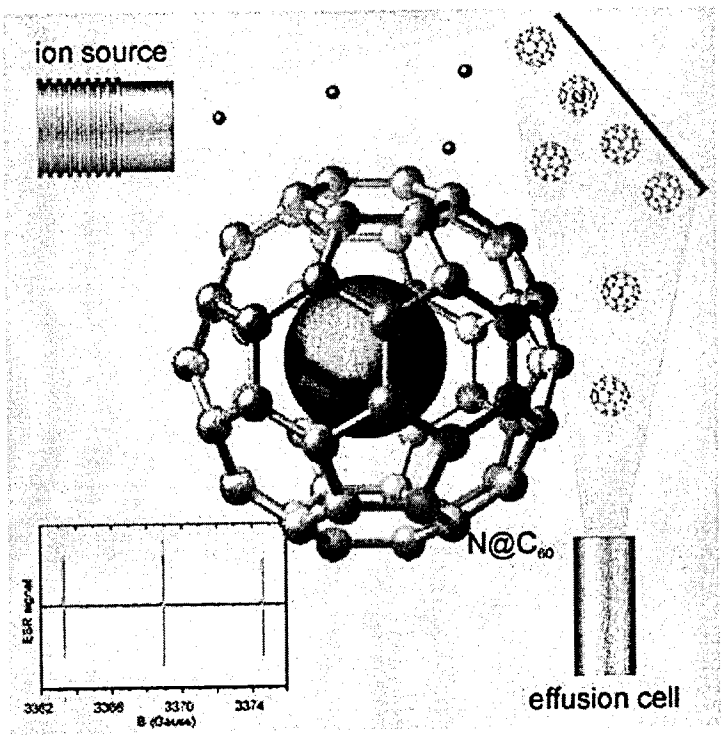

Figure 2.3: Implantation of nitrogen atoms into fullerene molecules. The inset on the left shows the the EPR lines of $N@C_{60}$ (taken from `http://www.hmi.de`).

details regarding this experiment see references [40, 42].

The observed sharp lines in the EPR spectrum indicate that the system is spherically symmetric, i.e. the fine-structure and quadrupole interactions are zero and the g factor and the hyperfine interaction are isotropic. Experiments and theoretical calculations suggest that there is a repulsive exchange interaction between the fullerene and the electronic cloud of the encapsulated atom [43, 44]. Therefore, the nitrogen atomic electrons are more tightly bound than in the free atom. Furthermore, studies on the charge distribution show a symmetrical charge contraction of the nitrogen electronic cloud. These findings along with the chemical inertness of the system show that the nitrogen can be considered as an independent particle encased within the C_{60} cage, and the experimentally observed spherical symmetry shows that the nitrogen sits in the centre of the shielding fullerene.

The most remarkable feature of $N@C_{60}$ is that a nitrogen atom, which is very reactive as a free atom, is stabilized in its electronic ground state and occupies a central position inside the hosting fullerene. Therefore, C_{60} can be considered as an ideal trap for the atomic nitrogen because it protects the hosted atom from the outer environment without introducing any charge transfer processes. Since charge interactions are completely screened, the only physical quantity of interest is the spin of the trapped particle. A nitrogen atom can be effectively described as a $\frac{3}{2}$-spin particle. This spin is associated with its electronic degrees of freedom. We will consider a more simple model assuming that the encased atoms are described as $\frac{1}{2}$-spin particles. The encased nitrogen atom therefore serves as a good candidate for encoding a qubit.

Other features which allow an endohedral fullerene to be considered as a good candidate as a building block for quantum computation is that they can be very easily maneuvered, see Sec. 2.2.1, and they are characterized by remarkably long relaxation times, see Sec. 2.2.2. The discussion related to these features is presented in the next two sections.

2.2.1 Assemblage of scalable systems

One of the most challenging requirements for reliable and useful quantum computation relies on the the possibility of building up scalable systems of qubits. With the use of buckyballs as encoding elements for qubits, it is possible to build up dimers or arrays [46] of buckyballs in nanotubes [46, 47, 48, 49]. The system composed of fullerenes arranged inside a nanotube is called *peapod*, see Fig. 2.4. Fullerenes can be assembled into ordered arrays in single walled nanotube (SWNT). Upon suitable heating conditions, fullerenes spontaneously enter nanotubes to form peapods [47]. Fullerene in SWNT locally alter

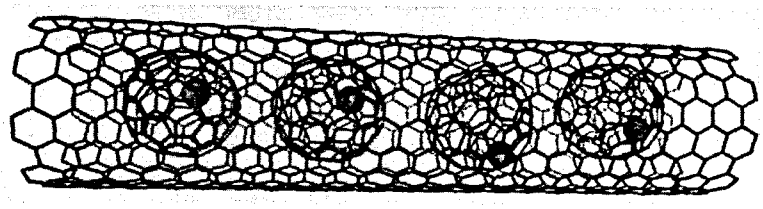

Figure 2.4: The schematic picture of the peapod: a nanotube filled with four endohedrals.

the electronic states of the nanotube [48, 49]. If the electronic states of the fullerene and the nanotube are coupled, then this effect could be used as a mechanism for distant qubits to interact through the nanotube. A pepapod can be seen as a molecular network, characterized by periodicity and geometry which are dictated by molecular interactions (usually non-covalent bonding).

For fullerene spins to be controlled locally by gates they need to be spaced at suitable distances which can allow the single addressing of each fullerene. It is possible to attach functional groups to $N@C_{60}$, which can be used as spacers so that the distance between fullerenes can be controlled [46]. Alternatively, it can be used as a global spin-addressing scheme [50, 51]. This addressing scheme, called *Quantum Cellular Automaton* (QCA) consists of an array of alternate species of endohedral fullerenes given by three [50] (ABCABC...) or two [51] (ABAB...) different types of qubits. An example of a QCA can be built through the use of the three endohedral fullerenes $^{14}N@C_{60}$, $^{15}N@C_{60}$ and $^{31}N@C_{60}$. In this setup, the addressing of qubits can be performed by utilizing the different resonance frequencies of the nitrogen and phosphorous atoms.

Fullerenes inside nanotubes are quasi one-dimensional systems. The fullerene can orient themselves relatively to the nanotube sidewall and to their nearest neighbors. Generally, the ordering of C_{60} fullerenes arrays is controlled by non-directional Van der Waals interactions. A new technique of low-temperature filling, see [46], after the insertion of functionalized fullerenes into a nanotube, leaves the functional groups and the electron spin unaltered and allows the formation of spin active arrays.

Endohedral fullerenes can not only be easily maneuvered to allow the possibility of building scalable systems, but they are also characterized by remarkably long relaxation times, see Sec. 2.2.2. Since in a peapod the nanotube acts as a shield to the encapsulated array of buckyballs from the outer environment, it is believed that relaxation times of the encased particles could be reduced. A detailed discussion about relaxation processes is presented in the next section.

2.2.2 Decoherence Times

It has been shown that endohedral systems provide a long lifetime for the trapped spins and that the fullerene molecules represent a good sheltering environment for the very sensitive spins trapped inside [43]. These endohedral systems are typically characterized by two relaxation times, T_1 and T_2.

Early studies on relaxation processes in endohedral fullerenes [52, 53], show that the first relaxation time T_1 is due to the interactions between a spin and the surrounding environment. The second T_2 is due to the dipolar interaction between the qubit encoding spin and the surrounding endohedral spins randomly distributed in the sample. While T_1 is dependent on temperature, T_2 is practically independent of it. The experimental measure of the two relaxation times shows that T_1 increases with decreasing temperature from about $100\mu s$ at $T = 300K$ to several seconds below $T = 5K$, and that the value of the other relaxation time T_2 remains constant, that is $T_2 \simeq 20\mu s$ [52, 53]. In comparison with T_2, the value of T_1 is very large, therefore the system decoherence is determined by the spin-spin relaxation processes. It is supposed that the value of T_2 can be increased if it could be possible to design a careful experimental architecture, which could screen the interaction of the spins with the surrounding magnetic moments. It is believed that in a system composed of arrays of endohedrals encapsulated in a nanotube [54] or buckyballs embedded on a substrate, it should be possible to reduce the relaxation time of the system due to the random spin-spin interactions. The above systems should be reliable for the realization of quantum gates. In such architectures the decoherence time for each encapsulated spin should be longer.

New findings about the relaxation processes of $N@C_{60}$ molecules have been recently published by Morton *et al.*, [55]. They found that both the relaxation time, T_1, and the coherence time, T_2, are temperature dependent and that there is a correlation between them, $T_2 \simeq \frac{2}{3}T_1$, which is constant over a broad temperature range. These findings suggest that both relaxation times are influenced by the same physical process. Fig. 2.5 (taken from [55]) shows the electron spin relaxation times (T_1 and T_2) of $N@C_{60}$ diluted in CS_2. The ratio $T_2 \simeq \frac{2}{3}T_1$ is constant over the full temperature range for which the solvent remains liquid. At temperatures below $160K$, the CS_2 solvent freezes as a polycrystal leaving regions of high fullerene concentrations around the grain boundaries. This dramatically increases the local spin concentration, and T_2 becomes extremely short due to dipolar spin coupling, which is due to the instantaneous diffusion effect [56, 57, 58].

In early studies investigating the relaxation of $N@C_{60}$ diluted in solvents, [59] the dominant process was found to be due to zero field splitting (ZFS) fluctuations. These

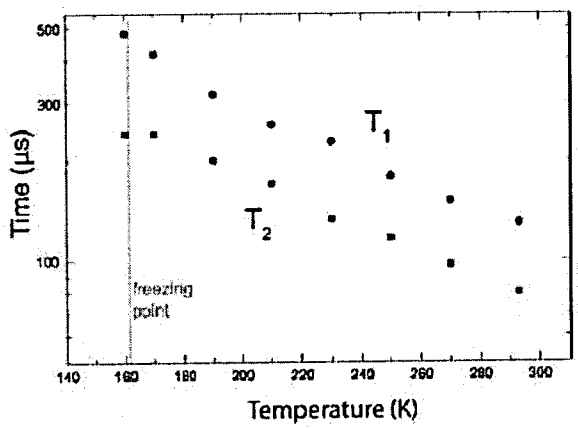

Figure 2.5: Electron spin relaxation times, T_1 and T_2, of $N@C_{60}$ in CS_2. The ratio $T_2 \simeq \frac{2}{3}T_1$ is constant over the full temperature range for which the solvent remains liquid. At temperatures below $160K$, the CS_2 solvent freezes as a polycrystal, leaving regions of high fullerene concentrations around grain boundaries. This dramatically increases the local spin concentration, and T_2 becomes extremely short due to dipolar spin coupling (taken from [55]).

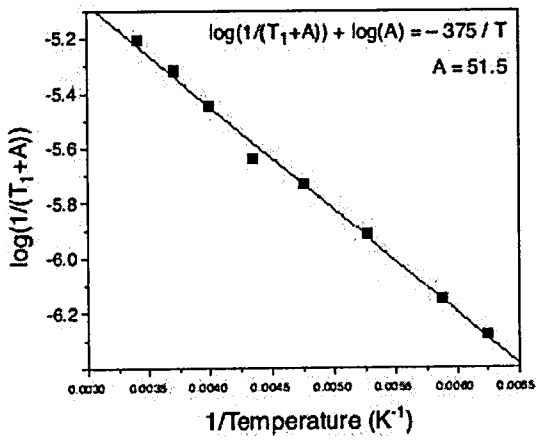

Figure 2.6: Temperature dependence of T_1 of $N@C_{60}$ is linear in Arrhenius coordinates, consistent with the Orbach relaxation mechanism (taken from [55]).

fluctuations are due to deformations of the spherically symmetrical $N@C_{60}$ cage caused by collisions with the molecules of the diluting solvent. Nevertheless, ZFS processes cannot explain the temperature dependence of both T_1 and T_2 and their correlation.

It was found that the physical process which describes the temperature dependence of relaxation times is well described by an Orbach relaxation mechanism, see Fig. 2.6 (Taken from [55]). This is a two-phonon relaxation process whose energies are resonant with a transition to an excited electronic state, such as a vibrational or orbital state which lies outside of the space considered by the spin Hamiltonian. The remarkable result provided by this research is the observation of a coherence time T_2 up to $0.25ms$, the longest for any molecular electron spin. As presented in Chapter 6, such times allow to perform a number proportional to 10^4 of high fidelity quantum gate operations, which subsequently allow us to meet the requirements for quantum error correction [60].

2.2.3 Readout

The possibility of measuring single spins is one of the most challenging aspects for endohedral fullerene molecule systems.

One of the most frequent technologies used for the study of buckyball systems are ESR experiments, which exploit the free induction decay of ensembles containing a number of molecules of the order of 10^4. Many other technologies developed so far can be

adopted as candidate for measuring single spins. The use of micro-SQUIDs (superconducting quantum interference devices) allows the measurement of small magnetic fields, but they limit current sensitivity to $\Delta m_s = 30$, which corresponds to the flipping of 30 electron spins [61]. Another promising experiment is based on magnetic resonance force microscopy (MRFM). It has been successful for detecting a single electron spin in silicon dioxide [62], but the process is slow. STM (scanning tunnel microscopy) assisted EPR allows the tunneling current to be modulated at the Larmor frequency of the individual spin to be detected, but since this does not allow vector measurements, it cannot make a projective measurement of an electron spin qubit [63]. As suggested in reference [64], electrical measurements could be exploited for single spin readout. At suitable low temperatures and magnetic fields, in a molecular-nanoelectronics hybrid device constituted by a fullerene molecule connected to a pair of electrical contacts [65], it may be possible to use Coulomb blockade to measure an endohedral electron spin [66].

Optical experiments seem to offer a valid alternative to electrical experiments for the detection of single spins. Actually, the direct optical detection of a spin in $N@C_{60}$ and $P@C_{60}$ is forbidden because the transition to the first excited state in atomic nitrogen falls far into the ultraviolet region (which cannot be measured with standard optics apparatuses) and well inside the primary absorption range of the C_{60} cage [64]. Other optical experiments could be improved for modeling optical readout devices for endohedral spins. In ODMR (Optically Detected Magnetic Resonance) experiments a sample (titanium-doped silicon carbide [67]) is irradiated with a magnetic field and its luminescence, due to transitions between electronic spin states is used to detect the electron spin. Other possible optical experiments can be based on spin to photon conversion [68], or on the coupling of the endohedral spin to solid-state magnetic optical dipole such as nitrogen-vacancy centres in nanocrystalline diamond [69, 70].

As suggested from a work by Benjamin *et al.* [64], promising candidates for optical single electron spin detection are erbium-doped fullerene. For example, a class of these fullerenes, the so-called TNT fullerenes (composed of a planar trigonal tri-lanthanide nitride group enclosed in a 78, 80 or 82-carbon cage) give a very good response in experiments aiming to single-spin readout. Examples of TNT fullerenes used in such experiments are $ErSc_2N@C_{80}$, $Er_2ScN@C_{80}$ and $Er_3N@C_{80}$ [71]. These experiments are based on cage-mediated photoluminescence. The cage states, which absorb the exciting visible laser source, are subsequently subjected to non-radiative relaxation to the ion and *intra* the ion, with a final luminescent decay. The uncontrolled and complex relaxation processes involved in these kind of experiments make them unsuitable as a readout scheme, which requires us to be able to perform precise coherent manipulations

of the ionic states. However, recent experiments show the possibility of direct excitation of ionic states in TNTs [72], which opens the opportunity of identifying useful readout transition and also to coherently and selectively excite these transitions.

Furthermore, recent experiments [72] show that, under the application of suitable external magnetic fields on TNT samples, the observed spectrum splits, confirming that the Er^{3+} ion maintain a two-fold degeneracy in its quantum states (Kramer ion), even under complete crystal-field splitting. This allows the encoding of a qubit in the arising pseudo-$\frac{1}{2}$-spin, and the possibility of exciting selective luminescent transitions could allow the detection of individual spin states in this species of endohedral fullerene molecules.

Quantum computing through the study of doped fullerene systems has been investigated in many works [44, 70, 73, 74, 75, 76, 77]. Although we have followed many ideas suggested in these previous papers, we consider a different approach for the realization of quantum gates, which is presented in the following chapters.

Chapter 3

Physical System

Following the description presented in the previous chapter, if we consider an $N@C_{60}$ molecule, the only physical quantity of interest is the spin of the encased nitrogen atom.

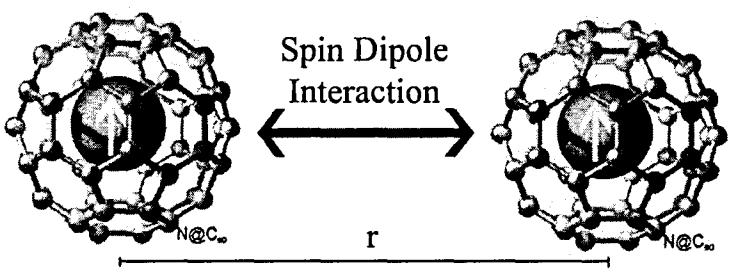

Figure 3.1: Our system: two interacting $N@C_{60}$ buckyballs. Each fullerene molecule hosts a nitrogen atom.

Our system is composed of two interacting $N@C_{60}$ buckyballs, see Fig.3.1, where we indicate the left spin as *spin 1* and the right spin as *spin 2*. In the two-buckyball system any charge interaction is screened and the fullerene cage does not contribute towards the interaction process [43]. Therefore, the mutual interaction between the two buckyballs is given only by the interaction between the spins of the two trapped nitrogen atoms. The Hamiltonian of the system can be written as

$$H = J_0 \vec{\hat{\sigma}}_1 \otimes \vec{\hat{\sigma}}_2 + g(r)[\vec{\hat{\sigma}}_1 \otimes \vec{\hat{\sigma}}_2 - 3(\vec{\hat{\sigma}}_1 \cdot \vec{n}) \otimes (\vec{\hat{\sigma}}_2 \cdot \vec{n})], \tag{3.1}$$

where J_0 is the exchange interaction coupling constant, $\vec{\hat{\sigma}}_1$ and $\vec{\hat{\sigma}}_2$ are the Pauli matrices related respectively to spin 1 and spin 2 , $g(r) = \gamma_1\gamma_2 \frac{\mu_0 \mu_B^2}{8\pi r^3}$ is the dipolar interaction

coupling constant, where μ_0 is the diamagnetic constant, μ_B is the Bohr magneton and r is the distance between the two trapped atoms, and $\vec{n}$ is the unit vector in the direction of the line joining the centers of the two encased atoms.

The most abundant $N@C_{60}$ molecules encase a ^{14}N nitrogen atom, whose electron spin is $S = \frac{3}{2}$. For the sake of simplicity, we will assume that the trapped nitrogens are $\frac{1}{2}$-spin particles, therefore they can be treated as electrons. Although the theoretical study is related to a simplified theoretical model, it gives a reliable overview on the behaviour of the system.

In the case where the trapped particles are electrons, the gyromagnetic ratio is given by $\gamma \simeq 2$, and $g(r) = \frac{\mu_0 \mu_B^2}{2\pi r^3}$. The study of fullerenes' spectra in ESR (Electron Spin Resonance) experiments, and theoretical studies [43, 44, 45], show that the exchange interaction is very small. Therefore, in Eq. (3.1), we can neglect the exchange term proportional to J_0, leaving the spin dipole-dipole interaction as the leading term of the mutual interaction between the two endohedrals. Therefore, the Hamiltonian of two interacting $N@C_{60}$ buckyballs is given by only the mutual dipole-dipole interaction between the spin of the two encased nitrogen atoms. Its expression is the following

$$H = g(r)[\vec{\hat{\sigma}}_1 \otimes \vec{\hat{\sigma}}_2 - 3(\vec{\hat{\sigma}}_1 \cdot \vec{n}) \otimes (\vec{\hat{\sigma}}_2 \cdot \vec{n})]. \tag{3.2}$$

Choosing the direction of vector $\vec{n}$ parallel to the x axis, the dipole-dipole interaction Hamiltonian is simplified as follows

$$H = g(r)(\hat{\sigma}_{z_1} \otimes \hat{\sigma}_{z_2} + \hat{\sigma}_{y_1} \otimes \hat{\sigma}_{y_2} - 2\hat{\sigma}_{x_1} \otimes \hat{\sigma}_{x_2}), \tag{3.3}$$

and its matrix form is the following

$$H = \begin{pmatrix} g(r) & 0 & 0 & -3g(r) \\ 0 & -g(r) & -g(r) & 0 \\ 0 & -g(r) & -g(r) & 0 \\ -3g(r) & 0 & 0 & g(r) \end{pmatrix}. \tag{3.4}$$

The eigenvalues and eigenvectors of matrix (3.4) are

$$\lambda_1 = 0 \rightarrow |e_1\rangle = \begin{pmatrix} 0 \\ -1 \\ 1 \\ 0 \end{pmatrix} \tag{3.5}$$

$$\lambda_2 = -2g(r) \rightarrow |e_2\rangle = \begin{pmatrix} 1 \\ 0 \\ 0 \\ 1 \end{pmatrix} \tag{3.6}$$

$$\lambda_3 = -2g(r) \rightarrow |e_3\rangle = \begin{pmatrix} 0 \\ 1 \\ 1 \\ 0 \end{pmatrix} \tag{3.7}$$

$$\lambda_4 = 4g(r) \rightarrow |e_4\rangle = \begin{pmatrix} -1 \\ 0 \\ 0 \\ 1 \end{pmatrix}. \tag{3.8}$$

If we assume that the two buckyballs are embedded on a silicon substrate, see [77], the suggested value for the distance between their centers is $r = 1.14nm$. Therefore, the numerical value of the energy related to each eigenvalue is

$$\lambda_1 = 0eV \tag{3.9}$$

$$\lambda_2 = \lambda_3 = 7.25 \times 10^{-8} eV \tag{3.10}$$

$$\lambda_4 = 1.45 \times 10^{-7} eV \tag{3.11}$$

These are the eigenvalues of the starting Hamiltonian (3.3), which describes the dipolar mutual interaction always present between the two spins.

In order to perform any quantum computation on our system we need to encode the qubit in our particles. In the following section we describe a way to represent a qubit with a spin particle.

3.1 Encoding a Qubit

Quantum computation and quantum information are based on the concept of the *qubit*. The qubit is the quantum counterpart of the classical bit. Any quantum computational operation can be performed by manipulating qubits. A qubit is a bi-dimensional Hilbert space whose basis is generally indicated as $\{|\ 0\rangle, |\ 1\rangle\}$. Therefore, to encode a qubit, we need a two-level system. Since our candidates for representing qubits are $\frac{1}{2}$-spin particles, a straightforward way to obtain a two level system is to apply to the particles a static magnetic field directed along the z axis. The Hamiltonian which describes a $\frac{1}{2}$-spin particle in a static magnetic field $\vec{B} = (0, 0, B_0)$ directed along z is given by the following expression

$$H_0 = -\frac{\mu_B \gamma B_0}{2}\sigma_z, \tag{3.12}$$

where μ_B is the Bohr magneton, γ is the gyromagnetic ratio, B_0 is the amplitude of the static magnetic field and

$$\sigma_z = \begin{pmatrix} 1 & 0 \\ 0 & -1 \end{pmatrix},$$

which is the z-Pauli matrix. Since we are supposing that the spin-particles are electrons, the gyromagnetic ratio $\gamma \simeq 2$, and equation 3.12 simplifies into

$$H_0 = -\mu_B B_0 \sigma_z. \tag{3.13}$$

The interpretation of Eq. 3.13 is that due to the Zeeman effect, the spin z-component will be split into two sub-components whose quantum numbers are $m_s = -\frac{1}{2}$ and $m_s = +\frac{1}{2}$. The arising two-level system is adopted as the two-level system which represents the qubit, see Fig.3.2. State $|\ 0\rangle$ corresponds to the spin-down component and its energy is $E_- = -\mu_B B_0$, and state $|\ 1\rangle$ corresponds to the spin-up component $E_+ = \mu_B B_0$. The difference in energy between these two state, known as the Zeeman splitting, is

$$\Delta E = E_+ - E_- = 2\mu_B B_0 = \hbar 2\omega_0 \tag{3.14}$$

from which we can derive the precession frequency of the spin

$$\omega_p = 2\omega_0. \tag{3.15}$$

The importance of the precession frequency will be relevant in performing single-qubit operation, see Chap. 4, which can be performed by applying resonant microwave fields.

From hereon, we assume that $\hbar = 1$. Therefore, Eq. 3.13 becomes

$$H_0 = -\mu_B B_0 \sigma_z. \tag{3.16}$$

Since the spin of a $N@C_{60}$ molecule encodes a qubit, an array of $N@C_{60}$ molecules can be considered as a multiple-qubit system. We limit our study to an array composed of two buckyballs, see Fig. 3.1, which represents a two-qubit system when it is subjected to a static magnetic field along the z axis.

The strength of the static magnetic field B_0 produces the splitting of energy levels. EPR spectrum of $N@C_{60}$ molecules consists of three lines. Generally, pulsed EPR are done using the center line of the EPR spectrum [78]. A sharp line triplet is observed with static magnetic field amplitudes B_0 in the range $0.36T - 0.39T$. Therefore, the angular resonance frequency of the spin ω_p, calculated through Eq. (3.15), is characterized by values in the range $63.3GHz - 68.6GHz$.

A system composed of two qubits can be described by a four dimensional Hilbert space. As a basis of this space, we consider the standard two-qubit computational basis, which is given by the set of vectors $\{|\,00\rangle, |\,01\rangle, |\,10\rangle, |\,11\rangle\}$, where

$$|\,00\rangle = \begin{pmatrix} 1 \\ 0 \\ 0 \\ 0 \end{pmatrix} \tag{3.17}$$

$$|\,01\rangle = \begin{pmatrix} 0 \\ 1 \\ 0 \\ 0 \end{pmatrix} \tag{3.18}$$

$$|\,10\rangle = \begin{pmatrix} 0 \\ 0 \\ 1 \\ 0 \end{pmatrix} \tag{3.19}$$

$$|\,11\rangle = \begin{pmatrix} 0 \\ 0 \\ 0 \\ 1 \end{pmatrix}. \tag{3.20}$$

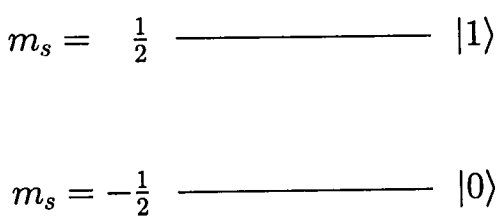

Figure 3.2: Two level system which encodes the qubit. It arises after applying a static magnetic field along the z-direction on a $\frac{1}{2}$-spin particle.

The wave-function of the system can be written as a superposition of the basis states in the following form

$$|\psi\rangle = \alpha\,|\,00\rangle + \beta\,|\,01\rangle + \gamma\,|\,10\rangle + \delta\,|\,11\rangle, \tag{3.21}$$

where α, β, γ and δ are complex coefficients which satisfy the probability normalization condition $|\,\alpha\,|^2 + |\,\beta\,|^2 + |\,\gamma\,|^2 + |\,\delta\,|^2 = 1$.

In a system composed of two $N@C_{60}$ molecules, the qubits are represented by the spins of the two encased nitrogen atoms. We assume that each of the two spins is subjected to a different static magnetic field along z, i.e. spin 1 is subjected to a static magnetic field of amplitude B_{0_1}, and it is described by Hamiltonian

$$H_{0_1} = -\mu_B B_{0_1} \sigma_{z_1}, \tag{3.22}$$

and spin 2 is subjected to the amplitude B_0^2, which allows this spin to be described by Hamiltonian

$$H_{0_2} = -\mu_B B_{0_2} \sigma_{z_2}. \tag{3.23}$$

The complete Hamiltonian of a two-qubit system represented by two interacting $N@C_{60}$ molecules, subjected to static magnetic fields directed along the z axis and to the always present mutual dipolar interaction, see Eq. (3.3), is the following

$$\begin{aligned} H' &= H + H_{0_1} + H_{0_2} \\ &= g(r)(\hat{\sigma}_{z_1} \otimes \hat{\sigma}_{z_2} + \hat{\sigma}_{y_1} \otimes \hat{\sigma}_{y_2} - 2\hat{\sigma}_{x_1} \otimes \hat{\sigma}_{x_2}) \\ &\quad -\mu_B B_{0_1} \sigma_{z_1} \otimes I_2 - \mu_B B_{0_2} I_1 \otimes \sigma_{z_2} \end{aligned} \tag{3.24}$$

We observe that the mutual interaction between the two spins naturally allows us to perform two-qubit operations by simply allowing the two-qubit system to evolve in time. Single-qubit transformations can be instead performed by applying suitable microwave fields on the system (see Chap. 4). However, the achievement of single-qubit operations relies on the possibility of acting distinctly on each single qubit. The description of a convenient single-qubit addressing scheme is presented in the following section.

3.2 Single addressing of each qubit

Our system is composed of two spins which interact with a static magnetic field. Applying a static magnetic field oriented in the direction of the z axis, for the Zeeman effect, we obtain the splitting of the spin z component into the spin-up and spin-down components. The difference between the energies of the two levels provides the resonance frequency of the particle. However, when we apply a static magnetic field on the whole sample, all the particles will have the same resonance frequency. To perform manipulations on each buckyball, we need to be able to distinguish between each of them. This setup leads to the most relevant experimental disadvantage for systems composed of arrays of buckyballs, which resides in the difficulty in addressing each of the qubit-encoding particles. This problem can be overcome by the use of external field gradients which can shift the electronic resonance frequency of the qubit-encoding spins [75, 77]. Magnetic field gradients can be generated by considering wires through which a current flows. If we place two parallel wires outside our two buckyball system, an additional magnetic field is generated in the space between the wires, Fig. 3.3. As described in a publication by Groth *et al.* [79], with the help of atom chip technology, wires with a high current density can be built. Recalling the Biot-Savart law, the magnetic field amplitude at a distance R from a long straight wire carrying a current I is given by the following equation

$$B_g = \frac{\mu_0}{2\pi}\frac{I}{R}. \tag{3.25}$$

As explained in the afore publication [79], if we choose the current intensity $I = 0.3A$, the distance between the two wires $d = 1\mu m$, and the radius of each wire $\rho = 1\mu m$, a buckyball at a distance x from the origin of the axes will be subjected to a magnetic field given by

$$B_g = \frac{\mu_0}{2\pi} I\left(\frac{1}{x+\rho+d/2} + \frac{1}{x-\rho-d/2}\right). \tag{3.26}$$

With the choice $I = 0.3A$, $d = 1\mu m$ and $\rho = 1\mu m$, applied to (3.26) as a numerical computation, we obtain the magnetic field distribution shown in Fig. (3.4). Since the

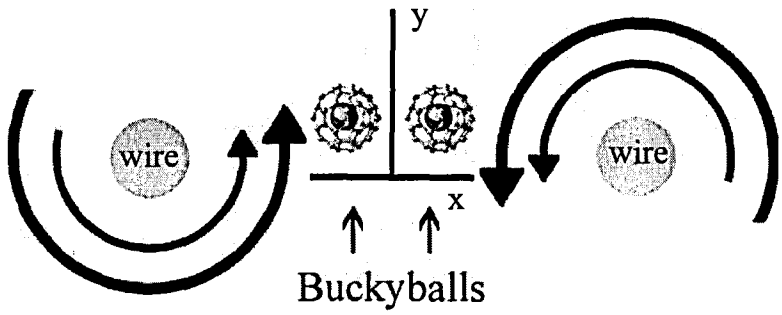

Figure 3.3: Schematic arrangement of the physical apparatus for the realization of a magnetic field gradient.

distance between the atoms encased in the two buckyballs is $r = 1.14nm$, the distance of the left particle from the origin of axes is $x_1 = -0.57nm$ and it is subjected to the gradient field amplitude $B_{g_1} = 6.8 \times 10^{-5}T$, while the right particle is placed at a distance $x_2 = 0.57nm$ from the origin and it is subjected to $B_{g_2} = -3.04 \times 10^{-5}T$. We could not consider a current greater than $I = 0.6A$ because the wires would face a too high heating process and eventually they could be destroyed. On the other hand, we could not consider currents smaller than $10^{-1}A$ because the arising magnetic field gradient would be too small for each buckyball. In this case, the resonance frequencies related to the buckyballs would differ by only a few MHz, which could be a too small gap to be realized by a frequency resonator.

Finally, the total static magnetic field strength on each particle is $B_{0_1} = B_z + B_{g_1}$ for spin 1 and $B_{0_2} = B_z + B_{g_2}$ for spin 2, where B_z is the amplitude of a static magnetic field directed along the z axis, which is applied on the whole system. The Hamiltonian describing a two-$N@C_{60}$ system is given by Eq. (3.24) where we have to substitute the static magnetic fields B_{0_1} and B_{0_2} as defined above.

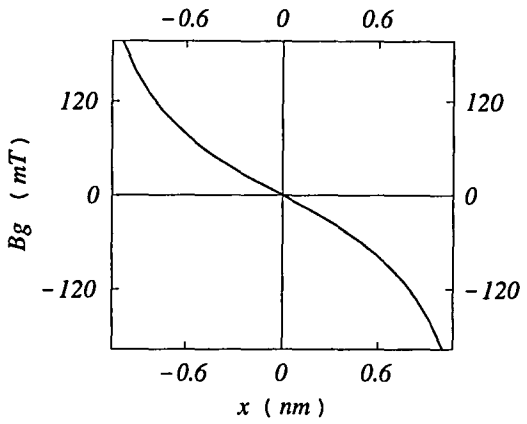

Figure 3.4: Magnetic field generated by two $1\mu m$-radius wires at a distance $d = 1\mu m$, which carry a current $I = 0.3A$. The two buckyballs are placed at a symmetrical distance x with respect to the origin of the axes.

3.3 Concurrence

When we consider a $\frac{1}{2}$-spin particle as the encoding system for the qubit, it may undergo to a *spin-flip* process. This phenomenon consists of the swapping between the spin-up and spin-down components, that is

$$|0\rangle \rightarrow |1\rangle, \tag{3.27}$$

$$|1\rangle \rightarrow |0\rangle. \tag{3.28}$$

If we consider, for example, the two-qubit state, known as *EPR pair*

$$\frac{|00\rangle + |11\rangle}{\sqrt{2}}, \tag{3.29}$$

we can see that it is unaffected by the spin-flip of both qubits. This state, for this feature, is said to be maximally *entangled.* Therefore, we can define the *entanglement* as the property of quantum states, which shows if the state is good enough for carrying quantum information. The most entangled is the quantum state and it is the most reliable for transferring quantum information. In our case, we will consider the *concurrence*, see Ref. [80] as a measure of the entanglement of the state describing the two-qubit system.

A *pure* state of a two-particle quantum system is said to be entangled if it cannot be factorisable, that is to say that it cannot be written as the direct product of the states

describing each particle. A *mixed* state is *entangled* if it cannot be represented as a mixture of factorisable pure states. In this Section we will refer to the *entanglement of formation*, which is intended to quantify the resources needed to create a given entangled state [81]. In order to show the definition of entanglement of formation, see Ref. [81] , we can consider a system composed of two subsystems, A and B. In the general case of a mixed state, the density matrix describing the whole system is given by

$$\rho = \sum_i p_i \mid \psi_i\rangle\langle\psi_i \mid \tag{3.30}$$

where the ensemble of pure states $\{\mid \psi_i\rangle\}$, with the respective probabilities p_i give all the possible pure state decomposition for the density matrix ρ. For each pure state $\mid \psi_i\rangle\langle\psi_i \mid$, the entanglement of formation is defined as the von Neumann entropy of both subsystems A and B. The von Neumann formula, which defines the entanglement of a pure state, $\mid \psi\rangle$, is described by the following equation

$$E(\psi) = -Tr(\rho_A \log_2 \rho_A) = -Tr(\rho_B \log_2 \rho_B). \tag{3.31}$$

where

$$\rho_A = Tr_B(\mid \psi\rangle\langle\psi \mid) \tag{3.32}$$

and

$$\rho_B = Tr_A(\mid \psi\rangle\langle\psi \mid). \tag{3.33}$$

The entanglement of formation of the mixed state ρ is then defined as the average entanglement of the pure states of its decomposition, minimized over all decompositions of ρ, that is

$$E(\rho) = min \sum_i p_i E(\psi_i). \tag{3.34}$$

In our system, in order to evaluate the degree of entanglement between the two particles, we consider the so called "spin-inversion" transformation, which, for a $\frac{1}{2}$-spin particle, is the standard time reversal transformation, see Ref. [82]. If we consider a single qubit pure state $\mid \psi\rangle$, which is expressed in the standard computational basis, the spin-inversion transformation is defined as follows

$$\mid \tilde{\psi}\rangle = \hat{\sigma}_y \mid \psi^*\rangle, \tag{3.35}$$

where $\hat{\sigma}_y = \begin{pmatrix} 0 & -\imath \\ \imath & 0 \end{pmatrix}$ is the Pauli y-matrix, and $\mid \psi^*\rangle$ is the complex conjugate of $\mid \psi\rangle$. Since the state describing our system is a two-qubit pure state, we can neglect mixed states

and focus our attention on the definition of entanglement for pure states as described by equation (3.31). We can now introduce the definition of concurrence, see Ref. [80], as

$$C(\psi) = \mid \langle \psi \mid \tilde{\psi} \rangle \mid, \tag{3.36}$$

and the corresponding entanglement reads

$$E(\psi) = f(C(\psi)), \tag{3.37}$$

where the function $f(C(\psi))$ is given by

$$f(C(\psi)) = h(\frac{1+\sqrt{1-C(\psi)^2}}{2}), \tag{3.38}$$

$$h(x) = -x\log_2 x - (1-x)\log_2(1-x). \tag{3.39}$$

The function $f(C(\psi))$ increases monotonically from 0 to 1 as $C(\psi)$ ranges from 0 to 1, consequently we can consider the concurrence as a measure of the entanglement.
The state describing our two-qubit system can be written as a superposition of the standard two-qubit computational basis states, which is described by the relation

$$\mid \psi \rangle = c1 \mid 00\rangle + c2 \mid 01\rangle + c3 \mid 10\rangle + c4 \mid 11\rangle. \tag{3.40}$$

To evaluate the concurrence of this state, we start with the evaluation of the complex conjugate of the state as follows

$$\mid \psi^* \rangle = c1^* \mid 00\rangle + c2^* \mid 01\rangle + c3^* \mid 10\rangle + c4^* \mid 11\rangle. \tag{3.41}$$

Then we apply the $\hat{\sigma}_y$ transformation to the state (3.41), that is to say that we need to act on it with the following two-body operator

$$S = \hat{\sigma}_{y_1} \otimes \hat{\sigma}_{y_2}. \tag{3.42}$$

Recalling that the action of the $\hat{\sigma}_y$ matrix on the standard computational basis states is

$$\hat{\sigma}_y \mid 0\rangle = \begin{pmatrix} 0 & -\imath \\ \imath & 0 \end{pmatrix} \begin{pmatrix} 1 \\ 0 \end{pmatrix} = \imath \begin{pmatrix} 0 \\ 1 \end{pmatrix} \Rightarrow \hat{\sigma}_y \mid 0\rangle = \imath \mid 1\rangle, \tag{3.43}$$

$$\hat{\sigma}_y \mid 1\rangle = \begin{pmatrix} 0 & -\imath \\ \imath & 0 \end{pmatrix} \begin{pmatrix} 0 \\ 1 \end{pmatrix} = -\imath \begin{pmatrix} 1 \\ 0 \end{pmatrix} \Rightarrow \hat{\sigma}_y \mid 1\rangle = -\imath \mid 0\rangle, \tag{3.44}$$

we obtain

$$\begin{aligned} S \mid 00\rangle &= -\mid 11\rangle \\ S \mid 01\rangle &= \mid 10\rangle \\ S \mid 10\rangle &= \mid 01\rangle \\ S \mid 11\rangle &= -\mid 00\rangle. \end{aligned} \tag{3.45}$$

Finally, the spin-inversion transformation on the state $|\psi\rangle$ reads

$$|\tilde{\psi}\rangle = -c1^* \mid 11\rangle + c2^* \mid 10\rangle + c3^* \mid 01\rangle - c4^* \mid 00\rangle. \tag{3.46}$$

Therefore, by substituting states (3.40) and (3.46) in equation (3.36), we obtain the concurrence for our system, whose normalized value is given by the following equation

$$C(\psi) = \frac{2 \mid c2^*c3^* - c1^*c4^* \mid}{\mid c1 \mid^2 + \mid c3 \mid^2 + \mid c3 \mid^2 + \mid c4 \mid^2}. \tag{3.47}$$

The result obtained in equation (3.47) will be very useful to know the degree of entanglement of our system during the time evolution. When the concurrence related to a wavefunction reaches its maximum value, i.e. $C(\psi) = 1$, the state is maximally entangled. Therefore, we can expect that the concurrence of the wavefunction, which describes our system, reaches its maximum or, at least, a value close to it in a shorter time in comparison to the decoherence time T_2.

3.4 Entanglement of the realistic system

The goal of any quantum computational proposal is the entanglement of the state of the system under consideration. For this purpose, it is interesting to study the concurrence, see Sec. 3.3. The knowledge of the degree of entanglement allows us to know if the quantum state is good enough for carrying quantum information, i.e. if it is a reliable state to be considered in a quantum channel for performing eventual quantum operations. We have studied the degree of entanglement of our two-qubit state in the case of a time-independent Hamiltonian, Sec. (3.4.1), and in the case of a time-dependent Hamiltonian, Sec. (3.4.2), obtained by applying time-dependent oscillating magnetic fields, see [73, 74].

3.4.1 Entanglement: Time Independent Hamiltonian

Considering the dipole-dipole interaction Hamiltonian of Eq. (3.3), the added static magnetic field along the z-direction, see Sec. 3.1, and the gradient field amplitudes, see Sec. 3.2, the resulting Hamiltonian of the system is given by the following equation

$$\begin{aligned} H = \; & g(r)(\hat{\sigma}_{z_1} \otimes \hat{\sigma}_{z_2} + \hat{\sigma}_{y_1} \otimes \hat{\sigma}_{y_2} - 2\hat{\sigma}_{x_1} \otimes \hat{\sigma}_{x_2}) \\ & -\mu_B B_{0_1} \hat{\sigma}_{z_1} \otimes I_2 \\ & -\mu_B B_{0_2} I_1 \otimes \hat{\sigma}_{z_2}, \end{aligned} \tag{3.48}$$

where μ_B is the Bohr magneton, $B_{0_1} = (B_z + B_{g_1})$ and $B_{0_2} = (B_z + B_{g_2})$ are the static magnetic fields acting on spin 1 and spin 2 respectively. B_z is the static magnetic field directed along the z axis which acts on the whole system, B_{g_1} and B_{g_2} are the field gradient amplitudes. The Hamiltonian matrix form is given by the following matrix

$$H = \begin{pmatrix} g(r)+m_1 & 0 & 0 & -3g(r) \\ 0 & -g(r)+m_2 & -g(r) & 0 \\ 0 & -g(r) & -g(r)-m_2 & 0 \\ -3g(r) & 0 & 0 & g(r)-m_1 \end{pmatrix}, \tag{3.49}$$

where

$$m_1 = -\mu_B(B_{0_1} + B_{0_2}) \tag{3.50}$$

and

$$m_2 = -\mu_B(B_{0_1} - B_{0_2}), \tag{3.51}$$

are the static magnetic field terms.

In order to check the degree of entanglement of the system during the time evolution, we need to evaluate the concurrence of the two-qubit quantum state through Eq. (3.47). Therefore, we need to check the time evolution of the wave-function of the two-qubit system. According to Eq. (3.21), we can write the wave-function of the system at a general time t as follows

$$\mid \psi(t)\rangle = c_1(t) \mid 00\rangle + c_2(t) \mid 01\rangle + c_3(t) \mid 10\rangle + c_4(t) \mid 11\rangle, \tag{3.52}$$

where $c_i(t)$, $i = 1,..4$, are the complex coefficients related to each computational basis state, which satisfy the condition $\sum_{i=1}^{4} \mid c_i(t) \mid^2 = 1$.

In order to calculate the concurrence, we need to evaluate the time evolution of each complex coefficient $c_i(t)$, $i = 1,..4$ and arrange them as in Eq. (3.47).

To obtain coefficients $c_i(t)$, we need to solve the Schrödinger equation

$$\imath \frac{\partial}{\partial t} \mid \psi(t)\rangle = H \mid \psi(t)\rangle, \tag{3.53}$$

where the vawe-function $\mid \psi(t)\rangle$ is given by Eq. (3.52), and the Hamiltonian H by Eq. (3.48). From the Schrödinger equation we obtain the following differential equation sys-

tem

$$
\begin{aligned}
\dot{c}_1(t) &= -\imath[(g(r)+m_1)c_1(t) - 3g(r)c_4(t)];\\
\dot{c}_2(t) &= -\imath[(-g(r)+m_2)c_2(t) - g(r)c_3(t)];\\
\dot{c}_3(t) &= -\imath[-g(r)c_2(t) + (-g(r)-m_2)c_3(t)];\\
\dot{c}_4(t) &= -\imath[-3g(r)c_1(t) + (g(r)-m_1)c_4(t)],
\end{aligned}
\tag{3.54}
$$

whose solution gives coefficients $c_i(t)$. The system of Eq. (3.54), is composed of two pairs of coupled first order linear differential equations. It can be solved analytically by integrating the pair $\dot{c}1(t)$ and $\dot{c}4(t)$ and the pair $\dot{c}2(t)$ and $\dot{c}3(t)$. The analytical solution, which has been found by using a Mathematica programme, is the following:

(3.55)

$$
\begin{aligned}
c_1(t) = {} & \frac{1}{2\sqrt{-9g(r)^2-m_1^2}}((\imath e^{(-\imath g(r)-\sqrt{-9g(r)^2-m_1^2})t}m_1 - \imath e^{(-\imath g(r)+\sqrt{-9g(r)^2-m_1^2})t}m_1\\
&+e^{(-\imath g(r)-\sqrt{-9g(r)^2-m_1^2})t}\sqrt{-9g(r)^2-m_1^2}\\
&+e^{(-\imath g(r)+\sqrt{-9g(r)^2-m_1^2})t}\sqrt{-9g(r)^2-m_1^2})\alpha)\\
&-3\imath((e^{(-\imath g(r)-\sqrt{-9g(r)^2-m_1^2})t} - e^{(-\imath g(r)+\sqrt{-9g(r)^2-m_1^2})t})g(r)\beta)),\\
c_4(t) = {} & \frac{1}{(2\sqrt{-9g(r)^2-m_1^2})}((-3\imath(e^{(-\imath g(r)-\sqrt{-9g(r)^2-m_1^2})t}\\
&-e^{(-\imath g(r)+\sqrt{-9g(r)^2-m_1^2})t})g(r)\alpha)\\
&+(-\imath e^{(-\imath g(r)-\sqrt{-9g(r)^2-m_1^2})t}m_1 + \imath e^{(-\imath g(r)+\sqrt{-9g(r)^2-m_1^2})t}m_1\\
&+e^{(-\imath g(r)-\sqrt{-9g(r)^2-m_1^2})t}\sqrt{-9g(r)^2-m_1^2}\\
&+e^{(-\imath g(r)+\sqrt{-9g(r)^2-m_1^2})t}\sqrt{-9g(r)^2-m_1^2})\beta)),
\end{aligned}
$$

where α and β are constants of integration. In analogy, integrating $\dot{c}2(t)$and $\dot{c}3(t)$, their solution is

$$
\begin{aligned}
c_2(t) = {} & \frac{1}{2\sqrt{-g(r)^2-m_2^2}}((\imath e^{(\imath g(r)-\sqrt{-g(r)^2-m_2^2})t}m_2 - \imath e^{(\imath g(r)+\sqrt{-g(r)^2-m_2^2})t}m_2\\
&+e^{(\imath g(r)-\sqrt{-g(r)^2-m_2^2})t}\sqrt{-g(r)^2-m_2^2}\\
&+e^{(\imath g(r)+\sqrt{-g(r)^2-m_2^2})t}\sqrt{-g(r)^2-m_2^2})\alpha)\\
&-\imath((e^{(\imath g(r)-\sqrt{-g(r)^2-m_2^2})t} - e^{(\imath g(r)+\sqrt{-g(r)^2-m_2^2})t})g(r)\beta)),\\
c_3(t) = {} & \frac{1}{(2\sqrt{-g(r)^2-m_2^2})}((-\imath(e^{(\imath g(r)-\sqrt{-g(r)^2-m_2^2})t}\\
&-e^{(-\imath g(r)+\sqrt{-g(r)^2-m_2^2})t})g(r)\alpha)\\
&+(-\imath e^{(\imath g(r)-\sqrt{-g(r)^2-m_2^2})t}m_2 + \imath e^{(\imath g(r)+\sqrt{-g(r)^2-m1^2})t}m_2\\
&+e^{(\imath g(r)-\sqrt{-g(r)^2-m_2^2})t}\sqrt{-g(r)^2-m_2^2}\\
&+e^{(\imath g(r)+\sqrt{-g(r)^2-m_2^2})t}\sqrt{-g(r)^2-m_2^2})\beta)).
\end{aligned}
\tag{3.56}
$$

We have numerically solved the differential equation system (3.54) with the Mathematica programme `concurrence-time-independent.nb`, see App. C.1. The numerical values chosen for the physical quantities involved in the calculations are $r = 1.14nm$ for the distance between two buckyballs embedded on a silicon substrate, $B_z = 10 \times 10^{-2}T$ for the static magnetic field amplitude along the z -direction, $B_{g_1} = 6.08 \times 10^{-5}T$ and $B_{g_2} = -6.08 \times 10^{-5}T$ for the gradient field amplitudes on the left and right particle respectively.

The solution of the Schrödinger equation allows to calculate coefficients $c_i(t)$, which can be finally arranged as in Eq. (3.47). Therefore, we can plot the time-evolution of the concurrence $C(\psi)$ from $t = 0$ to $t = t_{max} = 9.1 \times 10^{-9}s$, where t_{max} is the time at which the concurrence reaches its maximum, see Fig. 3.5. From this picture we observe that the

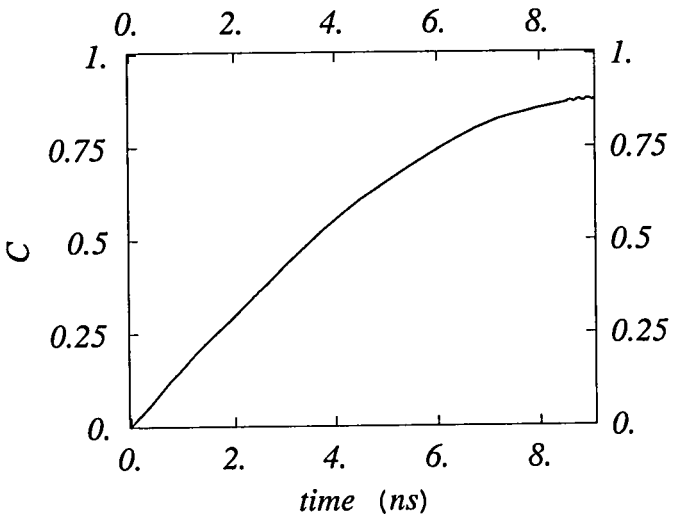

Figure 3.5: Time evolution of the concurrence, $C(\psi)$. In this case the two buckyballs, separated by a distance $r = 1.14nm$, are subjected to static magnetic fields directed along the z axis, whose amplitude is $B_{z_i} + B_{g_i}$, $i = 1, 2$. The numerical values chosen for these amplitudes are $B_z = 10 \times 10^{-2}T$, $B_{g_1} = 6.08 \times 10^{-5}T$ and $B_{g_2} = -6.08 \times 10^{-5}T$. The dipolar coupling constant is $g(r) = 5.505 \times 10^7 Hz$ and the spin precession frequencies are $\omega_{p_1} = 2\omega_{0_1} = 1.7599 \times 10^{10}s^{-1}$ and $\omega_{p_2} = 2\omega_{0_2} = 1.7577 \times 10^{10}s^{-1}$.

concurrence monotonically ranges from zero to its maximum $C(\psi(t_{max})) = 0.88$, which is reached at time $t = t_{max}$. Since the maximum concurrence differs from the ideal value $C = 1$ of a 12% error, allowing the time evolution for a time interval equal to t_{max}, the

system acquires a good degree of entanglement. Therefore, it can be considered as a good candidate for storing and carrying quantum information.

This result has been found for the chosen set of initial conditions $c_1 = 1/3$, $c_2 = \sqrt{7/2}/3$, $c_3 = 1/3$, $c_4 = \sqrt{7/2}/3$. However, we did many trials for different numerical values of the set $c_i(0)$, $i = 1,..4$. In all these cases, the concurrence shows a monotonically increasing behaviour in the time interval $[0, t_{max}]$and the resulting times t_{max} (at which $C(\psi)$ reaches its maximum) are all in the same range, which is of the order of $10^{-8}s$.

We need to comment on the particular choice that we made for the physical quantities involved in the calculations. The numerical value of the distance between the two buckyballs, r, is a fixed value which depends on the substrate where the buckyballs reside. Since we suppose that the buckyballs are embedded on a silicon substrate, the suggested distance is indeed $r = 1.14nm$, see [77]. The amplitude of the static magnetic field, B_z, has been found by considering the allowed experimental limits for its realization. The chosen value for this amplitude has been found by checking the response of the system, i.e. the concurrence after some trials. Therefore, we can say that t_{max}, the time which corresponds to the maximum value of concurrence depends on the distance between the two buckyballs and on the amplitude of the static magnetic field, but it is independent of the choice of the initial values $c_i(0)$, $i = 1,..4$.

If we compare t_{max} to the shortest decoherence time, $T_2 \simeq 0.25ms$, evaluating their ratio $\frac{T_2}{t_{max}} \simeq 2 \times 10^4$, we can deduce that it possible to generate entangled states and to eventually perform many manipulations on them (for example considering them as the starting state for two-qubit quantum gates) before the system relaxes.

It is convenient to investigate other system configurations, in order to check if it is possible to improve the concurrence. In the next Section, we will analyze the case of an additional magnetic field, which oscillates in time in the x-y plane.

3.4.2 Entanglement: Time Dependent Hamiltonian

In this Section, we apply to our system an additional time dependent magnetic field. To induce the transitions between the two Zeeman energy levels, we need to apply an oscillating magnetic field in the $x - y$ plane with angular frequency ω, equal to the spin resonance frequency.

In the case of a transverse linear oscillating magnetic field, the total applied mag-

netic field is given by

$$\vec{B}(t) = (B_l \cos\omega t, B_l \cos\omega t, (B_z + B_g)). \tag{3.57}$$

The Hamiltonian of the system reads

$$\begin{aligned} H &= g(r)(\sigma_{z_1} \otimes \sigma_{z_2} + \sigma_{y_1} \otimes \sigma_{y_2} - 2\sigma_{x_1} \otimes \sigma_{x_2}) \\ &-\mu_B B_{0_1} \sigma_{z_1} \otimes I_2 \\ &-\mu_B B_{0_2} I_1 \otimes \sigma_{z_2} \\ &-\mu_B B_{l_1}(\sigma_{x_1} \cos\omega_1 t + \sigma_{y_1} \cos\omega_1 t) \otimes I_2 \\ &+I_1 \otimes (-\mu_B B_{l_2}(\sigma_{x_2} \cos\omega_2 t + \sigma_{y_2} \cos\omega_2 t)), \end{aligned}$$

where ω_1 and ω_2 are the resonance frequencies of the left and right spin, respectively. From now on, as a shorthand we omit symbol $\otimes$ for indicating tensor products.

Knowing the total static magnetic field applied on each particle, we can evaluate the respective resonance frequencies through equation $\omega = \frac{2\mu_B B_z}{\hbar}$, which gives

$$\omega_1 = \frac{2\mu_B B_{0_1}}{\hbar} = 1.7599 \times 10^{10} Hz \tag{3.58}$$

and

$$\omega_2 = \frac{2\mu_B B_{0_2}}{\hbar} = 1.7577 \times 10^{10} Hz. \tag{3.59}$$

The Hamiltonian matrix form is given by

$$H = \begin{pmatrix} g(r) + m_1 & e_2(t) & e_1(t) & -3g(r) \\ d_2(t) & -g(r) + m_2 & -g(r) & e_1(t) \\ d_1(t) & -g(r) & -g(r) - m_2 & e_2(t) \\ -3g(r) & d_1(t) & d_2(t) & g(r) - m_1 \end{pmatrix}, \tag{3.60}$$

where

$$\begin{aligned} d_1(t) &= -\mu_B B_{l_1}(\cos\omega_1 t + \imath \cos\omega_1 t) \\ d_2(t) &= -\mu_B B_{1_2}(\cos\omega_2 t + \imath \cos\omega_2 t) \end{aligned} \tag{3.61}$$

and

$$\begin{aligned} e_1(t) &= -\mu_B B_{l_1}(\cos\omega_1 t - \imath \cos\omega_1 t) \\ e_2(t) &= -\mu_B B_{1_2}(\cos\omega_2 t - \imath \cos\omega_2 t). \end{aligned} \tag{3.62}$$

As in the time independent case, see Sec. 3.4.1, by solving the Schrödinger equation (3.53), where the Hamiltonian is given by Eq. (3.60), we obtain the four differential equation system

$$
\begin{aligned}
\dot{c}1(t) &= -\imath[g(r)c1(t) + e_2(t)c2(t) + e_1(t)c3(t) - 3g(r)c4(t)] \\
\dot{c}2(t) &= -\imath[d_2(t)c1(t) - g(r)c2(t) - g(r)c3(t) + e_1(t)c4(t)] \\
\dot{c}3(t) &= -\imath[d_1(t)c1(t) - g(r)c2(t) - g(r)c3(t) + e_2(t)c4(t)] \\
\dot{c}4(t) &= -\imath[-3g(r)c1(t) + d_1(t)c2(t) + d_2(t)c3(t) + g(r)c4(t)],
\end{aligned}
\tag{3.63}
$$

whose solution gives coefficients $c_i(t)$, $i = 1, ..4$, each of which is related to a computational basis state.

According to Eq. (3.47), we evaluated the concurrence related to the two-qubit system. In Fig. 3.6, it is represented the time evolution of the concurrence, $C(\psi(t))$ from

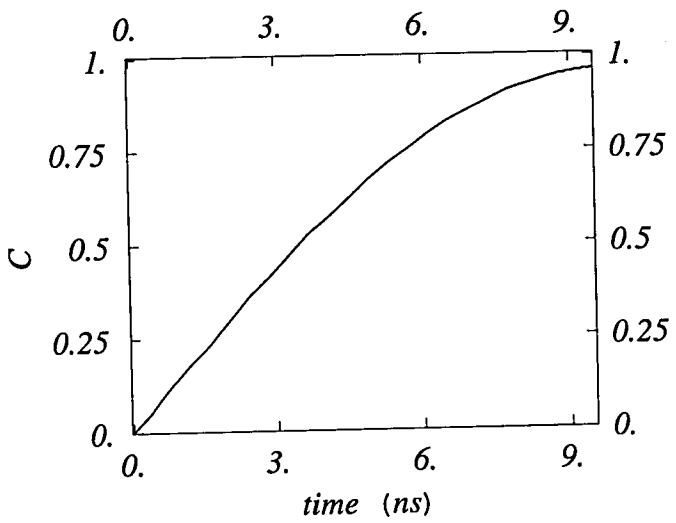

Figure 3.6: Time evolution of the concurrence, $C(\psi)$. In this case, the total magnetic field applied on each buckyball is $\vec{B}(t) = (B_{l_i}\cos\omega_i t, B_{l_i}\cos\omega_i t, B_0^i)$, $i = 1, 2$. The choice of the numerical values is $B_z = 10 \times 10^{-2}T$, $B_{g_1} = 6.08 \times 10^{-5}T$, $B_{g_2} = -6.08 \times 10^{-5}T$, $B_{l_1} = B_{l_2} = 5 \times 10^{-4}T$, $\omega_1 = 1.7599 \times 10^{10}Hz$ and $\omega_2 = 1.7577 \times 10^{10}Hz$.

$t = 0$ to $t = t_{max} = 9.8 \times 10^{-9}s$, which has been numerically evaluated with the Mathematica programme `concurrence-time-dependent.nb`, see App. C.2. It shows a monotonic behaviour and its maximum value, reached at time $t = t_{max}$, corresponds to

$C(\psi(t_{mac})) = 0.96$, which differs from the ideal value $C = 1$ of a 4% error. Therefore, it characterizes a highly entangled state.

Through the comparison between the value of the concurrence obtained in the time-dependent case, see Fig. 3.6, and the value obtained in the time-independent case, see Fig. 3.5, it can be seen that an additional linearly polarized oscillating field in the $x - y$ plane allows the system to be characterized by a better degree of concurrence.

In conclusion, the maximum value of concurrence is $C \simeq 0.88$ in the time independent case and $C \simeq 0.96$ in the time dependent one. Both values are acceptable because they are both related to a very high degree of entanglement for the state describing our two-qubit system. We can conclude that the best configuration for our system is the time dependent one, because it allows the two-qubit state to reach an high degree of entanglement described by the concurrence $C(\psi) \simeq 0.96$ in a very short time, $t_{max} = 9.8 \times 10^{-9} s$.

The possibility of obtaining highly entangled states in a time of the order of $10^{-8} s$, which is much shorter than the shortest decoherence time T_2, allows the use of these entangled states before the occurrence of relaxation processes. For example, they could be considered as input states of two-qubit quantum gates, or they could be used as elements for carrying information in quantum channels.

Chapter 4

Theoretical Realization of Quantum Gates

In this chapter we investigate our two-buckyball system from a purely theoretical point of view. In order to perform two qubit operations with a two-spin system, we borrow many ideas from NMR quantum computers, see [12, 22]. As in NMR quantum computers, our system is composed of two spins, but here, we are dealing with the electron spin of the particles. Single-qubit operations (spin rotations) can be performed using classical microwave pulses while two-qubit operations can be realized through the naturally existing exchange or dipolar interactions. In our two-spin system, the mutual interaction is dominated by the spin dipolar interaction, see discussion in Chap. 3. Therefore, under free evolution, the spin dipolar interaction allows to perform two-qubit gates.

When a sample of molecules exhibit paramagnetism as a result of unpaired electron spins, transitions between spin states can be induced by applying a magnetic field and then supplying electromagnetic energy, usually in the microwave range of frequencies. The resulting absorption spectra are described as Electron Spin Resonance (ESR) or Electron Paramagnetic Resonance (EPR). Therefore, when the frequency of the microwave field is equal to the precession frequency of the spin, i.e. they are in resonance, each spin can be controlled by means of ESR techniques. The range of frequencies of a microwave radiation is $\nu_m \simeq 1.6GHz - 30GHz$. Since the precession frequency of the spin is $\omega_0 = \mu_B B_0$, the microwave range of frequencies implies that the range, where the amplitude of the static magnetic field applied to the spin along the z axis should lie is $B_0 \simeq 0.05T - 1.1T$

4.1 Spin-Microwave Field Interaction: Single-Qubit gates

The state of a $\frac{1}{2}$-spin particle in a static magnetic field $\vec{B}_0$ along the z axis, described by the Hamiltonian (3.16), can be manipulated by applying a microwave field $\vec{B}_m = B_m(\cos(\omega_m t + \phi), -\sin(\omega_m t + \phi), 0)$, which rotates in the x-y plane at a frequency ω_m and is characterized by a phase ϕ and amplitude B_m. When the frequency of the applied microwave field is in resonance with the spin precession frequency, i.e. $\omega_m = 2\omega_0$, it is possible to perform rotation of the spin about the x-y plane. The Hamiltonian describing a single spin subjected to a microwave field $\vec{B}_m$ is analogous to the spin-static magnetic field Hamiltonian, Eq. (3.16), and is represented by the following formula

$$H_m = -\mu_B B_m[\cos(\omega_m t + \phi)\sigma_x - \sin(\omega_m t + \phi)\sigma_y], \tag{4.1}$$

where σ_x and σ_y are the x and y Pauli matrices, respectively. In Eq. (4.1) we observe that the minus sign in front of the sine term allows the MW field to evolve in the same sense of the spin evolution under H_0, Eq. (3.16). The total Hamiltonian of a $\frac{1}{2}$-spin particle subjected to both static and microwave fields is described by

$$\begin{aligned} H &= H_0 + H_m \\ &= -\mu_B B_0 \sigma_z - \mu_B B_m[\cos(\omega_m t + \phi)\sigma_x - \sin(\omega_m t + \phi)\sigma_y] \\ &= -\omega_0 \sigma_z - \omega_a[\cos(\omega_m t + \phi)\sigma_x - \sin(\omega_m t + \phi)\sigma_y], \end{aligned} \tag{4.2}$$

where $\omega_a = \mu_B B_m$. Hamiltonian (4.2) is described in the usual laboratory coordinate system. The motion of a single electron spin, described by (4.2), can be simplified by changing the coordinate system to a rotating frame. The rotating frame is a coordinate system which rotates about the z axis at a frequency ω_r, and is defined by the following transformation:

$$| \psi\rangle^{rot} = \exp[-\imath\omega_r t\sigma_z] \mid \psi\rangle. \tag{4.3}$$

By replacing the new definition of $| \psi\rangle$ in the Schrödinger equation

$$\imath\frac{d}{dt} \mid \psi\rangle = H \mid \psi\rangle, \tag{4.4}$$

with H given by Eq. (4.2), we obtain the Schrödinger equation for $| \psi\rangle^{rot}$:

$$\begin{aligned} \imath\tfrac{d}{dt} \mid \psi\rangle^{rot} &= -(\omega_0 - \omega_r)\sigma_z \\ &\quad -\omega_a[\cos[(\omega_m - 2\omega_r)t + \phi]\sigma_x \\ &\quad - \sin[(\omega_m - 2\omega_r)t + \phi]\sigma_y] \mid \psi\rangle^{rot}. \end{aligned} \tag{4.5}$$

We define

$$H^{rot} = -(\omega_0 - \omega_r)\sigma_z - \omega_a[\cos[(\omega_m - 2\omega_r)t + \phi]\sigma_x - \sin[(\omega_m - 2\omega_r)t + \phi]\sigma_y], \tag{4.6}$$

which is the Hamiltonian transformed in the rotating frame. The complete derivation of Eq. (4.5) is presented in A.1.

If we choose a frame rotating at a frequency $\omega_r = \omega_0$, Hamiltonian (4.6) simplifies as follows

$$H^{rot}_{\omega_0} = -\omega_a[\cos[(\omega_m - 2\omega_0)t + \phi]\sigma_x - \sin[(\omega_m - 2\omega_0)t + \phi]\sigma_y], \tag{4.7}$$

where the Zeeman term has been canceled and only the microwave field terms are left. We notice that a single-qubit rotation, Eq. (1.11), can be implemented in the rotating frame by using microwave pulses. If in Hamiltonian (4.7) a microwave field is applied at $\omega_m = 2\omega_0$, i.e. it is in *resonance* with the spin Larmor frequency, the Hamiltonian becomes time-independent and the spin time evolution operator is given by

$$U(t) = \exp[\imath\omega_a(\cos\phi\sigma_x - \sin\phi\sigma_y)t], \tag{4.8}$$

where time t represents the duration of the microwave pulse. Transformation $U(t)$ describes a rotation of an angle θ, proportional to $\omega_a t$, about an axis in the x-y plane which is determined by the phase ϕ. It is possible to vary with time both the amplitude B_m and the phase ϕ of a microwave field. On the other hand, the Larmor frequency depends on the amplitude of a static magnetic field, which cannot be varied with time. Therefore, Hamiltonian (4.7) can be considered as a *control Hamiltonian*, because it allows single-qubit rotations by controlling the microwave field amplitude and phase. For example, if we want to perform a $\frac{-\pi}{2}$-rotation about y, we need to choose $\phi = \frac{-\pi}{2}$, which gives

$$U(t) = \exp[\imath\omega_a\sigma_y t], \tag{4.9}$$

and we need to allow this evolution for a time $t = \frac{\pi}{4\omega_a} = \frac{\pi}{4\mu_B B_m}$, which finally gives

$$\exp[\imath\frac{\pi}{4}\sigma_y]. \tag{4.10}$$

From this we understand that the duration of time of an applied microwave field, required for performing a single-qubit rotation, depends on the inverse of the microwave field amplitude B_m. This example will be very useful to understand the realization of a single-qubit rotation when we solve the complete dynamics of the coupled two-spin system, see Chap. 5.

4.2 Two-Spin System

If we consider a system composed of two uncoupled spins, each one subjected to a different static magnetic field along the z axis, B_{0_1} for the first spin and B_{0_2} for the second one, and to a different microwave field which rotates in the x-y plane, $\vec{B}_{m_1} = B_{m_1}(\cos(\omega_{m_1}t+\phi), -(\sin(\omega_{m_1}t+\phi)), 0)$ and $\vec{B}_{m_2} = B_{m_2}(\cos(\omega_{m_2}t+\phi), -(\sin(\omega_{m_2}t+\phi)), 0)$, the Hamiltonian in the laboratory frame is the following

$$\begin{aligned} H_{US} &= -\omega_{0_1}\sigma_{z_1} - \omega_{0_2}\sigma_{z_2} \\ &-\omega_{a_1}[\cos(\omega_{m_1}t+\phi)\sigma_{x_1} - \sin(\omega_{m_1}t+\phi)\sigma_{y_1}] \\ &-\omega_{a_2}[\cos(\omega_{m_2}t+\phi)\sigma_{x_2} - \sin(\omega_{m_2}t+\phi)\sigma_{y_2}], \end{aligned} \tag{4.11}$$

where $\omega_{0_1} = \mu_B B_{0_1}$ and $\omega_{0_2} = \mu_B B_{0_2}$, $\omega_{a_1} = \mu_B B_{m_1}$ and $\omega_{a_2} = \mu_B B_{m_2}$ for the first and second spin respectively. In the rotating frame, defined by transformation 4.3, after having chosen $\omega_{r_1} = \omega_{0_1}$ and $\omega_{r_2} = \omega_{0_2}$ the Hamiltonian of two uncoupled spins reads as follows:

$$\begin{aligned} H_{US}^{rot} = &-\omega_{a_1}[\cos[(\omega_{m_1} - 2\omega_{0_1})t+\phi]\sigma_{x_1} - \sin[(\omega_{m_1} - 2\omega_{0_1})t+\phi]\sigma_{y_1}] \\ &-\omega_{a_2}[\cos[(\omega_{m_2} - 2\omega_{0_2})t+\phi]\sigma_{x_2} - \sin[(\omega_{m_2} - 2\omega_{0_2})t+\phi]\sigma_{y_2}], \end{aligned} \tag{4.12}$$

where for H_{US} the subscript means that this is the Uncoupled-Spins Hamiltonian.

4.2.1 Spin Mutual Interaction

In a system composed of two endohedral fullerene molecules, their mutual interaction is the spin dipole-dipole interaction, see Eq.(3.2). If we consider the case in which vector $\vec{n}$ is parallel to the z axis, the dipole-dipole Hamiltonian becomes

$$H_{DD} = g(r)(\sigma_{x_1}\sigma_{x_2} + \sigma_{y_1}\sigma_{y_2} - 2\sigma_{z_1}\sigma_{z_2}), \tag{4.13}$$

The matrix related to Hamiltonian (4.13) is the following

$$H_{DD} = \begin{pmatrix} -2g(r) & 0 & 0 & 0 \\ 0 & 2g(r) & 2g(r) & 0 \\ 0 & 2g(r) & 2g(r) & 0 \\ 0 & 0 & 0 & -2g(r) \end{pmatrix}, \tag{4.14}$$

whose eigenvalues and eigenvectors are

$$(4.15)\quad \delta_1 = 0 \rightarrow |\, l_1\rangle = \begin{pmatrix} 0 \\ -1 \\ 1 \\ 0 \end{pmatrix}; \quad \delta_2 = -2g(r) \rightarrow |\, l_2\rangle = \begin{pmatrix} 1 \\ 0 \\ 0 \\ 0 \end{pmatrix}$$

$$(4.16)\quad \delta_3 = -2g(r) \rightarrow |\, l_3\rangle = \begin{pmatrix} 0 \\ 0 \\ 0 \\ 1 \end{pmatrix}; \quad \delta_4 = 4g(r) \rightarrow |\, l_4\rangle = \begin{pmatrix} 0 \\ 1 \\ 1 \\ 0 \end{pmatrix}.$$

Whenever we consider two neighboring buckyballs, the mutual dipole-dipole interaction, Eq. (4.13), is always present. As described in Sec. (3.1), in order to encode the qubit in the spin, we need to apply a static magnetic field along the z axis on both particles. Therefore, in addition to the mutual spin dipolar interaction also the interaction between static magnetic fields along z and the spins, Eq. (3.16), is always present. The fundamental Hamiltonian describing a system composed of two buckyballs, each of which encode a qubit, is the following

$$(4.17)\quad H_f = H_{DD} + H_{0_1} + H_{0_2} = g(r)(\sigma_{x_1}\sigma_{x_2} + \sigma_{y_1}\sigma_{y_2} - 2\sigma_{z_1}\sigma_{z_2}) - \omega_{0_1}\sigma_{z_1} - \omega_{0_2}\sigma_{z_2},$$

where $H_{0_1} = -\omega_{0_1}\sigma_{z_1}$ and $H_{0_2} = -\omega_{0_2}\sigma_{z_2}$ describe the interaction of a static magnetic field along the z axis with the first and second qubit, respectively.

The matrix form of Hamiltonian (4.17) is given by

$$(4.18)\quad H_f = \begin{pmatrix} -2g(r) + m_1 & 0 & 0 & 0 \\ 0 & 2g(r) + m_2 & 2g(r) & 0 \\ 0 & 2g(r) & 2g(r) - m_2 & 0 \\ 0 & 0 & 0 & -2g(r) - m_1 \end{pmatrix},$$

where $m_1 = -\omega_{0_1} - \omega_{0_2}$ and $m_2 = -\omega_{0_1} + \omega_{0_2}$. The eigenvalues and eigenvectors of

matrix (4.18) are the following

$$\gamma_1 = -2g(r) + m_1 \rightarrow |\, n_1\rangle = \begin{pmatrix} 1 \\ 0 \\ 0 \\ 0 \end{pmatrix} \tag{4.19}$$

$$\gamma_2 = 2g(r) - \epsilon \rightarrow |\, n_2\rangle = \begin{pmatrix} 0 \\ \frac{m_2-\epsilon}{2g(r)} \\ 1 \\ 0 \end{pmatrix} \tag{4.20}$$

$$\gamma_3 = 2g(r) + \epsilon \rightarrow |\, n_3\rangle = \begin{pmatrix} 0 \\ \frac{m_2+\epsilon}{2g(r)} \\ 1 \\ 0 \end{pmatrix} \tag{4.21}$$

$$\gamma_4 = -2g(r) - m_1 \rightarrow |\, n_4\rangle = \begin{pmatrix} 0 \\ 0 \\ 0 \\ 1 \end{pmatrix} \tag{4.22}$$

where $\epsilon = \sqrt{4g(r)^2 + (m_2)^2}$. Fig. (4.1) shows the energy levels that are allowed for a system of two buckyballs subjected to static magnetic fields along the z axis.

4.2.2 Complete Hamiltonian

Considering Eq. (4.11) and Eq. (4.13), in the laboratory frame the complete Hamiltonian for a system composed of two spins, which interact via the dipole-dipole interaction and subjected to static and microwave fields, is given by

$$\begin{aligned} H &= H_{US} + H_{DD} \\ &= -\omega_{0_1}\sigma_{z_1} - \omega_{0_2}\sigma_{z_2} \\ &-\omega_{a_1}[\cos(\omega_{m_1}t + \phi)\sigma_{x_1} - \sin(\omega_{m_1}t + \phi)\sigma_{y_1}] \\ &-\omega_{a_2}[\cos(\omega_{m_2}t + \phi)\sigma_{x_2} - \sin(\omega_{m_2}t + \phi)\sigma_{y_2}] \\ &+g(r)(\sigma_{x_1}\sigma_{x_2} + \sigma_{y_1}\sigma_{y_2} - 2\sigma_{z_1}\sigma_{z_2}). \end{aligned} \tag{4.23}$$

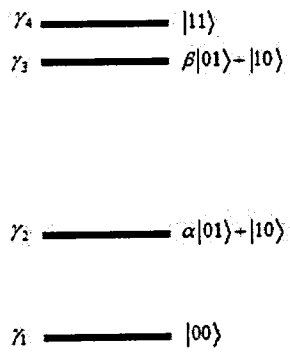

Figure 4.1: Energy-level diagram (in $\hbar$ units) for two spins coupled by Hamiltonian (4.17). The dipole-dipole interaction is the mutual interaction between the two spin, each of which is subjected to a static magnetic field along z.

To transform Hamiltonian (4.23) to the rotating frame, where we have already chosen $\omega_{r_1} = \omega_{0_1}$ and $\omega_{r_2} = \omega_{0_2}$, we need to perform the following change of coordinate on Hamiltonian H_{DD} (4.13)

$$\exp[-i\omega_{0_1} t\sigma_{z_1}] \exp[-i\omega_{0_2} t\sigma_{z_2}] H_{DD} \exp[i\omega_{0_1} t\sigma_{z_1}] \exp[i\omega_{0_2} t\sigma_{z_2}], \tag{4.24}$$

which describes the change of coordinate to the rotating frame for both particles. Therefore, the dipole-dipole Hamiltonian in the rotating frame system is the given by following expression

$$H_{DD}^{rot} = g(r)(\cos[(2\omega_{0_1} - 2\omega_{0_2})t](\sigma_{x_1}\sigma_{x_2} + \sigma_{y_1}\sigma_{y_2}) - 2\sigma_{z_1}\sigma_{z_2}), \tag{4.25}$$

whose complete derivation can be found in A.2.

Finally, we can write the total Hamiltonian of our two-spin system in a frame rotating at ω_0 as

$$\begin{aligned} H(t) &= H_{tot}^{rot} = H_{DD}^{rot} + H_{US}^{rot} \\ &= g(r)(\cos[(2\omega_{0_1} - 2\omega_{0_2})t](\sigma_{x_1}\sigma_{x_2} + \sigma_{y_1}\sigma_{y_2}) - 2\sigma_{z_1}\sigma_{z_2}) \\ &-\omega_{a_1}[\cos[(\omega_{m_1} - 2\omega_{0_1})t + \phi]\sigma_{x_1} - \sin[(\omega_{m_1} - 2\omega_{0_1})t + \phi]\sigma_{y_1}] \\ &-\omega_{a_2}[\cos[(\omega_{m_2} - 2\omega_{0_2})t + \phi]\sigma_{x_2} - \sin[(\omega_{m_2} - 2\omega_{0_2})t + \phi]\sigma_{y_2}]. \end{aligned} \tag{4.26}$$

4.3 Quantum Computation: realization of a π-gate

To perform quantum computations we need to be able to perform unitary transformations. In Eq. (4.8) we showed that in the case of a system composed of only one qubit, it is allowed to perform single-qubit gates by controlling the applied microwave field. This idea can be extended to a two-qubit system. Allowing the system to transform under single-qubit rotations, arbitrary unitary transformations can be performed on the two-qubit system.

We recall that the time evolution operator related to a time independent Hamiltonian H is simply (in $\hbar$ units)

$$U(t) = \exp[-\imath Ht]. \tag{4.27}$$

Otherwise, if the system is described by a time dependent Hamiltonian $H(t)$, the associated time-evolution operator is given by (in $\hbar$ units)

$$U(t, t_0) = T \exp[-\imath \int_{t_0}^{t} H(t\prime)dt\prime], \tag{4.28}$$

where T is the time ordering operator.

In order to easily perform unitary transformations we need to write the time evolution operator as in Eq. (4.27). To do this we need to cancel the time dependence in Eq. (4.25). Therefore, we assume $\omega_{0_1} = \omega_{0_2}$, i.e. the resonance frequencies of the two spins are equal. This allows the dipole-dipole Hamiltonian in the rotating system, Eq.(4.25), to simplify into the Hamiltonian in the laboratory system, Eq. (4.13).

Consider the two-spin Hamiltonian in the rotating frame, Eq. (4.26), with the choices $\omega_{0_1} = \omega_{0_2}$ and $\omega_{m_1} = 2\omega_{0_1}$ and $\omega_{m_2} = 2\omega_{0_2}$. These choices allow the Hamiltonian to be time-independent and its related time-evolution operator can be easily written as

$$U(t) = \exp[-\imath Ht]. \tag{4.29}$$

We assume that when a large microwave field is applied, we can make the following approximation

$$\exp[-\imath Ht] = \exp[-\imath(H_{DD} + H_{US})t] \simeq \exp[-\imath H_{US}t], \tag{4.30}$$

where H_{DD} is now given by Eq. (4.13), and H_{US} by Eq. (4.12). This approximation prescribes that the microwave field-spin interaction terms dominate the time evolution,

i.e. when a microwave is applied, H_{DD} becomes a small perturbation and its effect can be neglected. Therefore, single-qubit rotations can be performed because the coupling effect of the dipolar interaction is negligible. This approximation is true in the case of a single spin. Indeed, considering Eq. (4.8) at the resonance $\omega_m = 2\omega_0$, the B_0 contribution becomes negligible, and a small change in B_m can cause a considerable change in the state, corresponding to rotations about an axis in the x-y plane. Approximation (4.30) allows us to perform single-qubit operations on our two-qubit system.

Being able to perform single-qubit transformations on our spins, we can make use of a technique known as *refocusing*, which allows the removal of the off-diagonal coupling terms of H_{DD}, Eq. (4.13). The sequence of unitary transformations which allow the refocusing of H_{DD} is given by

$$\begin{aligned} U(t) &= \exp[-\imath H_{DD} t] \exp[-\imath \tfrac{\pi}{2}\sigma_{z_2}] \exp[-\imath H_{DD} t] \exp[\imath \tfrac{\pi}{2}\sigma_{z_2}] \\ &= U_b(t) \exp[-\imath \tfrac{\pi}{2}\sigma_{z_2}] U_a(t) \exp[\imath \tfrac{\pi}{2}\sigma_{z_2}] \\ &= \exp[\imath 4g(r)\sigma_{z_1}\sigma_{z_2} t], \end{aligned} \tag{4.31}$$

whose matrix form is

$$U(t) = \begin{pmatrix} e^{\imath 4g(r)t} & 0 & 0 & 0) \\ 0 & e^{-\imath 4g(r)t} & 0 & 0 \\ 0 & 0 & e^{-\imath 4g(r)t} & 0 \\ 0 & 0 & 0 & e^{\imath 4g(r)t} \end{pmatrix}, \tag{4.32}$$

where $\exp[-\imath \frac{\pi}{2}\sigma_{z_2}]$ and $\exp[\imath \frac{\pi}{2}\sigma_{z_2}]$ correspond respectively to a π and $-\pi$ rotation about the z axis of the second spin. $U_a(t)$ and $U_b(t)$ represent the time evolution when the system is allowed to evolve in time under the action of static magnetic fields along the z axis and the dipole-dipole interaction. Since the dipole-dipole interaction couples the two spins, transformations $U_a(t)$ and $U_b(t)$ can be interpreted as two-qubit operations. Fig. (4.2) shows the scheme of the gate-circuit represented by the sequence of transformations which define $U(t)$ in Eq. (4.31). The proof of (4.31) is presented in A.3.

Matrix (4.32) is diagonal and we can compare it to the definition of a phase-gate, see Sec. 1.3.2. From Eq. (4.32), by summing the phases of each term of matrix (4.32) as prescribed by Eq. (1.51), we can evaluate phase ϑ. In this case, we obtain $\vartheta = 16g(r)t$. By imposing the condition $\vartheta = \pi$, the π-gate is performed (up to $\frac{\pi}{2}$ rotation of both spins about the z axis and up to a global phase) by allowing evolution $U(t)$ for a time $t = \frac{\pi}{16g(r)}$, i.e.

$$\vartheta = 16g(r)t = \pi \quad \Rightarrow \quad t = \frac{\pi}{16g(r)}. \tag{4.33}$$

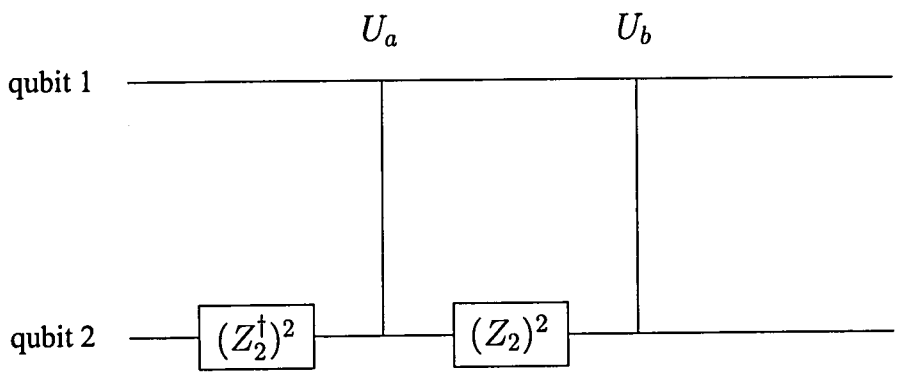

Figure 4.2: Schematic representation of the gate-circuit corresponding to the sequence of transformation in (4.31). Transformations $(Z_2^\dagger)^2 = \exp[\imath\frac{\pi}{2}\sigma_{z_2}]$ and $(Z_2)^2 = \exp[-\imath\frac{\pi}{2}\sigma_{z_2}]$ are respectively a $-\pi$ and a π rotation of the second qubit about the z axis. $U_a(t)$ and $U_b(t)$ represent the time evolution of the system under the action of only the dipole-dipole interaction, and they can be described as two-qubit operations.

Allowing the system to evolve for a time $t = \frac{\pi}{16g(r)}$, the output time-evolution matrix naturally realizes a $\frac{\pi}{4}$-phase-gate, whose expression is given by

$$U_{PG} = U(t = \frac{\pi}{16g(r)}) = \begin{pmatrix} e^{\imath\frac{\pi}{4}} & 0 & 0 & 0) \\ 0 & e^{-\imath\frac{\pi}{4}} & 0 & 0 \\ 0 & 0 & e^{-\imath\frac{\pi}{4}} & 0 \\ 0 & 0 & 0 & e^{\imath\frac{\pi}{4}} \end{pmatrix}, \tag{4.34}$$

where the explicit numerical values for the exponentials are $\exp[\imath\frac{\pi}{4}] = 0.707107 + 0.707107\imath$ and $\exp[-\imath\frac{\pi}{4}] = 0.707107 - 0.707107\imath$. Therefore, if we allow evolution $U(t)$, Eq. (4.32), to evolve for a time $t = \frac{\pi}{16g(r)}$, it gives a $\frac{\pi}{4}$-phase-gate, which allows us to achieve a π-gate, up to a $\frac{\pi}{2}$ rotation of each qubit about the z axis and up to an overall phase, by combining the phases of each output state as in Eq. (1.51).

Alternatively, if after the refocusing, Eq. (4.31), we consider a $\frac{\pi}{2}$- rotation about the z axis of both qubits, we can exactly perform a π-gate without summing the phases as in

(1.51). This set of transformations is accomplished through the following expression

$$
\begin{aligned}
G_\pi &= \sqrt{\imath}\exp[-\imath\tfrac{\pi}{4}\sigma_{z_1}]\exp[-\imath\tfrac{\pi}{4}\sigma_{z_2}]U(t=\tfrac{\pi}{16g(r)}) \\
&= \begin{pmatrix} 1 & 0 & 0 & 0 \\ 0 & 1 & 0 & 0 \\ 0 & 0 & 1 & 0 \\ 0 & 0 & 0 & -1 \end{pmatrix}.
\end{aligned} \tag{4.35}
$$

The circuit representing the set of transformation of Eq. (4.35) is shown in Fig. (4.3).

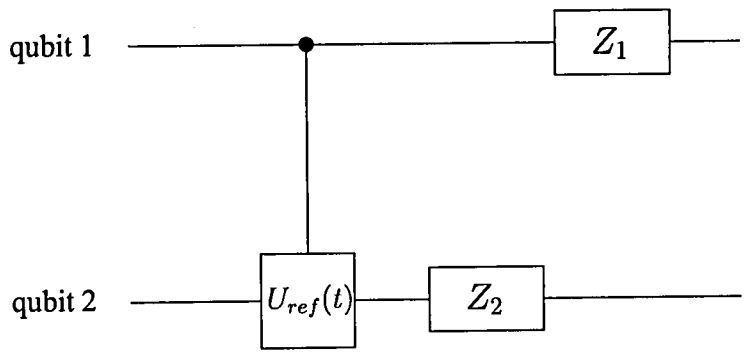

Figure 4.3: Schematic representation of the gate-circuit for the realization of a π-gate, which corresponds to the sequence of transformation in (4.35). $U_{ref}(t)$ represents the sequence of single and two-qubit operations which define the refocusing, Eq. (4.31). Transformations $Z_2 = \exp[-\imath\frac{\pi}{4}\sigma_{z_2}]$ and $Z_1 = \exp[-\imath\frac{\pi}{4}\sigma_{z_1}]$ are $\frac{\pi}{2}$-rotations about the z axis on the second and first qubit, respectively.

In equation (4.35), $\sqrt{\imath} = \exp[\imath\frac{\pi}{4}]$ is an overall phase, which is irrelevant, and

$$
\exp[-\imath\frac{\pi}{4}\sigma_{z_1}] = \cos\frac{\pi}{4} - \imath\sin\frac{\pi}{4}\sigma_{z_1} = \frac{1}{\sqrt{2}}\begin{pmatrix} 1-\imath & 0 \\ 0 & 1+\imath \end{pmatrix}_1, \tag{4.36}
$$

is a $\frac{\pi}{2}$ rotation about the z axis on the first qubit (denoted by footer 1), and analogously

$$
\exp[-\imath\frac{\pi}{4}\sigma_{z_2}] = \frac{1}{\sqrt{2}}\begin{pmatrix} 1-\imath & 0 \\ 0 & 1+\imath \end{pmatrix}_2, \tag{4.37}
$$

is a $\frac{\pi}{2}$ rotation about z on the second qubit (footer 2).

Since

$$\exp[-\imath\frac{\pi}{4}\sigma_{z_1}]\exp[-\imath\frac{\pi}{4}\sigma_{z_2}] = \begin{pmatrix} -\imath & 0 & 0 & 0 \\ 0 & 1 & 0 & 0 \\ 0 & 0 & 1 & 0 \\ 0 & 0 & 0 & \imath \end{pmatrix}, \tag{4.38}$$

and

$$U(t = \frac{\pi}{16g(r)}) = \begin{pmatrix} \frac{1+\imath}{\sqrt{2}} & 0 & 0 & 0 \\ 0 & \frac{1-\imath}{\sqrt{2}} & 0 & 0 \\ 0 & 0 & \frac{1-\imath}{\sqrt{2}} & 0 \\ 0 & 0 & 0 & \frac{1+\imath}{\sqrt{2}} \end{pmatrix}, \tag{4.39}$$

thus the matrix products in (4.35) are explicitly given by the following expression

$$\begin{aligned} G_\pi &= \exp[\imath\tfrac{\pi}{4}] \begin{pmatrix} -\imath & 0 & 0 & 0 \\ 0 & 1 & 0 & 0 \\ 0 & 0 & 1 & 0 \\ 0 & 0 & 0 & \imath \end{pmatrix} \begin{pmatrix} \frac{1+\imath}{\sqrt{2}} & 0 & 0 & 0 \\ 0 & \frac{1-\imath}{\sqrt{2}} & 0 & 0 \\ 0 & 0 & \frac{1-\imath}{\sqrt{2}} & 0 \\ 0 & 0 & 0 & \frac{1+\imath}{\sqrt{2}} \end{pmatrix} \\ &= \exp[\imath\tfrac{\pi}{4}]\tfrac{1}{\sqrt{2}} \begin{pmatrix} 1-\imath & 0 & 0 & 0 \\ 0 & 1-\imath & 0 & 0 \\ 0 & 0 & 1-\imath & 0 \\ 0 & 0 & 0 & -(1-\imath) \end{pmatrix} \\ &= \exp[\imath\tfrac{\pi}{4}] \underbrace{\frac{1}{\sqrt{2}}(1-\imath)}_{=\exp[-\imath\frac{\pi}{4}]} \begin{pmatrix} 1 & 0 & 0 & 0 \\ 0 & 1 & 0 & 0 \\ 0 & 0 & 1 & 0 \\ 0 & 0 & 0 & -1 \end{pmatrix} \\ &= \begin{pmatrix} 1 & 0 & 0 & 0 \\ 0 & 1 & 0 & 0 \\ 0 & 0 & 1 & 0 \\ 0 & 0 & 0 & -1 \end{pmatrix}. \end{aligned} \tag{4.40}$$

Finally, we found that the theoretical procedure of refocusing allows the realization of a π-gate. The refocusing of the dipole-dipole Hamiltonian has been performed by assuming

two approximations. We will need to check if in the realistic system treated in Chap. 5 these assumptions are satisfied.

4.4 Quantum Computation: realization of a $CNOT$-gate

As described in Sec. 1.3, the $CNOT$-gate is the universal two-qubit quantum gate, through which along with single-qubit rotations, any two-qubit quantum gate can be built. Once a two-qubit π-gate is performed, a $CNOT$-gate can be accomplished by performing single-qubit operation in addition to a π-gate. The sequence of single-qubit operations involved in the realization of a $CNOT$-gate can be single qubit Hadamard gates, see Eq. (1.43), [12]. Alternatively, following [22], the sequence of transformations which can be adopted to perform a $CNOT$-gate is given by

$$CNOT = \imath \exp[-\imath\frac{\pi}{2}\sigma_{z_1}] \exp[\imath\frac{\pi}{4}\sigma_{y_2}] G_\pi \exp[-\imath\frac{\pi}{4}\sigma_{y_2}], \tag{4.41}$$

which differs from a π-gate by a π rotation about the z axis of the first qubit (control qubit), represented by $\exp[-\imath\frac{\pi}{2}\sigma_{z_1}]$, and by a basis change of the second qubit (target qubit), represented by transformation $\exp[\imath\frac{\pi}{4}\sigma_{y_2}]G_\pi \exp[-\imath\frac{\pi}{4}\sigma_{y_2}]$. The schematic circuit which represents the sequence of transformations for the realization of a $CNOT$-gate, Eq. (4.41), is shown in Fig. (4.4).

Substituting the definition of G_π (given by Eq. (4.35)) in Eq. (4.41), we obtain the following expression

$$\begin{aligned} CNOT = \; & \imath \exp[-\imath\tfrac{\pi}{2}\sigma_{z_1}] \exp[\imath\tfrac{\pi}{4}\sigma_{y_2}] \\ & \sqrt{\imath} \exp[-\imath\tfrac{\pi}{4}\sigma_{z_1}] \exp[-\imath\tfrac{\pi}{4}\sigma_{z_2}] U(t = \tfrac{\pi}{16g(r)}) \\ & \exp[-\imath\tfrac{\pi}{4}\sigma_{y_2}] \\ = \; & \exp[\imath\tfrac{3\pi}{4}] \exp[-\imath\tfrac{3\pi}{4}\sigma_{z_1}] \exp[-\imath\tfrac{\pi}{4}\sigma_{z_2}] \exp[\imath\tfrac{\pi}{4}\sigma_{x_2}] \\ & U(t = \tfrac{\pi}{16g(r)}) \\ & \exp[-\imath\tfrac{\pi}{4}\sigma_{y_2}] \\ = \; & \begin{pmatrix} 1 & 0 & 0 & 0 \\ 0 & 1 & 0 & 0 \\ 0 & 0 & 0 & 1 \\ 0 & 0 & 1 & 0 \end{pmatrix}. \end{aligned} \tag{4.42}$$

The sequence of calculations involved in Eq. (4.42) is presented in Appendix A.4.

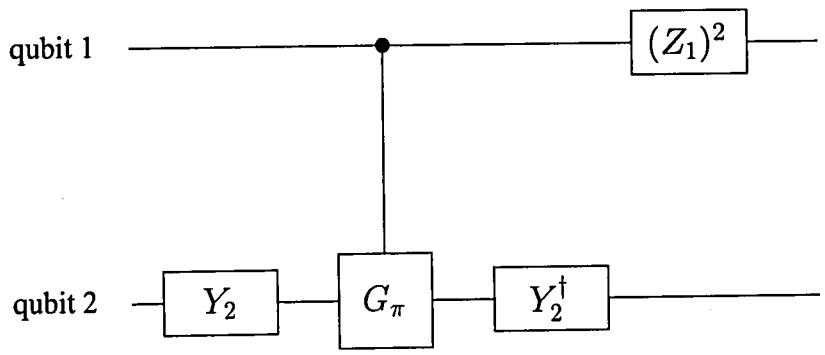

Figure 4.4: Schematic representation of the gate-circuit for the realization of a $CNOT$-gate, which corresponds to the sequence of transformation in (4.41). G_π realizes a π-gate. Transformation $(Z_1)^2 = \exp[-\imath\frac{\pi}{2}\sigma_{z_1}]$ is a π rotation about the z axis of the first qubit. Transformations $Y_2 = \exp[-\imath\frac{\pi}{4}\sigma_{y_2}]$ and $Y_2^\dagger = \exp[\imath\frac{\pi}{4}\sigma_{y_2}]$ are respectively a $\frac{\pi}{2}$ and a $-\frac{\pi}{2}$ rotations about the y axis of the second qubit.

In this chapter we have presented a theoretical model which shows a way of performing quantum gates. In the next chapter we apply this theory to a realistic system composed of two interacting endohedral fullerene molecules subjected to external microwave fields. Through the study of the dynamics of the realistic system, which requires the solution of Schrödinger equations, we present how it could be possible to perform single-qubit rotations and two-qubit operations. As a proof of the reliability of these transformations with respect to their theoretical definition, we present a study of the fidelity of the achievable two-qubit operations.

Chapter 5

Realistic Dynamics

In this chapter we investigate the possibility of realization of single-qubit and two-qubit gates by considering the realistic dynamics of a two-buckyball system. In Chapter 4 we presented a theoretical model for the implementation of single-qubit and two-qubit gates. This theory is based on two approximations, i.e. that when we apply a sufficiently large microwave field we can neglect the dipolar spin interaction, see Eq. (4.30), and that the resonance frequencies of the two particles are equal, i.e. $\omega_{0_1} = \omega_{0_2}$, in order to have a time-independent Hamiltonian. In the actual context, we cannot take into account these two assumptions because they are generally not satisfied in a realistic system. Therefore, we will perform our study by considering the complete Hamiltonian of the two-qubit system given by Eq. (4.26), which well describes a realistic situation. However, after having studied the dynamics of the realistic system, we will check if in this case the two assumptions are satisfied, see Secs. 5.6-5.7 and the comments on matrices (5.31), (5.43) and (5.50).

For performing quantum gates, we provide sets of transformations which are based on the theoretical model of quantum-gates presented in Chap. 4. The transformations in this chapter are *intended* to reproduce a $\frac{\pi}{4}$-phase gate (Eq. (4.34)), a π-gate (Eq. (1.42)) and a $CNOT$-gate (Eq. (1.31)).

Since the Hamiltonian of the system is time dependent, we cannot provide an analytical solution of its time evolution. Therefore, we have to solve the Schrödinger equation

$$\imath \frac{d}{dt} \mid \psi \rangle^{rot} = H(t) \mid \psi \rangle^{rot}, \tag{5.1}$$

where the wave-function $\mid \psi\rangle^{rot}$ can be expanded over the computational basis as

$$\mid \psi\rangle^{rot} = c_1(t) \mid 00\rangle + c_2(t) \mid 01\rangle + c_3(t) \mid 10\rangle + c_4(t) \mid 11\rangle. \tag{5.2}$$

Notice that the Schrödinger equation is a system of four differential equations, one for each coefficient $c_i(t)$, $i = 1, .., 4$.

The numerical results of the Schrödinger equation will be compared to the theoretically predicted outcomes. From this comparison and from the study of the gate fidelity, see Sec. 5.4, we will show the agreement between the scheme for reproducing quantum-gates through a realistic system and the theoretical predictions.

5.1 Single-Qubit Rotations

In order to perform quantum-gates, we need to refocus the Hamiltonian as prescribed in Eq. (4.31). The refocusing procedure requires to perform single-qubit rotations about the z axis. These transformations can be realized by applying microwave fields on the system, whose action on uncoupled spins is described by Hamiltonian H_{US}^{rot}, see Eq. (4.12). The terms contained in H_{US}^{rot} are proportional to $\sigma_{x_{1,2}}$ and $\sigma_{y_{1,2}}$. Therefore, it is convenient to express a rotation about the z axis in terms of rotations about x and y axes. From Bloch's theorem, see Eq. (1.27), a single-spin θ-rotation about the z axis can be decomposed in terms of rotation about the x and y axes in the following way:

$$\exp[-\imath\frac{\theta}{2}\sigma_z] = \exp[-\imath\frac{\pi}{4}\sigma_y]\exp[\imath\frac{\theta}{2}\sigma_x]\exp[\imath\frac{\pi}{4}\sigma_y]. \tag{5.3}$$

For example, a single-spin π-rotation about the z axis is given by

$$\exp[-\imath\frac{\pi}{2}\sigma_z] = \exp[-\imath\frac{\pi}{4}\sigma_y]\exp[\imath\frac{\pi}{2}\sigma_x]\exp[\imath\frac{\pi}{4}\sigma_y]. \tag{5.4}$$

The scheme which represents the realization of a π-rotation about the z axis as a circuit composed of rotations about the x and y axes, Eq. (5.4), is shown in Fig. (5.1).

If we want to perform rotations on the second qubit, we can *switch off* the interaction between the microwave field and the first qubit. Therefore, in Eq. (4.26) we take $B_{m_1} = 0$, which implies $\omega_{a_1} = 0$. From an experimental point of view, the interaction between the microwave field and the first qubit can be neglected if the microwave pulse, whose frequency is in resonance with the precession frequency of the second qubit, i.e. $\omega_{m_2} = 2\omega_{0_2}$, is characterized by a very tight spectral bandwidth. This allows the second qubit to be rotated and leaves the first qubit unaltered, see the discussion in Sec. 5.7.

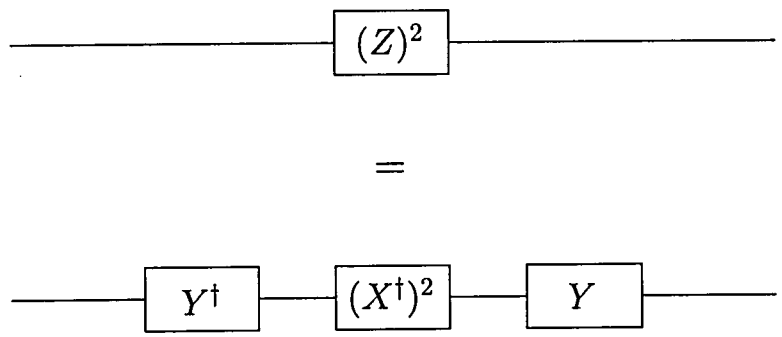

Figure 5.1: In the upper line $(Z)^2 = \exp[-\imath\frac{\pi}{2}\sigma_z]$ represents a π-rotation about the z axis. In the lower line it is shown the sequence of rotations about the x and y axis, which corresponds to $\exp[-\imath\frac{\pi}{2}\sigma_z]$. Transformation $Y^\dagger = \exp[\imath\frac{\pi}{4}\sigma_y]$ represents a $\frac{-\pi}{2}$-rotation about the y axis, $Y = \exp[-\imath\frac{\pi}{4}\sigma_y]$ is a $\frac{\pi}{2}$-rotation about the y axis, and $(X^\dagger)^2 = \exp[\imath\frac{\pi}{2}\sigma_x]$ is a $-\pi$-rotation about the x axis.

Therefore, the Hamiltonian to be inserted in the Schrödinger equation, whose solution provides the time evolution matrix intended to reproduce a rotation of the second qubit, is the following

$$\begin{aligned} H_{SQR2}(t) &= g(r)(\cos[(2\omega_{0_1} - 2\omega_{0_2})t](\sigma_{x_1}\sigma_{x_2} + \sigma_{y_1}\sigma_{y_2}) - 2\sigma_{z_1}\sigma_{z_2}) \\ &\quad -\omega_{a_2}[\cos[(\omega_{m_2} - 2\omega_{0_2})t + \phi]\sigma_{x_2} - \sin[(\omega_{m_2} - 2\omega_{0_2})t + \phi]\sigma_{y_2}], \end{aligned} \tag{5.5}$$

where the footer $SQR2$ means single-qubit rotation of the second qubit. As shown in Eq. (4.8), the microwave field has to be in resonance with the spin precession frequency, i.e. $\omega_{m_2} = 2\omega_{0_2}$. Therefore, equation (5.5) simplifies into

$$\begin{aligned} H^{res}_{SQR2}(t) &= g(r)(\cos[(2\omega_{0_1} - 2\omega_{0_2})t](\sigma_{x_1}\sigma_{x_2} + \sigma_{y_1}\sigma_{y_2}) - 2\sigma_{z_1}\sigma_{z_2}) \\ &\quad -\omega_{a_2}[\cos(\phi)\sigma_{x_2} - \sin(\phi)\sigma_{y_2}], \end{aligned} \tag{5.6}$$

where B_{m_2}, contained in $\omega_{a_2} = \mu_B B_{m_2}$, and ϕ are the only parameters that we can control

in order to perform single qubit rotations. Its matrix form is given by

$$H^{res}_{SQR2}(t) = \begin{pmatrix} -2g(r) & -\omega_{a_2} f & 0 & 0) \\ -\omega_{a_2} f^* & 2g(r) & 2g(r)l(t) & 0 \\ 0 & 2g(r)l(t) & 2g(r) & -\omega_{a_2} f \\ 0 & 0 & -\omega_{a_2} f^* & -2g(r) \end{pmatrix}, \tag{5.7}$$

where $l(t) = \cos[(2\omega_{0_1} - 2\omega_{0_2})t]$, $f = \cos(\phi) + \imath \sin(\phi)$ and f^* is its complex conjugate.

If we want to perform a single-qubit rotation on the first particle, we can *switch off* the interaction between the microwave field and the second particle by choosing $B_{m_2} = 0$ in Eq. (4.26). With this choice, we obtain the Hamiltonian to be considered in the Schrödinger equation for the reproduction of a rotation on the first qubit

$$\begin{aligned} H_{SQR1}(t) &= g(r)(\cos[(2\omega_{0_1} - 2\omega_{0_2})t](\sigma_{x_1}\sigma_{x_2} + \sigma_{y_1}\sigma_{y_2}) - 2\sigma_{z_1}\sigma_{z_2}) \\ &\quad -\omega_{a_1}[\cos[(\omega_{m_1} - 2\omega_{0_1})t + \phi]\sigma_{x_1} - \sin[(\omega_{m_1} - 2\omega_{0_1})t + \phi]\sigma_{y_1}], \end{aligned} \tag{5.8}$$

which at the resonance, $\omega_{m_1} = 2\omega_{0_1}$, becomes

$$\begin{aligned} H^{res}_{SQR1}(t) &= g(r)(\cos[(2\omega_{0_1} - 2\omega_{0_2})t](\sigma_{x_1}\sigma_{x_2} + \sigma_{y_1}\sigma_{y_2}) - 2\sigma_{z_1}\sigma_{z_2}) \\ &\quad -\omega_{a_1}[\cos(\phi)\sigma_{x_1} - \sin(\phi)\sigma_{y_1}]. \end{aligned} \tag{5.9}$$

The matrix form of Hamiltonian (5.9) is given by

$$H^{res}_{SQR1}(t) = \begin{pmatrix} -2g(r) & 0 & -\omega_{a_1} f & 0) \\ 0 & 2g(r) & 2g(r)l(t) & -\omega_{a_1} f \\ -\omega_{a_1} f^* & 2g(r)l(t) & 2g(r) & 0 \\ 0 & -\omega_{a_1} f^* & 0 & -2g(r) \end{pmatrix}. \tag{5.10}$$

To perform rotations on the second and first qubits, we need to solve the Schrödinger equation Eq. (5.1), with the Hamiltonians given respectively by Eq. (5.6) and by Eq. (5.9).

As examples of single-qubit rotations, we consider the sequence of transformations in Eq. (4.31), which has to be read from right to left. The first transformation is a $-\pi$-rotation of the second qubit about the z axis. By virtue of Eq. (5.4), we can write

$$\exp[\imath\frac{\pi}{2}\sigma_{z_2}] = \exp[-\imath\frac{\pi}{4}\sigma_y]\exp[-\imath\frac{\pi}{2}\sigma_x]\exp[\imath\frac{\pi}{4}\sigma_y], \tag{5.11}$$

which expresses a $-\pi$-rotation about z in terms of rotations about the y and x axes. The sequence of transformations in (5.11) starts with a $-\frac{\pi}{2}$ rotation of the second qubit about

the y axis. In order to perform this rotation, we have to remove the dependence on σ_{x_2} from the Hamiltonian, which can be realized by choosing $\phi = -\frac{\pi}{2}$. Under this condition, the Hamiltonian becomes

$$\begin{aligned} H(t) &= g(r)(\cos[(2\omega_{0_1} - 2\omega_{0_2})t](\sigma_{x_1}\sigma_{x_2} + \sigma_{y_1}\sigma_{y_2}) - 2\sigma_{z_1}\sigma_{z_2}) \\ &\quad -\omega_{a_2}[\sigma_{y_2}], \end{aligned} \tag{5.12}$$

and considering Eq. (5.7), its matrix form is

$$H(t) = \begin{pmatrix} -2g(r) & \imath\omega_{a_2} & 0 & 0) \\ -\imath\omega_{a_2} & 2g(r) & 2g(r)l(t) & 0 \\ 0 & 2g(r)l(t) & 2g(r) & \imath\omega_{a_2} \\ 0 & 0 & -\imath\omega_{a_2} & -2g(r) \end{pmatrix}. \tag{5.13}$$

By integrating the Schrödinger equation with the Hamiltonian given by Eq. (5.13) for a time interval $\Delta t = \frac{\pi}{4\omega_{a_2}} = \frac{\pi}{4\mu_B B_{m_2}}$, we find the time evolution matrix which performs a $-\frac{\pi}{2}$-rotation about the y axis of the second qubit. The time interval Δt has been found following the procedure considered for the theoretical transformation of Eq. (4.9).

The next single-qubit rotation in Eq. (5.11) is a π-rotation about the x axis of the second qubit. Analogous to what we did for the previous single-qubit rotation, in this case we need to remove the dependence on σ_{y_2} which can be accomplished with the choice $\phi = \pi$. The related Hamiltonian becomes

$$\begin{aligned} H(t) &= g(r)(\cos[(2\omega_{0_1} - 2\omega_{0_2})t](\sigma_{x_1}\sigma_{x_2} + \sigma_{y_1}\sigma_{y_2}) - 2\sigma_{z_1}\sigma_{z_2}) \\ &\quad -\omega_{a_2}[-\sigma_{x_2}], \end{aligned} \tag{5.14}$$

whose matrix form is

$$H(t) = \begin{pmatrix} -2g(r) & \omega_{a_2} & 0 & 0) \\ \omega_{a_2} & 2g(r) & 2g(r)l(t) & 0 \\ 0 & 2g(r)l(t) & 2g(r) & \omega_{a_2} \\ 0 & 0 & \omega_{a_2} & -2g(r) \end{pmatrix}. \tag{5.15}$$

Allowing the time evolution for a time interval $\Delta t = \frac{\pi}{2\mu_B B_{m_2}}$, a π-rotation about the x axis of the second qubit can be accomplished.

The same procedure can be adopted for the realization of a $\frac{\pi}{2}$-rotation about the y axis, which requires $\phi = \frac{\pi}{2}$ and gives

$$\begin{aligned} H(t) &= g(r)(\cos[(2\omega_{0_1} - 2\omega_{0_2})t](\sigma_{x_1}\sigma_{x_2} + \sigma_{y_1}\sigma_{y_2}) - 2\sigma_{z_1}\sigma_{z_2}) \\ &\quad -\omega_{a_2}[-\sigma_{y_2}], \end{aligned} \tag{5.16}$$

whose matrix form is

$$H(t) = \begin{pmatrix} -2g(r) & -\imath\omega_{a_2} & 0 & 0) \\ \imath\omega_{a_2} & 2g(r) & 2g(r)l(t) & 0 \\ 0 & 2g(r)l(t) & 2g(r) & -\imath\omega_{a_2} \\ 0 & 0 & \imath\omega_{a_2} & -2g(r) \end{pmatrix}, \tag{5.17}$$

with the related integration time interval $\Delta t = \frac{\pi}{4\mu_B B_{m_2}}$.

For the realization of $-\pi$-rotation about the x axis, we need to choose $\phi = 0$ whose choice gives

$$\begin{aligned} H(t) &= g(r)(\cos[(2\omega_{0_1} - 2\omega_{0_2})t](\sigma_{x_1}\sigma_{x_2} + \sigma_{y_1}\sigma_{y_2}) - 2\sigma_{z_1}\sigma_{z_2}) \\ &\quad -\omega_{a_2}[\sigma_{x_2}], \end{aligned} \tag{5.18}$$

and whose matrix form is

$$H(t) = \begin{pmatrix} -2g(r) & -\omega_{a_2} & 0 & 0) \\ -\omega_{a_2} & 2g(r) & 2g(r)l(t) & 0 \\ 0 & 2g(r)l(t) & 2g(r) & -\omega_{a_2} \\ 0 & 0 & -\omega_{a_2} & -2g(r) \end{pmatrix}. \tag{5.19}$$

In this case, to perform a $-\pi$-rotation about the x axis of the second qubit, the time evolution matrix can be found through the integration of the Schrödinger equation for a time interval $\Delta t = \frac{\pi}{2\mu_B B_{m_2}}$.

5.2 Two-Qubit Interaction

Transformation (4.31) contains two two-qubit transformations, $U_a(t)$ and $U_b(t)$, due to the interaction of the two spins that are subjected only to the action of static magnetic fields oriented along the direction of the z axis. In the absence of any applied microwave field the dominant term in the Hamiltonian of the system is H_{DD}, i.e. the dipole-dipole interaction term. Since the dipole-dipole term describes the mutual interaction which couples the two spins, transformations $U_a(t)$ and $U_b(t)$ can be interpreted as two-qubit gates. These transformations can be obtained by solving the Schrödinger equation (5.1), with $H(t)$ given by H_{DD}^{rot}, see Eq. (4.25). The integration time is given by condition (4.33). Therefore, in order to perform $U_a(t)$ and $U_b(t)$ we need to solve for each of them the related Schrödinger equation for a time interval $\Delta t = \frac{\pi}{16g(r)}$.

5.3 Realization of Transformation $U(t)$

To reproduce the series of transformations in Eq. (4.31) with the final goal of the implementation of a π-gate, we need to solve a set of Schrödinger equations. Each transformation can be evaluated by solving a Schrödinger equation of the form (5.1), with a suitable choice for the Hamiltonian, according to the transformation which is intended to be reproduced. We present the set of Hamiltonians which have to be considered in the Schrödinger equation at each step and the related integration time.

$-\frac{\pi}{2}$-rotation of the second qubit about the y axis, $\exp[\imath\frac{\pi}{4}\sigma_{y_2}]$:

$$H_1(t) = \begin{pmatrix} -2g(r) & \imath\omega_{a_2} & 0 & 0) \\ -\imath\omega_{a_2} & 2g(r) & 2g(r)l(t) & 0 \\ 0 & 2g(r)l(t) & 2g(r) & \imath\omega_{a_2} \\ 0 & 0 & -\imath\omega_{a_2} & -2g(r) \end{pmatrix} \quad , \Delta t_1 = \frac{\pi}{4\mu_B B_{m_2}} \tag{5.20}$$

π-rotation of the second qubit about x, $\exp[-\imath\frac{\pi}{2}\sigma_{x_2}]$:

$$H_2(t) = \begin{pmatrix} -2g(r) & \omega_{a_2} & 0 & 0) \\ \omega_{a_2} & 2g(r) & 2g(r)l(t) & 0 \\ 0 & 2g(r)l(t) & 2g(r) & \omega_{a_2} \\ 0 & 0 & \omega_{a_2} & -2g(r) \end{pmatrix} \quad , \Delta t_2 = \frac{\pi}{2\mu_B B_{m_2}} \tag{5.21}$$

$\frac{\pi}{2}$-rotation of the second qubit about the y axis, $\exp[-\imath\frac{\pi}{4}\sigma_{y_2}]$:

$$H_3(t) = \begin{pmatrix} -2g(r) & -\imath\omega_{a_2} & 0 & 0) \\ \imath\omega_{a_2} & 2g(r) & 2g(r)l(t) & 0 \\ 0 & 2g(r)l(t) & 2g(r) & -\imath\omega_{a_2} \\ 0 & 0 & \imath\omega_{a_2} & -2g(r) \end{pmatrix} \quad , \Delta t_3 = \frac{\pi}{4\mu_B B_{m_2}} \tag{5.22}$$

The two-qubit transformation $U_a(t)$ can be realized by allowing the two-spin system subjected only to a static magnetic field along z direction to evolve for a time Δt_4. Since the mutual dipole-dipole interaction couples the two spins, it naturally realizes a two-qubit gate.

$$H_4(t) = \begin{pmatrix} -2g(r) & 0 & 0 & 0) \\ 0 & 2g(r) & 2g(r)l(t) & 0 \\ 0 & 2g(r)l(t) & 2g(r) & 0 \\ 0 & 0 & 0 & -2g(r) \end{pmatrix} \quad , \Delta t_4 = \frac{\pi}{16g(r)} \tag{5.23}$$

$-\frac{\pi}{2}$-rotation of the second qubit about the y axis, $\exp[\imath\frac{\pi}{4}\sigma_{y_2}]$:

$$H_5(t) = H_1(t) \quad , \Delta t_5 = \Delta t_1 \tag{5.24}$$

$-\pi$-rotation of the second qubit about x, $\exp[\imath\frac{\pi}{2}\sigma_{x_2}]$:

$$H_6(t) = \begin{pmatrix} -2g(r) & -\omega_{a_2} & 0 & 0) \\ -\omega_{a_2} & 2g(r) & 2g(r)l(t) & 0 \\ 0 & 2g(r)l(t) & 2g(r) & -\omega_{a_2} \\ 0 & 0 & -\omega_{a_2} & -2g(r) \end{pmatrix} \quad , \Delta t_6 = \frac{\pi}{2\mu_B B_{m_2}} \tag{5.25}$$

$\frac{\pi}{2}$-rotation of the second qubit about y, $\exp[-\imath\frac{\pi}{4}\sigma_{y_2}]$:

$$H_7(t) = H_3(t) \quad , \Delta t_7 = \Delta t_3 \tag{5.26}$$

The system is subjected to Hamiltonian H_{DD}^{rot} for the realization of transformation $U_b(t)$

$$H_8(t) = H_4(t) \quad , \Delta t_8 = \Delta t_4 \tag{5.27}$$

The set of Schrödinger equations which descends from the substitution of matrices (5.20-5.27) is explicitly presented in App. B, Eqs. (B.1-B.8).

Fig. (5.2) shows the quantum gate which is represented by the unitary transformation obtained through the solution of the realistic Schrödinger equations (with matrices given by (5.20-5.27)) as a global unitary transformation.

5.3.1 Realization of a π-gate: First approach

The first approach that we consider towards performing a π-gate is based on the realization of a $\frac{\pi}{4}$-phase gate of Eq. (4.34), where the output phases are arranged as prescribed in Eq. (1.51). In order to evaluate phase ϑ, see Eq. (1.51), we had solved the set of Schrödinger equations with the Hamiltonians (5.20-5.27) four times, i.e. for each component of the wave-function (5.2). This corresponds to set a different input state at each time, i.e.

$$\begin{aligned} &c_1 = 1, \quad c_2 = c_3 = c_4 = 0 \quad \Rightarrow \quad |\,\text{in}\rangle = |\,00\rangle \\ &c_2 = 1, \quad c_1 = c_3 = c_4 = 0 \quad \Rightarrow \quad |\,\text{in}\rangle = |\,01\rangle \\ &c_3 = 1, \quad c_1 = c_2 = c_4 = 0 \quad \Rightarrow \quad |\,\text{in}\rangle = |\,10\rangle \\ &c_4 = 1, \quad c_1 = c_2 = c_3 = 0 \quad \Rightarrow \quad |\,\text{in}\rangle = |\,11\rangle \end{aligned} \tag{5.28}$$

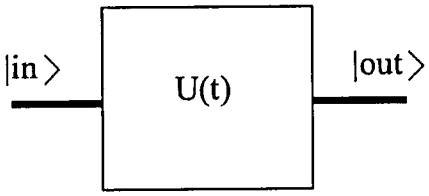

Figure 5.2: Schematic representation of the gate operation which is represented by the set of transformations (5.20-5.27). The input state | in⟩ and the output state | out⟩ are two-qubit states.

Therefore, in order to check if equations (5.20-5.27) allow a phase-gate to be realized, we have to evaluate $\vartheta(t_{out})$, as follows

(5.29) $\vartheta(t_{out}) = Arg[c_{11}(t_{out}))] - Arg[c_{22}(t_{out}))] - Arg[c_{33}(t_{out}))] + Arg[c_{44}(t_{out})]$,

where t_{out} is the output time, and $c_{ii}(t_{out})$, $i = 1,..4$, are the diagonal elements of the numerical output matrix (see Eqs. (A.42) and (5.31)) .The output time t_{out} is given by the sum of the integration intervals in (5.20-5.27), i.e.

(5.30) $$t_{out} = \sum_i \Delta t_i,$$

with $i = 1,..8$.

In order to see if the time evolution performs a π-gate we have to check if $\vartheta(t_{out}) = \pi$. The numerical values chosen for the physical quantities involved in the calculations are the following:

- for the distance between the two buckyballs $r = 1.14nm$
- for the static magnetic field along the z axis $B_{0_1} = B_z + B_{g_1} = (0.3 + 3.04 \times 10^{-5})T$, $B_{0_2} = B_z + B_{g_2} = (0.3 - 3.04 \times 10^{-5})T$, where B_{g_1} and B_{g_2} are due to the magnetic field gradient, see Sec. 3.2;
- for the angular frequencies $\omega_{m_1} = 2\omega_{0_1} = 2\pi\nu_1 = 2\pi\mu_B B_{0_1} = 5.2769 \times 10^{10} Hz$ and $\omega_{m_2} = \omega_{0_1} = 2\pi\nu_2 = 2\pi\mu_B B_{0_1} = 5.2758 \times 10^{10} Hz$, from which $\nu_1 = 8.398 GHz$ and $\nu_2 = 8.396 GHz$, which are in the range of microwave frequencies;

- for the amplitude of the microwave fields $B_{m_1} = 0$ and $B_{m_2} = 0.5T$.

With this choice for the numerical quantities we have used the Mathematica programme `Phase-gate.nb`, see App. C.3, to solve the set of Scrhrödinger equations (5.20-5.27). The realistic time-evolution matrix which reproduces a $\frac{\pi}{4}$-phase gate obtained through the numerical calculations is the following

(5.31)

$$U_{\pi 1} = \begin{pmatrix} 0.703 + 0.711i & 0.003 + 0.002i & -0.002 + 0.006i & 0.002 + 0.002i \\ -0.002 + 0.002i & 0.704 - 0.710i & 0.001 - 0.001i & -0.002 - 0.004i \\ 0.002 + 0.006i & -0.001 + 0.001i & 0.703 - 0.711i & -0.005 + 0.002i \\ -0.002 - 0.002i & 0.002 - 0.004i & 0.005 + 0.002i & 0.703 + 0.711i \end{pmatrix}$$

From a comparison between matrix $U_{\pi 1}$ and matrix U_{PG}, Eq. (4.34), we notice that the realistic time-evolution introduces in each term of matrix (5.31) a phase. In particular, the off-diagonal terms of (5.31) are all different from zero. This means that the output state after the realistic time-evolution is a superposition of all the computational basis states. This is due to the fact that through the study of the realistic dynamics of the system, single-qubit rotations are performed under the influence of the dipole-dipole interaction which couples the two spins. In order to perform a single-qubit operation in perfect agreement with the ideal theoretical single-qubit rotation, the system should not be affected by any mutual interaction term. In our case, we cannot switch off the mutual dipole-dipole interaction because it is naturally always present. Therefore, the presence of the mutual interaction influences any single-qubit rotation (and in turn two-qubit gates like a π-gate and a $CNOT$-gate, which by definition are composed also of single-qubit rotations) by introducing phases as presented in $U_{\pi 1}$, which prevent this matrix to be exactly equal to a $\frac{\pi}{4}$-phase gate. However, since the dipolar coupling constant $g(r) = 5.505 \times 10^7 Hz$ is much smaller than the spin-microwave field interaction term $\omega_{a_{1,2}} = \mu_B B_{m_{1,2}} = 4.397 \times 10^{10} Hz$, the dipolar interaction can be considered as a perturbation which influences the achievement of the desirable quantum gate. This outcome allows approximation (4.30) to be satisfied. Further comments on the dipolar interaction as a perturbative term are presented in Sec. 5.7. Another source of error is the intrinsic numerical error due to the precision of the programming software. However, this error is estimated to be of the order of $10^{-4}\% - 10^{-7}\%$, which is negligible in comparison with the influence of imperfect single-qubit rotations.

With the study of the fidelity (Sec. 5.4), which allows a quantitative comparison between the realistic time evolution $U_{\pi 1}$ and the ideal $\frac{\pi}{4}$-phase gate, we will know the

degree of agreement between them.

According to Eq. (5.30), with the presented choice for the numerical quantities, we can evaluate the output time t_{out}, whose numerical value is

$$t_{out} = 4\frac{\pi}{4\mu_B B_{m_2}} + 2\frac{\pi}{2\mu_B B_{m_2}} + 2\frac{\pi}{16g(r)} = 7.277ns. \tag{5.32}$$

The numerical calculations show that

$$\vartheta(t_{out}) = 3.16167. \tag{5.33}$$

Since the expected value is $\vartheta(t_{out}) = \pi$, we find that the calculated value of $\vartheta(t_{out})$ differs from the expected by an error of 2%. Since this error is very small, we can conclude that the realistic dynamics of the sytem reproduces a π-gate in very good agreement with the theoretical predictions. This result allows us to confirm that approximation (4.30) is valid in the realistic system composed of two interacting buckyballs. Finally, the dipolar interaction weakly influences the perfect realization of single-qubit rotations, but it is essential for the realization of two-qubit gates because it couples the two qubits.

5.3.2 Realization of a π-gate: Second Approach

Here, to perform a π-gate we consider the set of transformations in Eq. (4.35). Therefore, in addition to the set of differential equation systems whose Hamiltonians are given by Eqs. (5.20-5.27), we consider two more single-qubit rotation, i.e. a $\frac{\pi}{2}$ rotation about the z axis on each qubit. Following Eq. (5.4), these two single-qubit rotations are given by

$$\exp[-\imath\frac{\pi}{4}\sigma_{z_1}] = \exp[-\imath\frac{\pi}{4}\sigma_{y_1}]\exp[\imath\frac{\pi}{4}\sigma_{x_1}]\exp[\imath\frac{\pi}{4}\sigma_{y_1}], \tag{5.34}$$

for the first qubit, and for the second qubit

$$\exp[-\imath\frac{\pi}{4}\sigma_{z_2}] = \exp[-\imath\frac{\pi}{4}\sigma_{y_2}]\exp[\imath\frac{\pi}{4}\sigma_{x_2}]\exp[\imath\frac{\pi}{4}\sigma_{y_2}]. \tag{5.35}$$

The set of rotations (5.34) on the first qubit can be realized by solving the Schrödinger equation where the Hamiltonian is given by Eq. (5.9).

The sequence of rotations involved in the matrix tensor product

$$\exp[-\imath\frac{\pi}{4}\sigma_{z_1}]\exp[-\imath\frac{\pi}{4}\sigma_{z_2}] \tag{5.36}$$

can be reproduced by solving a set of Schrödinger equations of the form (5.1) where the Hamiltonian are the following :

$-\frac{\pi}{2}$-rotation of the second qubit about the y axis, $\exp[\imath\frac{\pi}{4}\sigma_{y_2}]$

$$H_9(t) = H_1(t) \quad , \Delta t_9 = \Delta t_1 \tag{5.37}$$

$-\frac{\pi}{2}$-rotation on the second qubit about the x axis, $\exp[\imath\frac{\pi}{4}\sigma_{x_2}]$:

$$H_{10}(t) = \begin{pmatrix} -2g(r) & -\omega_{a_2} & 0 & 0) \\ -\omega_{a_2} & 2g(r) & 2g(r)l(t) & 0 \\ 0 & 2g(r)l(t) & 2g(r) & -\omega_{a_2} \\ 0 & 0 & -\omega_{a_2} & -2g(r) \end{pmatrix} \quad , \Delta t_{10} = \frac{\pi}{4\mu_B B_{m_2}} \tag{5.38}$$

$\frac{\pi}{2}$-rotation on the second qubit about the y axis, $\exp[-\imath\frac{\pi}{4}\sigma_{y_2}]$:

$$H_{11}(t) = H_3(t) \quad , \Delta t_{11} = \Delta t_3 \tag{5.39}$$

$-\frac{\pi}{2}$-rotation about the y axis on the first qubit, $\exp[\imath\frac{\pi}{4}\sigma_{y_1}]$

$$H_{12}(t) = \begin{pmatrix} -2g(r) & 0 & \imath\omega_{a_1} & 0) \\ 0 & 2g(r) & 2g(r)l(t) & \imath\omega_{a_1} \\ -\imath\omega_{a_1} & 2g(r)l(t) & 2g(r) & 0 \\ 0 & -\imath\omega_{a_1} & 0 & -2g(r) \end{pmatrix} \quad , \Delta t_{12} = \frac{\pi}{4\mu_B B_{m_1}} \tag{5.40}$$

$-\frac{\pi}{2}$-rotation on the first qubit about the x axis, $\exp[\imath\frac{\pi}{4}\sigma_{x_1}]$:

$$H_{13}(t) = \begin{pmatrix} -2g(r) & 0 & -\omega_{a_1} & 0) \\ 0 & 2g(r) & 2g(r)l(t) & -\omega_{a_1} \\ -\omega_{a_1} & 2g(r)l(t) & 2g(r) & 0 \\ 0 & -\omega_{a_1} & 0 & -2g(r) \end{pmatrix} \quad , \Delta t_{13} = \frac{\pi}{4\mu_B B_{m_1}} \tag{5.41}$$

$\frac{\pi}{2}$-rotation on the first qubit about the y axis, $\exp[-\imath\frac{\pi}{4}\sigma_{y_1}]$:

$$H_{14}(t) = \begin{pmatrix} -2g(r) & 0 & -\imath\omega_{a_1} & 0) \\ 0 & 2g(r) & 2g(r)l(t) & -\imath\omega_{a_1} \\ \imath\omega_{a_1} & 2g(r)l(t) & 2g(r) & 0 \\ 0 & \imath\omega_{a_1} & 0 & -2g(r) \end{pmatrix} \quad , \Delta t_{14} = \frac{\pi}{4\mu_B B_{m_1}} \tag{5.42}$$

The set of Schrödinger equations with Hamiltonians (5.20-5.27) together with those characterized by Hamiltonians (5.37-5.42) has been solved with the Mathematica programme

`Pi-gate.nb`, see App. C.4. The explicit expressions of the set of Schrödinger equations with Hamiltonians (5.37-5.42) is presented in App. (B), Eqs. (B.9-B.14). The numerical values chosen are the same as in Sec. 5.3.1. In Hamiltonians (5.40-5.42) a microwave field acts on the first qubit and we set $B_{m_2} = 0$ and $B_{m_1} = 0.5T$.

By solving the presented set of Schrödinger equations with the numerical Mathematica programme we obtain the realistic time-evolution matrix. From Eq. (4.35), through the study of the actual dynamics of the system, we can reproduce a π-gate up to a $\sqrt{\imath} = \exp[\imath\frac{\pi}{4}]$ global phase, which is irrelevant. Therefore, the calculated time-evolution matrix is the following

(5.43)

$$U_{\pi 2} = \sqrt{\imath} U_{real}(t_{out}) =$$

$$\begin{pmatrix} 0.9999 + 0.0100\imath & 0.0058 + 0.0040\imath & 0.0075 + 0.0085\imath & 0.0005 - 0.00002\imath \\ -0.0057 + 0.0040\imath & 0.9999 - 0.0091\imath & -0.0024 - 0.0044\imath & 0.0061 - 0.0021\imath \\ -0.0075 + 0.0085\imath & 0.0023 - 0.0045\imath & 0.9999 - 0.0109\imath & -0.0025 + 0.0022\imath \\ 0.0005 + 0.00004\imath & 0.0061 + 0.0021\imath & -0.0025 - 0.0023\imath & -0.9999 - 0.0101\imath \end{pmatrix}$$

We notice that the realistic time evolution affects each term of $U_{\pi 2}$ by introducing phases, which prevent the realization of the perfect G_π matrix, Eq. (4.35). Also in this case, the account for these phases resides in the reproduction of single-qubit rotations through the study of the actual realistic dynamics of the system. Indeed, in order to produce a single-qubit rotation in perfect agreement with the theoretical prediction, the two spins should not be coupled by any mutual interaction, see Sec. 4.1. In our realistic system, the two spins under consideration are always subjected to the mutual dipole-dipole coupling. However, as discussed above for matrix (5.31), the dipolar coupling constant is much smaller than the interaction between the spin and the microwave field, i.e. $g(r) << \omega_{a_{1,2}}$, and it can be considered as a perturbation which weakly influences the dynamics of the system when it is subjected to external microwave fields.

A quantitative evaluation of the degree of agreement between the realistic time evolution $U_{\pi 2}$ and a theoretical π-gate is provided by the study of the fidelity, see Sec. 5.4.

With the presented choice for the numerical quantities, the time required for performing a π-gate can be evaluated through Eq. (5.30), which gives

$$t^{\pi}_{out} = 7\frac{\pi}{4\mu_B B_{m_2}} + 3\frac{\pi}{4\mu_B B_{m_1}} + 2\frac{\pi}{2\mu_B B_{m_2}} + 2\frac{\pi}{16g(r)} = 7.38ns. \tag{5.44}$$

By comparing the gate time $t^{\pi}_{out} = 7.38ns$ with the shortest decoherence time $T_2 \simeq 0.25ms$, see Sec. 2.2.2, it is allowed to perform a number of quantum π-gates equal to $n = T_2/t^{CNOT}_{out} \simeq 3 \times 10^4$ before the occurrence of decoherence processes. This is a

very important outcome in the frame of quantum error correcting. It is believed that in order to apply error correcting codes (which would be essential in any realistic quantum computer for the safe transmission of quantum information and for ensuring fault tolerant gates), it is required to be able to perform on the system a number of quantum operations of the order of 10^4. Therefore, from a theoretical point of view, the system considered is a very good candidate as a building block for quantum computers. It presents very short operational times (of the order of $10^{-9}s$), which allow the completion of a large number of quantum operations (of the order of 10^4) before the occurrence of relaxation processes. This also allows error correcting codes to be reasonably applied, with a resulting reduction of the errors due to the action of faulty gates or faulty quantum channels and opens the possibility of building a scalable system composed of buckyballs.

5.3.3 Realization of a $CNOT$-gate

The set of transformation in Eq. (4.42) allows us to perform a $CNOT$-gate. The set of transformations involved in the realization of a $CNOT$-gate, up to a $\exp[\imath\frac{\pi}{2}]$ global phase, is given by the composition of a $\frac{\pi}{2}$ rotation about the y axis of the second (target) qubit, $\exp[-\imath\frac{\pi}{4}\sigma_{y_2}]$, followed by a π-gate G_π, followed by a $-\frac{\pi}{2}$-rotation about the y axis of the second qubit, $\exp[\imath\frac{\pi}{4}\sigma_{y_2}]$, finally followed by a π-rotation about the z axis of the first (control) qubit. We need to reproduce these transformations by solving the dynamics of the system through the solution of suitable Schrödinger equations.

The first transformation that we need to reproduce is $\exp[-\imath\frac{\pi}{4}\sigma_{y_2}]$. This can be achieved by solving the Schrödinger equation (5.1). Since we want to reproduce a $\frac{\pi}{2}$-rotation of the second qubit about the y axis, in Hamiltonian (4.26) we choose $\omega_{a_1} = 0$ and $\phi = \frac{\pi}{2}$. From these choices, the Hamiltonian which has to be inserted in the related Schrödinger equation whose solution allows the reproduction the second qubit $\frac{\pi}{2}$-rotation about the y axis, is the following

(5.45)

$$H_{15}(t) = H_3(t) = \begin{pmatrix} -2g(r) & -\imath\omega_{a_2} & 0 & 0) \\ \imath\omega_{a_2} & 2g(r) & 2g(r)l(t) & 0 \\ 0 & 2g(r)l(t) & 2g(r) & -\imath\omega_{a_2} \\ 0 & 0 & \imath\omega_{a_2} & -2g(r) \end{pmatrix} , \Delta t_{15} = \Delta t_3$$

In Eq. (4.41) the $\frac{\pi}{2}$-rotation about the y axis on the second qubit is followed by the transformation represented by matrix G_π, Eq. (1.42), which represents a π-gate. The set of Schrödinger equations whose solution reproduces a π-gate up to a $\exp[\imath\frac{\pi}{4}]$ global

irrelevant phase, which has been presented in Secs. (5.3.1) and (5.3.2), is given by the set of differential equations (B.1-B.8) followed by equations (B.9-B.14).

After the transformation represented by G_π, in Eq. (4.41) we find a $-\frac{\pi}{2}$-rotation about the y axis of the second qubit. This transformation can be reproduced with all the same choices made for the realization of a $\frac{\pi}{2}$-rotation about the y axis with a different choice of $\phi = -\frac{\pi}{2}$. The Schrödinger equation resulting from these choices has to be integrated for a time interval Δt_{16} and contains the following Hamiltonian

(5.46)
$$H_{16}(t) = H_1(t) = \begin{pmatrix} -2g(r) & \imath\omega_{a_2} & 0 & 0) \\ -\imath\omega_{a_2} & 2g(r) & 2g(r)l(t) & 0 \\ 0 & 2g(r)l(t) & 2g(r) & \imath\omega_{a_2} \\ 0 & 0 & -\imath\omega_{a_2} & -2g(r) \end{pmatrix} \quad , \Delta t_{16} = \Delta t_1$$

Finally, in order to complete the procedure which allows us to perform a $CNOT$-gate up to a global phase $\exp[\imath\frac{\pi}{2}]$, we need to reproduce the last transformation in Eq. (4.41), which is represented by a π-rotation about the z axis on the first qubit. Following Eq. (5.4), a π-rotation about the z axis can be represented as the composition of a $-\frac{\pi}{2}$-rotation about the y axis, followed by a $-\pi$-rotation about the x axis, finally followed by a $\frac{\pi}{2}$-rotation about the y axis. To perform a rotation of only the first qubit, we need to switch off the microwave field interaction with second qubit and to switch it on with the first particle by choosing $B_{0_2} = 0$ and $B_{0_1} = 0.5T$ respectively. The Hamiltonian which describes this situation is given by Eq. (5.9). Following the procedure described in Sec. 5.1, the set of three rotations which correspond to a π-rotation about the z axis of the first qubit can be reproduced by solving a Schrödinger equation with the Hamiltonian given by Eq. (5.9) and by choosing $\phi = -\frac{\pi}{2}$ to perform a $-\frac{\pi}{2}$-rotation about the y axis, $\phi = \pi$ to perform a $-\pi$-rotation about the x axis and finally $\phi = \frac{\pi}{2}$ to realize a $\frac{\pi}{2}$-rotation about the y axis. The set of Hamiltonians to be inserted into the Scrhödinger equations for reproducing a π-rotation about the z axis of the first qubit is the following:

$-\frac{\pi}{2}$-rotation about the y axis:

(5.47)
$$H_{17}(t) = H_{12}(t) \quad , \Delta t_{17} = \Delta t_{12}$$

$-\pi$-rotation about the x axis:

(5.48)
$$H_{18}(t) = \begin{pmatrix} -2g(r) & 0 & -\omega_{a_1} & 0) \\ 0 & 2g(r) & 2g(r)l(t) & -\omega_{a_1} \\ -\omega_{a_1} & 2g(r)l(t) & 2g(r) & 0 \\ 0 & -\omega_{a_1} & 0 & -2g(r) \end{pmatrix} \quad , \Delta t_{18} = \frac{\pi}{2\mu_B B_{m_1}}$$

$\frac{\pi}{2}$-rotation about the y axis:

$$H_{19}(t) = H_{14}(t) \quad , \Delta t_{19} = \Delta t_{14} \tag{5.49}$$

With the numerical choices already presented, we have used the Mathematica programme `CNOT-gate.nb`, see App. C.5, which allows us to evaluate the time-evolution matrix for the realization of a $CNOT$-gate. Eq. (4.42) represents the set of transformations which have been reproduced through the study of the realistic evolution of the system for performing a $CNOT$-gate. Therefore, the realistic time-evolution matrix which is able to reproduce a $CNOT$-gate up to a global phase equal to $\exp[\imath\frac{3\pi}{4}]$ is given by the following matrix

(5.50)

$$U_{CN_{real}} = \exp[\imath\tfrac{3\pi}{4}]U_{real}(t_{out})$$
$$= \begin{pmatrix} 0.9998 + 0.0094\imath & 0.0058 - 0.0088\imath & 0.0071 & 0.0032 - 0.0020\imath \\ -0.0056 - 0.0088\imath & 0.9998 - 0.0085\imath & -0.0048 - 0.0097\imath & 0.0065 + 0.0076\imath \\ -0.0032 - 0.0021\imath & -0.0064 + 0.0077\imath & 0.0026 + 0.0098\imath & 0.9999 - 0.0051\imath \\ -0.0072 - 0.0001\imath & 0.0046 - 0.0097\imath & 0.9998 + 0.0043\imath & -0.0026 + 0.0098\imath \end{pmatrix}$$

Even in this case, all terms of the realistic time evolution $U_{CN_{real}}$ (Eq. (5.50)) differ from the ideal $CNOT$-gate (Eq. (1.31)) for a phase. The dipolar interaction is responsible for these phases and it prevents to perform single-qubit rotations in perfect agreement with the theory. Indeed, the mutual dipolar interaction between the two spins is always present and cannot be switched off for performing single-qubit rotations. However, the spin dipolar coupling constant $g(r)$ is estimated to be weaker than the strength of the spin-microwave field interaction. Therefore, the mutual coupling term can be considered as a perturbation in comparison with the interaction between the spin and the microwave field, which is the term responsible for performing a single-qubit rotation. The reliability of the quantum system for the realization of a $CNOT$-gate through the realistic transformation $U_{CN_{real}}$ can be estimated with the study of the minimum fidelity, see Sec. 5.4, which allows us to make a comparison between the realistic and theoretical matrices.

The time required to complete a $CNOT$-gate can be evaluated through Eq. (5.30). The numerical value obtained is the following

$$\begin{aligned} t_{out}^{CNOT} = \; & 9\tfrac{\pi}{4\mu_B B_{m_2}} + 5\tfrac{\pi}{4\mu_B B_{m_1}} \\ & +2\tfrac{\pi}{2\mu_B B_{m_2}} + \tfrac{\pi}{2\mu_B B_{m_1}} + 2\tfrac{\pi}{16g(r)} \\ & = 7.49ns. \end{aligned} \tag{5.51}$$

From a comparison between the gate time $t_{out}^{CNOT} = 7.49ns$ and the shortest decoherence time $T_2 \simeq 0.25ms$, see Sec. 2.2.2, before the system relaxes we could perform on

our system a number of quantum operations equal to $n = T_2/t_{out}^{CNOT} \simeq 3 \times 10^4$. As discussed above for the case of a π-gate, the possibility of performing a number of operations $n \geq 10^4$ enables the application of error correcting codes. Error correcting codes allow the detection and correction of faulty gates and enable the safe transmission of quantum information.

We have presented a theory which allows the realization of $CNOT$-gates and single-qubit operations through which we can build a set of universal quantum gates. This finding, which is a requirement of DiVincenzo criteria, see Sec. 1.10, allows the fulfillment of other two criteria. Indeed, a large number of quantum operations can be performed before the system relaxes, and also, since buckyballs can be easily maneuvered, they are good elements for building scalable quantum systems, see Sec. 2.2.1.

The results obtained so far are related to the rapidity in performing a two-qubit quantum operation and to the possibility of repeating many quantum operations before the relaxation of the system. We still need to have an insight into the quality of the performed quantum operations. Does the actual realistic transformation reproduce well a $\frac{\pi}{4}$-phase gate, a π-gate and a $CNOT$-gate? In the following two sections we theoretically present and numerically calculate the *fidelity*, which quantifies how reliably these quantum gates work.

5.4 Quantum Gate Fidelity

To check the efficiency and the reliability of a quantum gate we need to compare the realistic output state, evolved through the actual dynamics of the system, with the ideal output state. The quantity we need to evaluate is the *quantum gate fidelity*. Its definition can be derived starting from a more general definition of fidelity.

Following [12], the fidelity is defined as a measure of the distance between two states. The classical definition of fidelity of two probability distributions $\{p_x\}$ and $\{q_x\}$ is given by

$$F(p_x, q_x) = \sum_x \sqrt{p_x q_x}, \tag{5.52}$$

from which it is clear that when the two probability distributions are equal, the fidelity is maximum and equal to one.

The analogous quantum measure of fidelity for two quantum states described by

their density matrices σ and ρ is given by

$$F(\rho,\sigma) = \mathrm{tr}\sqrt{\rho^{1/2}\sigma\rho^{1/2}}. \tag{5.53}$$

Despite the apparent asymmetry in its expression, the fidelity is symmetric in its inputs ρ and σ, and has many other properties. For example, it is invariant under unitary transformations

$$F(U\rho U^{\dagger}, U\sigma U^{\dagger}) = F(\rho,\sigma), \tag{5.54}$$

whose proof is given in Ref. [12]. An important example is the fidelity between a pure state $\mid \psi\rangle$ and an arbitrary state described by the density matrix ρ. In this case, the expression which defines the fidelity simplifies to

$$\begin{aligned} F(\mid \psi\rangle, \rho) &= \mathrm{tr}\sqrt{\langle\psi \mid \rho \mid \psi\rangle \mid \psi\rangle\langle\psi \mid} \\ &= \sqrt{\langle\psi \mid \rho \mid \psi\rangle}. \end{aligned} \tag{5.55}$$

Another example is the fidelity between two pure states $\mid \psi\rangle$ and $\mid \phi\rangle$, whose formula is given by

$$F(\mid \psi\rangle, \mid \phi\rangle) = \mid \langle\phi \mid \psi\rangle \mid, \tag{5.56}$$

which is simply the overlap between the two states.

Since the fidelity quantifies the distance between two quantum states, i.e. how much they differ from each other, we can use it to compare the realistic output state with the ideal output state which is intended to be reproduced through the realistic unitary evolution of the system. Therefore, the fidelity between these two states gives information about how well the quantum gate operates.

An arbitrary starting state describing our two-qubit system can be written as

$$\begin{aligned} \mid \psi\rangle &= c_{00} \mid 00\rangle + c_{01} \mid 01\rangle + c_{10} \mid 10\rangle + c_{11} \mid 11\rangle \\ &= \textstyle\sum_{\alpha} c_{\alpha} \mid \alpha\rangle. \end{aligned} \tag{5.57}$$

In a realistic situation, the input state of a quantum control sequence is better described by a density matrix

$$\sigma = \mid \psi\rangle\langle\psi \mid . \tag{5.58}$$

The realistic output density matrix is given by applying to σ the unitary evolution U. The derivation of matrix U is presented in App. A.5. The formula which describes the realistic output density matrix is the following

$$\sigma\prime = U\sigma U^{\dagger} \tag{5.59}$$

From Eq. (5.55) which defines the fidelity between a pure state and a density matrix, we can evaluate the fidelity between the ideal pure state $\mid \psi\rangle_{ideal}$ and the realistic output density matrix

$$F(\mid \psi\rangle_{ideal}, \sigma\prime) = \sqrt{{}_{ideal}\langle\psi \mid \sigma\prime \mid \psi\rangle_{ideal}} = \sqrt{{}_{ideal}\langle\psi \mid U \mid \psi\rangle\langle\psi \mid U^{\dagger} \mid \psi\rangle_{ideal}}. \tag{5.60}$$

Generally, in a realistic situation we do not know in advance what is the initial state of the system $\mid \psi\rangle$. However, we can evaluate the *minimum fidelity*, which minimizes over all possible initial states. This quantity quantifies the worst-case behaviour of the quantum gate and is described by the following expression

$$\mathcal{F} = \min_{c_\alpha} F(\mid \psi\rangle_{ideal}, \sigma\prime), \tag{5.61}$$

where the minimization is over coefficients c_α of the initial state, Eq.(5.57).

Since through the study of the dynamics of our two-buckyball system we have reproduced a $\frac{\pi}{4}$-phase gate (5.31), a π-gate (5.43) and a $CNOT$-gate (5.50), we have evaluated the minimum fidelity for these three cases.

In each of these three cases the ideally transformed state $\mid \psi\rangle_{ideal}$ can be found by acting on the starting state $\mid \psi\rangle$ with the ideal matrix which describes the transformation (respectively, matrices (4.34), (1.42) and (1.31)), and its expression is given by

$$\begin{aligned} \mid \psi\rangle_{ideal} &= U_{PG} \mid \psi\rangle \\ &= \begin{pmatrix} e^{\imath\frac{\pi}{4}} & 0 & 0 & 0) \\ 0 & e^{-\imath\frac{\pi}{4}} & 0 & 0 \\ 0 & 0 & e^{-\imath\frac{\pi}{4}} & 0 \\ 0 & 0 & 0 & e^{\imath\frac{\pi}{4}} \end{pmatrix} \begin{pmatrix} c_{00} \\ c_{01} \\ c_{10} \\ c_{11} \end{pmatrix} \\ &= e^{\imath\frac{\pi}{4}} c_{00} \mid 00\rangle + e^{-\imath\frac{\pi}{4}} c_{01} \mid 01\rangle + e^{-\imath\frac{\pi}{4}} c_{10} \mid 10\rangle + e^{\imath\frac{\pi}{4}} c_{11} \mid 11\rangle, \end{aligned} \tag{5.62}$$

for the $\frac{\pi}{4}$-phase gate,

$$\begin{aligned} \mid \psi\rangle_{ideal} &= G_\pi \mid \psi\rangle \\ &= \begin{pmatrix} 1 & 0 & 0 & 0 \\ 0 & 1 & 0 & 0 \\ 0 & 0 & 1 & 0 \\ 0 & 0 & 0 & -1 \end{pmatrix} \begin{pmatrix} c_{00} \\ c_{01} \\ c_{10} \\ c_{11} \end{pmatrix} \\ &= c_{00} \mid 00\rangle + c_{01} \mid 01\rangle + c_{10} \mid 10\rangle - c_{11} \mid 11\rangle, \end{aligned} \tag{5.63}$$

for a π-gate, and finally

$$
\begin{aligned}
|\psi\rangle_{ideal} &= U_{CNOT}\,|\psi\rangle \\
&= \begin{pmatrix} 1 & 0 & 0 & 0 \\ 0 & 1 & 0 & 0 \\ 0 & 0 & 0 & 1 \\ 0 & 0 & 1 & 0 \end{pmatrix} \begin{pmatrix} c_{00} \\ c_{01} \\ c_{10} \\ c_{11} \end{pmatrix} \\
&= c_{00}\,|00\rangle + c_{01}\,|01\rangle + c_{11}\,|10\rangle + c_{10}\,|11\rangle,
\end{aligned} \tag{5.64}
$$

for a $CNOT$-gate.

The minimum fidelity has been evaluated through Mathematica programmes. Programme `fidelity-phase-gate.nb` allows us to evaluate the minimum fidelity for the $\frac{\pi}{4}$-phase gate , see App. C.6, programme `fidelity-pi-gate.nb` for the π-gate, see App. C.7, and programme `fidelity-CNOT-gate.nb` for the $CNOT$-gate, see App. C.8. The set of initial values for coefficients c_α has been found by generating random numbers while matrix U, which has been reconstructed by solving the set of Schrödinger equations, is given by matrix $U_{\pi 1}$ (Eq. (5.31)) for the $\frac{\pi}{4}$-phase gate, by matrix $U_{\pi 2}$ (Eq. (5.43)) for the π-gate and by matrix $U_{CN_{real}}$ (Eq. (5.50)) for the $CNOT$-gate.

The calculated value for the minimum fidelity is

$$\mathcal{F}_{\pi 1} = 0.999892, \tag{5.65}$$

for the $\frac{\pi}{4}$-phase gate

$$\mathcal{F}_{\pi 2} = 0.999664, \tag{5.66}$$

for the π-gate and

$$\mathcal{F}_{CN_{real}} = 0.999525, \tag{5.67}$$

for the $CNOT$-gate. The ideal value of the minimum fidelity is $\mathcal{F} = 1$. The difference between the calculated values of $\mathcal{F}$ in all three cases and the ideal value 1 is of the order of $10^{-2}\%$. The calculated values are very close to the ideal value even if they represent the worst case scenario. Therefore, the realistic transformations considered for the realization of a $\frac{\pi}{4}$-phase gate, a π-gate and a $CNOT$-gate are in high accordance with the theoretical predictions. However, we can observe that the numerical value of the minimum fidelity decreases on going from a $\frac{\pi}{4}$-phase gate to a $CNOT$-gate, see Eqs. (5.65-5.67). This behaviour is due to the fact that for the realization of a π-gate and a $CNOT$-gate we need

to add more single-qubit rotations with respect to the number of single-qubit rotations required for achieving a $\frac{\pi}{4}$-phase gate. Following the comments made for the numerical error in the realistic time-evolution matrices $U_{\pi 1}$, $U_{\pi 2}$ and $U_{CN_{real}}$, any single-qubit rotation cannot be performed perfectly because of the always present spin dipolar interaction. Therefore, the decreasing of the fidelity is attributed to the impossibility of reproducing perfect single-qubit rotations.

In conclusion, the realistic transformations $U_{\pi 1}$, $U_{\pi 2}$ and $U_{CN_{real}}$ are in very high agreement with the respective ideal transformations. By increasing the number of single-qubit rotations, the numerical value of the minimum fidelity shows a slight decrease. However, this decrease of the fidelity is of the order of $10^{-2}\%$, see Eq. (5.65-5.67), and we can conclude that the presented two-qubit transformations can be reproduced with a very high fidelity (within a $10^{-2}\%$ error in comparison with the ideal value $\mathcal{F} = 1$) through the study of the proper realistic time-evolution of the system. Therefore, the system composed of two buckyballs is highly reliable for reproducing two-qubit gates and it could be considered in a quantum circuit or in a quantum channel for reproducing complex sets of quantum operations.

5.5 Quantum State Fidelity

In this section we focus on a particular case of fidelity, the *quantum state fidelity*, see [12]-[22]. In this case, we treat the study of the fidelity for only the case of a $CNOT$-gate because it is the most complete two-qubit gate which naturally includes single-qubit gates and $\frac{\pi}{4}$-phase gates.

For the study of the quantum gate fidelity, Sec. 5.4, we considered the most general realistic input state described by a density matrix (5.58). For the study of the quantum state fidelity, we assumed to be able to select the computational basis states as realistic input states. This is an ideal situation which generally cannot be experimentally realized, but through which we can have a further knowledge of the behaviour of our realistic $CNOT$-gate.

The quantum state fidelity allows us to compare the realistic output state $\mid \psi\rangle_{out} = U_{CN_{real}} \mid \psi\rangle$ with the ideal output state $\mid \psi\rangle_{ideal}$, Eq. (5.64). Since both $\mid \psi\rangle_{out}$ and $\mid \psi\rangle_{ideal}$ are pure states, from Eq. (5.56), which defines the fidelity between two pure states, we obtain the following expression

$$F(\mid \psi\rangle_{ideal}, \mid \psi\rangle_{out}) = \mid_{ideal}\langle \psi \mid \psi\rangle_{out} \mid . \tag{5.68}$$

As described in Refs. [22, 23], we will consider as quantum state fidelity the square of Eq. (5.68). This is very convenient because $F(\mid \psi\rangle_{ideal}, \mid \psi\rangle_{out})^2$ can be interpreted as the probability that a system described by state $\mid \psi\rangle_{out}$ can be found to be in the state $\mid \psi\rangle_{ideal}$.

In our case, the output state $\mid \psi\rangle_{out}$ can be written as a general superposition of all computational basis states

$$\begin{aligned} \mid \psi\rangle_{out} &= U_{CN_{real}} \mid \psi\rangle \\ &= c_1(t_{out}) \mid 00\rangle + c_2(t_{out}) \mid 01\rangle + c_3(t_{out}) \mid 10\rangle + c_4(t_{out}) \mid 11\rangle. \end{aligned} \tag{5.69}$$

Since we assume to know exactly the input state $\mid \psi\rangle$, the ideal output state $\mid \psi\rangle_{out}$ is automatically known as follows

$$\begin{aligned} \mid \psi\rangle &= \mid 00\rangle \quad \Rightarrow \quad \mid \psi\rangle_{ideal} = \mid 00\rangle; \\ \mid \psi\rangle &= \mid 01\rangle \quad \Rightarrow \quad \mid \psi\rangle_{ideal} = \mid 01\rangle; \\ \mid \psi\rangle &= \mid 10\rangle \quad \Rightarrow \quad \mid \psi\rangle_{ideal} = \mid 11\rangle; \\ \mid \psi\rangle &= \mid 11\rangle \quad \Rightarrow \quad \mid \psi\rangle_{ideal} = \mid 10\rangle. \end{aligned} \tag{5.70}$$

Therefore, for each input state $\mid \psi\rangle$ the quantum state fidelity $F^2 = F(\mid \psi\rangle_{ideal}, \mid \psi\rangle_{out})^2$ can be easily calculated as follows

$$\begin{aligned} \mid \psi\rangle &= \mid 00\rangle \quad \Rightarrow \quad F_{00}^2 = F(\mid \psi\rangle_{ideal}, \mid \psi\rangle_{out}) = \mid c_1(t_{out}) \mid^2; \\ \mid \psi\rangle &= \mid 01\rangle \quad \Rightarrow \quad F_{01}^2 = F(\mid \psi\rangle_{ideal}, \mid \psi\rangle_{out}) = \mid c_2(t_{out}) \mid^2; \\ \mid \psi\rangle &= \mid 10\rangle \quad \Rightarrow \quad F_{10}^2 = F(\mid \psi\rangle_{ideal}, \mid \psi\rangle_{out}) = \mid c_4(t_{out}) \mid^2; \\ \mid \psi\rangle &= \mid 11\rangle \quad \Rightarrow \quad F_{11}^2 = F(\mid \psi\rangle_{ideal}, \mid \psi\rangle_{out}) = \mid c_3(t_{out}) \mid^2 . \end{aligned} \tag{5.71}$$

From the solution of programme `CNOT-gate.nb`, see App. C.5, we obtain the numerical values for coefficients $c_i(t_{out})$, $i = 1, .., 4$

$$\begin{aligned} c_1(t_{out}) &= -0.700368 - 0.713657\imath, \\ c_2(t_{out}) &= -0.713016 - 0.700913\imath, \\ c_4(t_{out}) &= -0.703959 - 0.710049\imath, \\ c_3(t_{out}) &= -0.710656 - 0.703384\imath, \end{aligned} \tag{5.72}$$

from which we obtain the numerical values of the quantum state fidelity for each input state:

$$\begin{aligned} F_{00}^2 &= 0.9998; \\ F_{01}^2 &= 0.9997; \\ F_{10}^2 &= 0.9998; \\ F_{11}^2 &= 0.9997. \end{aligned} \tag{5.73}$$

Since all values of fidelity F_i^2, $i = 00,..11$, differ from the ideal value 1 by of the order of $10^{-2}\%$, we can conclude that the output state $\mid \psi\rangle_{out}$ represents the transformed state $\mid \psi\rangle_{ideal}$ with a very high fidelity.

By knowing $F^2 = F(\mid \psi\rangle_{ideal}, \mid \psi\rangle_{out})^2$, we can easily evaluate the error committed by the realistic quantum operation U in order to reproduce a $CNOT$-gate. The *probabilistic error* is defined as follows

$$\epsilon = 1 - F^2 = 1 - F(\mid \psi\rangle_{ideal}, \mid \psi\rangle_{out})^2 = 1 - \mid_{ideal}\langle \psi \mid \psi\rangle_{out} \mid^2, \tag{5.74}$$

and it gives an estimate of the gate failure probability. From the numerical values of the fidelity we obtain the following results for the probabilistic error

$$\begin{aligned} \epsilon_{00} &= 1 - 0.9998 = 0.0002; \\ \epsilon_{01} &= 1 - 0.9997 = 0.0003; \\ \epsilon_{10} &= 1 - 0.9998 = 0.0002; \\ \epsilon_{11} &= 1 - 0.9997 = 0.0003, \end{aligned} \tag{5.75}$$

which in each case is of the order of 10^{-4}.

The definition of the error probability ϵ gives the upper limit to the probability of failure per quantum operation, p, i.e.

$$p \leq \epsilon = 1 - F^2 \tag{5.76}$$

The importance of the probabilistic error is related to the accuracy threshold of a quantum operation, for what concerns the application of error correcting codes. This is an alternative to check if the realistic system is suitable for the application of error correcting codes.

To build a system which could perform reliable quantum gates, the probability of error per operation, p, has to be below the threshold accuracy p_{th}. When the condition $p < p_{th}$ is satisfied, a quantum error correcting circuit can be built using unreliable components. The error introduced by faulty gates is compensated by the error correcting codes.

The generally accepted theoretical value of p_{th} is 10^{-4} [24, 25] and a more optimistic estimate rises it up to 10^{-3} [26]. Since the calculated ϵ for the completion of a $CNOT$-gate is of the order of 10^{-4}, from Eq. (5.76) the probability of failure is $p \leq 10^{-4}$. Therefore the condition $p \leq p_{th}$ is verified and the proposed system composed of two-buckyballs could be a reliable system for building quantum circuits. This result also

allows us to conclude that on a quantum circuit composed of buckyballs we could apply error correcting schemes which would ensure fault tolerant quantum gates. Furthermore, this result opens a new road for the design of a scalable quantum computer composed of endohedral fullerene molecules.

5.6 Check of Approximations

In Sec. 4.3, in order to perform the refocusing we needed to cancel the time dependence in the Hamiltonian (4.26). We assumed that the resonance frequencies of the two particles are equal to each other, i.e. $\omega_{0_1} = \omega_{0_2}$. This assumption allows the time dependent function in Eq. (4.26), given by $l(t) = \cos[2(\omega_{0_1} - \omega_{0_2})t]$, to be constantly equal to one. With this choice for the resonance frequencies of the two particles, in Secs. 4.3-4.4 we were able to develop the theory which leads to the realization of π-gates and $CNOT$-gates.

In this Chapter we have checked the validity of the theory by considering the real dynamics of the two-qubit system through the solution of the Schrödinger equation. We need now to check if the assumption, which states that $l(t)$ is constant, is well approximated in the actual physical system. With the numerical choices (5.3.1) for the physical quantities we evaluate the evolution in time of function $l(t)$. Fig. (5.3) shows the profile of $l(t)$ during the time evolution up to the time value $t_{out}^{CNOT} = 7.49ns$, which is the time required to perform a $CNOT$-gate. From this picture, we observe that the time profile of function $l(t)$ shows a deviation less than 1% with respect to the ideal profile which is constantly equal to one. Therefore, in very good approximtion, function $l(t)$ is constant in the time interval $[0, t_{out}^{CNOT}]$, which coincides with the time needed to perform a $CNOT$-gate. This justifies the study of the actual dynamics of the system by applying the theory presented in Secs. 4.3-4.4. Furthermore, since function $l(t)$is approximately constant in the time interval $[0, t_{out}^{CNOT}]$, we are allowed to integrate each step of the set of Schrödinger equations, whose Hamiltonians are given by Eqs. (5.20-5.27,5.37-5.42,5.45-5.46), starting from the integration time $t = 0$.

5.7 Comments and Considerations

This Section presents some considerations with respect to theoretical and experimental limits which can be encountered in performing single-qubit operations.

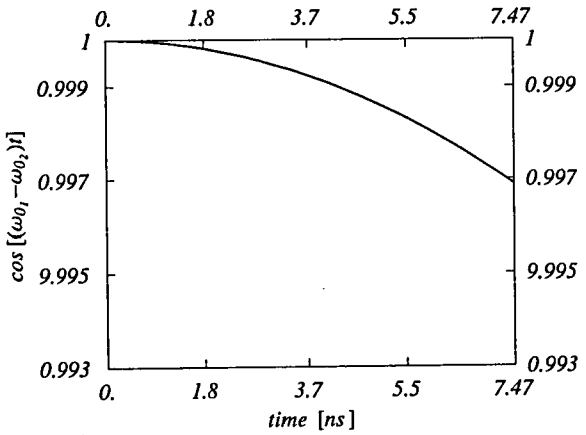

Figure 5.3: Time dependence of function $l(t) = \cos[(\omega_{0_1} - \omega_{0_2})t]$ up to the time $t_{out}^{CNOT} = 7.49ns$. The profile of $l(t)$ shows a deviation less than 1% with respect to the ideal profile which is constantly equal to one.

Firstly, we investigate the theoretical possibility of performing single-qubit operations. We need to make a comparison between the time required to perform a single-qubit rotation and the period of action of the mutual dipolar interaction. With the choice made for the numerical values of the physical quantities involved in the calculations, the time required for completing a single-qubit rotation is $t_{SQ} = \frac{\pi}{2\mu_B B_{m_{1,2}}} = 3.57 \times 10^{-11} s$ for a π-rotation of spin 1 or spin 2, and $t_{SQ} = \frac{\pi}{4\mu_B B_{m_{1,2}}} = 1.79 \times 10^{-11} s$ for a $\frac{\pi}{2}$-rotation. The period of time in which the system is influenced by the spin dipolar interaction is $T = \frac{2\pi}{g(r)} = 1.14 \times 10^{-7} s$, where the coupling strength $g(r)$ is in $\hbar$ units. We can observe that $t_{SQ} \ll T$, i.e. the time required for performing a single-qubit rotation is much smaller than T. Therefore, during the completion of a single-qubit operation we can consider the system as being unaffected by the mutual spin interaction. During a time equal to t_{SQ}, the dipole-dipole interaction can be considered as a small perturbation, and the two spins behave as two uncoupled particles, which can be described by Hamiltonian (4.11). These considerations allow assumption (4.30) to be satisfied in the realistic system.

Since the two spins are characterized by different resonance frequencies, see Sec. 3.2, during the short time interval t_{SQ}, the possibility of controlling microwave fields could allow us to act separately on each single spin. The control of the interaction between the microwave field and the particle can be accomplished by centering the microwave pulse on the resonance frequency of the particle whose spin has to be rotated. However,

even if in the considered time interval the direct coupling is weak, we notice that, when centering the microwave pulse on the resonance frequency of one particular particle, the other one could also be excited. Therefore, in this case the system would undergo a rotation of both spins, and the single spin rotation could not be performed.

In order to be sure that only the selected particle is rotated, the microwave pulse has to be characterized by a very tight spectral bandwidth Δf. An estimate of the bandwidth can be performed by comparing it with the difference between the resonance frequencies of the two particles, $\Delta\nu = \nu_1 - \nu_2 = 2MHz$. If the experimental device can achieve a spectral bandwidth $\Delta f \leq \Delta\nu$, the other particle should not be affected by the applied microwave pulse. However, the bandwidth theorem implies that any wave phenomenon that occurs over a time interval Δt has to have a spread of frequencies Δf given by:

$$\Delta f \simeq \frac{1}{\Delta t}, \tag{5.77}$$

In our case the time interval Δt corresponds to the time required for performing a single-qubit rotation t_{SQ}. Since the time interval of interest for performing a single-qubit rotation is of the order of $10^{-11}s$ and the upper limit of the frequency bandwidth is $\Delta\nu = 2MHz$, the bandwidth theorem is not satisfied. To satisfy the bandwidth theorem, we can consider the following two cases:

- if $t_{SQ} \propto 10^{-11}s$, the microwave pulse frequency bandwidth should be $\Delta f \propto 10^{11}Hz$. This implies that the difference between the resonance frequencies of the two spins has to be $\Delta\nu \geq 10^{11}Hz$;
- if the frequency bandwidth is $\Delta f \simeq 2MHz$, the time required for performing a single-qubit operation should be $t_{SQ} \simeq 0.5\mu s$.

According to the single addressing scheme of Sec. 3.2, the considered values for the resonance frequencies of the two particles correspond to the maximum experimentally achievable. Therefore, it is experimentally forbidden to achieve a value $\Delta\nu \geq 10^{11}Hz$. Nevertheless, the case where $\Delta f \simeq 2MHz$ and $t_{SQ} \simeq 0.5\mu s$ is in agreement with the experimental ranges, but the time required for performing a single-qubit rotation is very long in comparison with the relaxation time T_2. Furthermore, since the aim of our study is to perform the universal quantum $CNOT$-gate, we need to perform at least 17 single-qubit rotations (see Sec. 5.3.3), which would raise the output time of a $CNOT$-gate to approximately $t_{out}^{CNOT} \simeq 10\mu s$, see Eq. (5.51). This allows a number of quantum operations $n = T_2/t_{out}^{CNOT} \simeq 20$ before the occurrence of relaxation processes. Since in order to apply error correcting codes we need to perform at least 10^4 quantum operations,

the calculated value of n is very small for allowing the system to be a reliable component of a quantum circuit.

However, in recent experiments [78], the typical time for performing a single-qubit rotation is $t_{SQ}^{exp} \simeq 32ns$. A θ rotation can be realized by applying an on-resonance microwave pulse of amplitude B_m for a time duration t_{SQ}, which can be calculated through the following expression

$$t_{SQ} = \frac{\theta\hbar}{g\mu_B B_m}. \tag{5.78}$$

In order to rise the calculated time required for a single-qubit rotation $t_{SQ} \simeq 3.57\times10^{-11}s$ to a numerical value equal to the experimental typical time $t_{SQ}^{exp} \simeq 32ns$, considering Eq. (5.78) we see that we should reduce the strength of microwave pulse from the actual considered value $B_m = 0.5T$ (see Sec. 5.3.1). For performing a $\pi/2$ rotation we should reduce B_m to a value that is at least equal to $B_m \simeq 0.28mT$. From hereon, in our calculations we will switch the value of microwave amplitude to $B_m \simeq 0.28mT$. With this value for the microwave pulse amplitude we can perform single-qubit rotations within the experimental limits.

In order to satisfy the bandwidth theorem, the frequency bandwidth of a microwave pulse for the realization of a single-qubit rotation in a time interval $\Delta t = 32ns$ has to be equal to $\Delta f = 31.25MHz$, which implies that the difference between the resonance frequencies of the two spins has to be $\Delta\nu \geq 31.25MHz$. This value of $\Delta\nu$ differs from the experimentally achievable value $\Delta\nu = 2MHz$ of one order of magnitude. In order to enable the realization of single-qubit rotations with the system under consideration, we need to provide an addressing scheme which would allow the achievement of the desirable difference between the two resonance frequencies, i.e. $\Delta\nu \geq 31.25MHz$. The possible alternative designs which can be investigated are the following:

- *Quantum Cellular Automaton: different species of encased particles.*

  Consider different encased particles, characterized by resonance frequencies whose difference has to be of the order of $\Delta\nu \geq 31.25MHz$. This is an example of QCA, see Sec. 2.2.1, which provides an alternative way of addressing qubits. Since the resonance frequency of a particle in a static magnetic field B_0 is $\omega_p = 2\mu_B B_0$, we should apply static magnetic fields with a strength of the order of a few Tesla, but the two particles have to be characterized by a very different value of the gyromagnetic ratio g.

- *New design for the magnetic field gradient.*

The design of a new experimental architecture for addressing each single spin. For example, a more steep magnetic field gradient could be realized. This would subject the two particles to very different magnetic field amplitudes.

The study of these two architectures could allow us to set the numerical value of the physical quantity $\Delta\nu$ in the desirable range and, finally, enable the control of single qubits.

Chapter 6

Quantum Gates with two Distant Buckyballs

In this chapter we investigate a system composed of two $N@C_{60}$ buckyballs separated by a greater distance with respect to the system treated before.

Here we suppose that the buckyballs are placed inside a nanotube. To increase the distance which separates the two buckyballs, we suppose to place between them a sequence of empty fullerene molecules. Following Ref. [83], the diameter of a buckyball is $d \approx 0.7nm$, and, due to van der Waals forces, the distance between two buckyballs in a nanotube is $dist \approx 0.3nm$. Therefore, if we place nine empty fullerenes between the two buckyballs, the distance between the two buckyball-encased Nitrogen atoms is approximately $r = 7nm$. With such a distance, the coupling constant of the dipole-dipole interaction (in $\hbar$ units) is $g(r) = \frac{\mu_0 \mu_B^2}{2\pi r^3} = 2.38 \times 10^5 Hz$.

Furthermore, in this case, by applying a magnetic field gradient as described in Sec. 3.2, the two encased particles would be subjected to a higher magnetic field amplitude in comparison with the previous case, where the two spins were separated by a distance $r = 1.14nm$. With the use of Eq. (3.26), by choosing a distance $x = r = 7nm$ and a current intensity $I = 0.3A$, the two encased particles are respectively subjected to the magnetic field amplitudes $B_{g_1} = 1.87 \times 10^{-4} T$ and $B_{g_2} = -1.87 \times 10^{-4} T$. Since the two particles are also subjected to a static magnetic field in the z axis direction $B_{z_1} = B_{z_2} = 0.3T$, which acts on the whole sample, the total static magnetic field on each particle is $B_{0_1} = B_{z_1} + B_{g_1} = (0.3 + 1.87 \times 10^{-4})T$ for the first particle, and $B_{0_2} = B_{z_2} + B_{g_2} = (0.3 - 1.87 \times 10^{-4})T$ for the second. Knowing the value of the static magnetic field

strength, the resonance frequencies of the particles are respectively $\nu_0^1 = 2\omega_{0_1}/2\pi = 8.40 \times 10^9 Hz$ for the first spin, and $\nu_0^2 = 2\omega_{0_2}/2\pi = 8.39 \times 10^9 Hz$ for the second.

From the comparison between the difference of the angular resonance frequencies $\Delta\omega_p = \mid \omega_{p_1} - \omega_{p_2} \mid = \mid 2\omega_{0_1} - 2\omega_{0_2} \mid = 6.28 \times 10^7 Hz$ and the dipole-dipole interaction coupling constant strength $g(r) = 2.38 \times 10^5 Hz$, we see that

$$\omega_p \gg g(r). \tag{6.1}$$

When this condition is satisfied, the transverse coupling terms in the dipole-dipole Hamiltonian, Eq. (3.2) can be omitted, see [22], and the mutual interaction Hamiltonian can be approximately written as

$$H_{approx} = g(r)(1 - 3\cos^2\theta)\sigma_{z_1}\sigma_{z_2}, \tag{6.2}$$

where θ is the angle between the static magnetic field and the direction of the line joining the centers of the buckyballs, $\vec{n}$. In our system, since the static magnetic field and $\vec{n}$ are parallel and in the same direction, we obtain $\theta = 0$. Therefore, the mutual interaction Hamiltonian is given by the following equation

$$H_{approx} = -2g(r)\sigma_{z_1}\sigma_{z_2}, \tag{6.3}$$

which is a diagonal matrix

$$H_{approx} = -2g(r)\begin{pmatrix} 1 & 0 & 0 & 0 \\ 0 & -1 & 0 & 0 \\ 0 & 0 & -1 & 0 \\ 0 & 0 & 0 & 1 \end{pmatrix}. \tag{6.4}$$

Since this matrix is diagonal, its eigenvectors are represented by the computational basis states $\{\mid ij\rangle;\ \ i,j = 0,1\}$, and its eigenvalues are two double degenerate energy levels $\delta_1 = \delta_2 = -2g(r)$ and $\delta_3 = \delta_4 = 2g(r)$.

To encode the qubit, see Sec. 3.1, we need to apply the already mentioned static magnetic field along the z axis, B_{z_1} on the first particle and B_{z_2} on the second. To single address each qubit, see Sec. 3.2, we apply a magnetic field gradient which allows each particle to be subjected to the additional amplitudes B_{g_1} and B_{g_2} for the first and second spins respectively. The Hamiltonian which describes the interaction between a $\frac{1}{2}$-spin particle and a static magnetic field is given by Eq. (3.16). Therefore, from Eq. (3.16) and Eq. (6.3), the total Hamiltonian which describes two distant buckyballs subjected to static fields along the z axis is

$$H_{tot} = H_{approx} + H_{0_1} + H_{0_2} = -2g(r)\sigma_{z_1}\sigma_{z_2} - \omega_{0_1}\sigma_{z_1} - \omega_{0_2}\sigma_{z_2}, \tag{6.5}$$

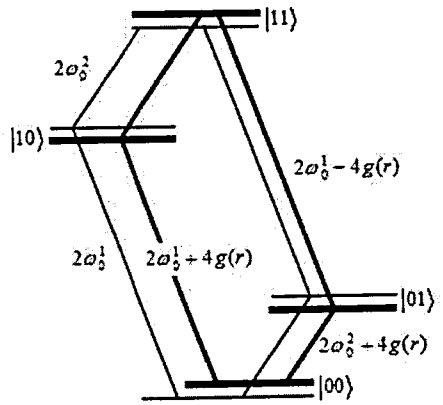

Figure 6.1: Energy-level diagram (in $\hbar$ units) for two uncoupled spins (light lines), and two spins coupled by a Hamiltonian of the form of Eq. (6.5)(solid lines).

where $\omega_{0_{1,2}} = \mu_B B_{0_{1,2}}$ and its matrix form is

$$H_{approx} = \begin{pmatrix} -2g(r) + m_1 & 0 & 0 & 0 \\ 0 & 2g(r) + m_2 & 0 & 0 \\ 0 & 0 & 2g(r) - m_2 & 0 \\ 0 & 0 & 0 & -2g(r) - m_1 \end{pmatrix}, \tag{6.6}$$

where $m_1 = -\omega_{0_1} - \omega_{0_2}$ and $m_2 = -\omega_{0_1} + \omega_{0_2}$. We notice that the approximated matrices (6.4) and (6.6) are respectively equal to matrices (4.14) and (4.18), with the off-diagonal terms dropped. The eigenvectors of matrix (6.6) are the computational basis states and its eigenvalues are given by the elements on the diagonal, i.e. $\lambda_1 = -2g(r) + m_1$, $\lambda_2 = 2g(r) + m_2$, $\lambda_3 = 2g(r) - m_2$, $\lambda_4 = -2g(r) - m_1$. The meaning of the scalar coupling term in Eq. (6.3) is that a spin feels a static magnetic field along the $\pm$z axis produced by the neighboring spins, in addition to the externally applied $B_{z_{1,2}}$ field. This additional field shifts the energy levels as in Fig. (6.1).

6.1 Microwave fields

As described in Sec. 4.1, the state of a $\frac{1}{2}$-spin particle in a static magnetic field B_z directed along the z axis can be manipulated by applying an electromagnetic field $\vec{B}_m(t)$, which rotates in the x-y plane at the resonance frequency $\omega_m = 2\omega_0$. Following the discussion presented in Sec. 5.7, according to experimental limitations , the chosen numerical value for the microwave pulse amplitude is $B_m = 0.28mT$. The Hamiltonian of a single spin interacting with a microwave field is given by Eq. (4.1).

From Eq. (4.11), which describes two uncoupled spins each interacting with a microwave field, and from Eq. (6.3), which describes the mutual interaction for two distant buckyballs, we can write the Hamiltonian of two distant buckyballs subjected to static fields along the z axis and interacting with a microwave field rotating in the x-y plane

$$\begin{aligned} H &= H_{approx} + H_{US} \\ &= -2g(r)\sigma_{z_1}\sigma_{z_2} - \omega_{0_1}\sigma_{z_1} - \omega_{0_2}\sigma_{z_2} \\ &-\omega_{a_1}[\cos(\omega_{m_1}t+\phi)\sigma_{x_1} - \sin(\omega_{m_1}t+\phi)\sigma_{y_1}] \\ &-\omega_{a_2}[\cos(\omega_{m_2}t+\phi)\sigma_{x_2} - \sin(\omega_{m_2}t+\phi)\sigma_{y_2}], \end{aligned} \tag{6.7}$$

where all quantities have the same meaning as in Sec. 4.1.

6.2 Rotating Frame

To simplify the motion of our two-spin system, as in Sec. 4.1, we can perform a change of coordinates for both spins to a system of coordinates rotating at a frequency ω_{0_1} for the first particle and ω_{0_2} for the second, which is defined by

$$|\psi\rangle^{rot} = \exp[-\imath\omega_{0_1}t\sigma_{z_1}]\exp[-\imath\omega_{0_2}t\sigma_{z_2}]\,|\psi\rangle. \tag{6.8}$$

Under this change of coordinates, the uncoupled spin Hamiltonian H_{US} transforms as Eq. (4.12), while the mutual interaction Hamiltonian H_{approx}, Eq. (6.3), is left unchanged because, since its matrix is proportional to $\sigma_{z_1}\sigma_{z_2}$, it obviously commutes with both $\exp[\sigma_{z_1}]$ and $\exp[\sigma_{z_2}]$, which give the matrix structure of the rotating frame transformation, Eq. (6.8).

Therefore, the Hamiltonian of our system in the rotating frame becomes

$$
\begin{aligned}
H &= H_{approx} + H_{US}^{rot} \\
&= -2g(r)\sigma_{z_1}\sigma_{z_2} \\
&-\omega_{a_1}[\cos[(\omega_{m_1} - 2\omega_{0_1})t + \phi]\sigma_{x_1} - \sin[(\omega_{m_1} - 2\omega_{0_1})t + \phi]\sigma_{y_1}] \\
&-\omega_{a_2}[\cos[(\omega_{m_2} - 2\omega_{0_2})t + \phi]\sigma_{x_2} - \sin[(\omega_{m_2} - 2\omega_{0_2})t + \phi]\sigma_{y_2}].
\end{aligned} \tag{6.9}
$$

When the microwave field and the spin resonance frequencies are in resonance, i.e. $\omega_{m_1} = 2\omega_{0_1}$ and $\omega_{m_2} = 2\omega_{0_2}$, the matrix form of the Hamiltonian is given by

$$
H = \begin{pmatrix}
-2g(r) + m_1 & -\omega_{a_2} f & -\omega_{a_1} f & 0 \\
-\omega_{a_2} f^* & 2g(r) + m_2 & 0 & -\omega_{a_1} f \\
-\omega_{a_1} f^* & 0 & 2g(r) - m_2 & -\omega_{a_2} f \\
0 & -\omega_{a_1} f^* & -\omega_{a_2} f^* & -2g(r) - m_1
\end{pmatrix}, \tag{6.10}
$$

where $f = \cos\phi + \imath \sin\phi$ and f^* is its complex conjugate.

6.3 Two-Qubit Gates

The mutual spin dipolar interaction couples the two spins and it gives rise to the most general two-qubit gate. The time evolution operator related to Hamiltonian (6.3), which has the same form in the laboratory frame and the rotating frame, represents the most straightforward two-qubit gate. From Eq. (4.27), the expression of the time evolution operator related to H_{approx} is

$$
U(t) = \exp[2\imath g(r)\sigma_{z_1}\sigma_{z_2}t], \tag{6.11}
$$

and its matrix form is

$$
U(t) = \begin{pmatrix}
e^{2\imath g(r)t} & 0 & 0 & 0 \\
0 & e^{-2\imath g(r)t} & 0 & 0 \\
0 & 0 & e^{-2\imath g(r)t} & 0 \\
0 & 0 & 0 & e^{2\imath g(r)t}
\end{pmatrix}. \tag{6.12}
$$

If we allow this time evolution to occur for a time $t = \frac{\pi}{8g(r)}$, we obtain a *controlled phase gate* up to a $\frac{\pi}{2}$-phase shift on each qubit and an overall and thus irrelevant phase. This treatment is similar to what we did for the refocusing in Eqs. (4.31-4.32). Since in this case the dipolar Hamiltonian is already diagonal, see Eq. (6.3), we do not need to perform the refocusing procedure.

6.3.1 Realization of a π-gate

To obtain the π-gate, we can evaluate ϑ, Eq. (1.51), which combines the phases of each state at the end of the time evolution, or we can perform the complete transformation (4.35) where, in addition to transformation (6.12) with $t = \frac{\pi}{8g(r)}$, we need to carry out a $\frac{\pi}{2}$-rotation about the z axis of the second and first spins.

The set of rotations included in transformation (4.35) can be evaluated following the treatment shown in Sec. 5.3.2. In this case, the controlled phase gate can be achieved by allowing the time-evolution, which is represented by matrix (6.12), to evolve for a time $t = \frac{\pi}{8g(r)}$. Therefore, Eq. (4.35) becomes

$$
\begin{aligned}
G_\pi &= \sqrt{i}\exp[-i\tfrac{\pi}{4}\sigma_{z_1}]\exp[-i\tfrac{\pi}{4}\sigma_{z_2}]U(t=\tfrac{\pi}{8g(r)}) \\
&= \begin{pmatrix} 1 & 0 & 0 & 0 \\ 0 & 1 & 0 & 0 \\ 0 & 0 & 1 & 0 \\ 0 & 0 & 0 & -1 \end{pmatrix},
\end{aligned} \tag{6.13}
$$

where $U(t = \frac{\pi}{8g(r)})$ is obtained by allowing matrix (6.12) to evolve for a time $t = \frac{\pi}{8g(r)}$.

The set of transformations in Eq. (6.13) can be reproduced (up to a global phase equal to $\sqrt{i}$) by solving a set of Schrödinger equations whose Hamiltonians and the related integration times are presented below.

The realization of the controlled phase-gate $U(t = \frac{\pi}{8g(r)})$ is obtained by allowing the system to evolve freely:

$$
H_1(t) = \begin{pmatrix} -2g(r) & 0 & 0 & 0) \\ 0 & 2g(r) & 0 & 0 \\ 0 & 0 & 2g(r) & 0 \\ 0 & 0 & 0 & -2g(r) \end{pmatrix}, \Delta t_1 = \frac{\pi}{8g(r)} \tag{6.14}
$$

$-\frac{\pi}{2}$-rotation about the y axis on the second qubit, $\exp[i\frac{\pi}{4}\sigma_{y_2}]$:

$$
H_2(t) = \begin{pmatrix} -2g(r) & i\omega_{a_2} & 0 & 0) \\ -i\omega_{a_2} & 2g(r) & 0 & 0 \\ 0 & 0 & 2g(r) & i\omega_{a_2} \\ 0 & 0 & -i\omega_{a_2} & -2g(r) \end{pmatrix}, \Delta t_2 = \frac{\pi}{4\mu_B B_{m_2}} \tag{6.15}
$$

$-\frac{\pi}{2}$-rotation on the second qubit about the x axis, $\exp[\imath\frac{\pi}{4}\sigma_{x_2}]$:

$$H_3(t) = \begin{pmatrix} -2g(r) & -\omega_{a_2} & 0 & 0) \\ -\omega_{a_2} & 2g(r) & 0 & 0 \\ 0 & 0 & 2g(r) & -\omega_{a_2} \\ 0 & 0 & -\omega_{a_2} & -2g(r) \end{pmatrix} \quad , \Delta t_3 = \frac{\pi}{4\mu_B B_{m_2}} \tag{6.16}$$

$\frac{\pi}{2}$-rotation on the second qubit about the y axis, $\exp[-\imath\frac{\pi}{4}\sigma_{y_2}]$:

$$H_4(t) = \begin{pmatrix} -2g(r) & -\imath\omega_{a_2} & 0 & 0) \\ \imath\omega_{a_2} & 2g(r) & 0 & 0 \\ 0 & 0 & 2g(r) & -\imath\omega_{a_2} \\ 0 & 0 & \imath\omega_{a_2} & -2g(r) \end{pmatrix} \quad , \Delta t_4 = \frac{\pi}{4\mu_B B_{m_2}} \tag{6.17}$$

$-\frac{\pi}{2}$-rotation about the y axis on the first qubit, $\exp[\imath\frac{\pi}{4}\sigma_{y_1}]$

$$H_5(t) = \begin{pmatrix} -2g(r) & 0 & \imath\omega_{a_1} & 0) \\ 0 & 2g(r) & 0 & \imath\omega_{a_1} \\ -\imath\omega_{a_1} & 0 & 2g(r) & 0 \\ 0 & -\imath\omega_{a_1} & 0 & -2g(r) \end{pmatrix} \quad , \Delta t_5 = \frac{\pi}{4\mu_B B_{m_1}} \tag{6.18}$$

$-\frac{\pi}{2}$-rotation on the first qubit about the x axis, $\exp[\imath\frac{\pi}{4}\sigma_{x_1}]$:

$$H_6(t) = \begin{pmatrix} -2g(r) & 0 & -\omega_{a_1} & 0) \\ 0 & 2g(r) & 0 & -\omega_{a_1} \\ -\omega_{a_1} & 0 & 2g(r) & 0 \\ 0 & -\omega_{a_1} & 0 & -2g(r) \end{pmatrix} \quad , \Delta t_6 = \frac{\pi}{4\mu_B B_{m_1}} \tag{6.19}$$

$\frac{\pi}{2}$-rotation on the first qubit about the y axis, $\exp[-\imath\frac{\pi}{4}\sigma_{y_1}]$:

$$H_7(t) = \begin{pmatrix} -2g(r) & 0 & -\imath\omega_{a_1} & 0) \\ 0 & 2g(r) & 0 & -\imath\omega_{a_1} \\ \imath\omega_{a_1} & 0 & 2g(r) & 0 \\ 0 & \imath\omega_{a_1} & 0 & -2g(r) \end{pmatrix} \quad , \Delta t_7 = \frac{\pi}{4\mu_B B_{m_1}} \tag{6.20}$$

To check the theoretical predictions through the study of the realistic time evolution of the system, we numerically solved the set of Schrödinger equations with Hamiltonians

(6.14-6.20) through the Mathematica programme `Pi-gate-distant.nb`, see App. C.9, which allows us to calculate the realistic matrix intended to reproduce a π-gate. The numerically calculated matrix is the following

(6.21)

$$U_{\pi 2} = \sqrt{i}U_{real}(t_{out})$$

$$\begin{pmatrix} 0.998+0.038i & 0.019+0.020i & 0.020+0.019i & -3\times 10^{-11}+0.001i \\ -0.019+0.020i & 0.998-0.039i & -0.001+3\times 10^{-11}i & 0.019+0.020i \\ -0.020+0.019i & -0.001-1\times 10^{-11}i & 0.998-0.039i & 0.020+0.019i \\ 8\times 10^{-12}+0.001i & 0.019-0.020i & 0.020-0.019i & -0.998-0.039i \end{pmatrix}.$$

From a comparison between the realistic time-evolution matrix (6.21) and the ideal matrix (1.42), we observe that all terms of $U_{\pi 2}$ differs from those of G_π for a phase. These phases are due to the fact that the realistic transformations intended to reproduce single-qubit rotations also contain the spin dipolar coupling term. Theoretically, a single-qubit rotation can be performed by manipulating a microwave field which acts on a single particle. Nevertheless, in the realistic system, the mutual interaction between the two spins is always present and this prevents the exact reproduction of any single-qubit transformation. This subsequently influences the achievement of a perfect π-gate, because by definition its realization includes single-qubit rotations. Values proportional to $10^{-11} - 10^{-12}$ are due to intrinsic errors of the software used to perform the calculations.

In this case, the time required to complete a π-gate is

$$t^{\pi}_{out} = 3\frac{\pi}{4\mu_B B_{m_2}} + 3\frac{\pi}{4\mu_B B_{m_1}} + \frac{\pi}{8g(r)} = 1.84\mu s. \tag{6.22}$$

By calculating the ratio between the operational time t^{π}_{out} and the relaxation time T_2, it is allowed a number of quantum operations equal to $n = T_2/t^{\pi}_{out} \simeq 10^2$. However, in order to apply quantum correcting codes we need to be able to perform a number of operations at least equal to 10^4. Such a limited number of possible quantum operations is due to the value of the operational time t^{π}_{out}. We observe that in this case the time required for performing a π-gate is greater than in the case treated in Chap. 5, see (5.44). The dominant terms in calculating the output time of two-qubit gates are those related to the realization of controlled phase gates, Eq. (6.14), which are proportional to $\frac{1}{g(r)}$. Since in this case the two buckyballs are separated by a larger distance, the spin dipolar coupling constant $g(r)$ acquires a smaller value with respect to Chap.5. This outcome justifies that here we need a longer operational time to perform a π-gate with respect to Chap. 5. However, if the decoherence time T_2 can be increased of two orders of magnitude, the number of allowed quantum operations n would meet the requirements for the application of error correcting

codes. In order to achieve such a value of T_2, we propose to investigate experiments for the study of relaxation processes based on architectures composed of buckyballs in a nanotube. This setup would reduce dipolar interactions between the encased spin and the randomly distributed spins in the sample and the nanotube would represent a further shield for the encased spin against the outer environment.

Also, in this case, we have evaluated the quantum gate fidelity, see Sec. 5.4, with the Mathematica programme `fidelity-pi-gate-distant.nb`, see App. C.11. The minimum quantum gate fidelity which gives the worst numerical value acquired by the gate fidelity is

$$\mathcal{F} = 0.998. \tag{6.23}$$

Since the calculated value of $\mathcal{F}$ differ from the ideal value 1 of a 0.2%, we observe that the realistic transformation $U_{real}(t_{out})$ is in very good agreement with the ideal $\pi-$gate. Therefore, the system considered is higly reliable for reproducing a π-gate through the study of its time evolution when the system is subjected to the set of transformations presented in Eq. (6.13).

6.3.2 Realization of a $CNOT$-gate

To perform a $CNOT$-gate we need to reproduce the set of transformation of Eq. (4.41). These transformations differ from a π-gate for a change of base of the second qubit and a phase shift on the first as in Eq. (4.42). In this case, analogous to Eq. (4.42), the set of transformations required for performing a $CNOT$-gate is the following

$$\begin{aligned} CNOT = \; & \imath \exp[-\imath\tfrac{\pi}{2}\sigma_{z_1}] \exp[\imath\tfrac{\pi}{4}\sigma_{y_2}] \\ & \sqrt{\imath} \exp[-\imath\tfrac{\pi}{4}\sigma_{z_1}] \exp[-\imath\tfrac{\pi}{4}\sigma_{z_2}] U(t = \tfrac{\pi}{8g(r)}) \\ & \exp[-\imath\tfrac{\pi}{4}\sigma_{y_2}] \\ = \; & \exp[\imath\tfrac{3\pi}{4}] \exp[-\imath\tfrac{3\pi}{4}\sigma_{z_1}] \exp[-\imath\tfrac{\pi}{4}\sigma_{z_2}] \exp[\imath\tfrac{\pi}{4}\sigma_{x_2}] \\ & U(t = \tfrac{\pi}{8g(r)}) \\ & \exp[-\imath\tfrac{\pi}{4}\sigma_{y_2}] \\ = \; & \begin{pmatrix} 1 & 0 & 0 & 0 \\ 0 & 1 & 0 & 0 \\ 0 & 0 & 0 & 1 \\ 0 & 0 & 1 & 0 \end{pmatrix}. \end{aligned} \tag{6.24}$$

Therefore, in addition to the realization of a π-gate we need to solve a set of Schrödinger equations which reproduce the needed single-qubit rotations.

Considering Eq.(6.24), the first transformation we need to reproduce is $\exp[-\imath\frac{\pi}{4}\sigma_{y_2}]$. The Hamiltonian which has to be inserted in the related Schrödinger equation for reproducing this transformation and the related integration interval are

$$H_8(t) = H_4(t) = \begin{pmatrix} -2g(r) & -\imath\omega_{a_2} & 0 & 0) \\ \imath\omega_{a_2} & 2g(r) & 0 & 0 \\ 0 & 0 & 2g(r) & -\imath\omega_{a_2} \\ 0 & 0 & \imath\omega_{a_2} & -2g(r) \end{pmatrix} \quad , \Delta t_8 = \Delta t_4 \tag{6.25}$$

In Eq. (6.24), after the realization of a π-gate represented by matrix G_π, we find a $-\frac{\pi}{2}$ rotation of the second qubit about the y axis. The Hamiltonian through which we want to perform this single-qubit rotation and the integration time of the Schrödinger equation are the following

$$H_9(t) = H_2(t) = \begin{pmatrix} -2g(r) & \imath\omega_{a_2} & 0 & 0) \\ -\imath\omega_{a_2} & 2g(r) & 0 & 0 \\ 0 & 0 & 2g(r) & \imath\omega_{a_2} \\ 0 & 0 & -\imath\omega_{a_2} & -2g(r) \end{pmatrix} \quad , \Delta t_9 = \Delta t_2 \tag{6.26}$$

The last transformation required to achieve a $CNOT$-gate up to a global phase $\exp[\imath\frac{\pi}{2}]$, see Eq. (6.24), is a π-rotation of the first qubit about the z axis. Starting from the right, this rotation can be represented by the composition of a $-\frac{\pi}{2}$-rotation about the y axis, followed by a $-\pi$-rotation about the x axis, finally followed by a $\frac{\pi}{2}$-rotation about the y axis, see Eq. (5.4). Therefore, a π-rotation about the z axis of the first spin is performed by the composition of three separate rotations. In order to reproduce this set of rotations, the Hamiltonians which have to be inserted in the Schrödinger equations and the related integration time intervals are presented below.

$-\frac{\pi}{2}$-rotation of the first spin about the y axis:

$$H_{10}(t) = H_5(t) \quad , \Delta t_{10} = \Delta t_5 \tag{6.27}$$

$-\pi$-rotation of the first spin about the x axis:

$$H_{11}(t) = \begin{pmatrix} -2g(r) & 0 & -\omega_{a_1} & 0) \\ 0 & 2g(r) & 0 & -\omega_{a_1} \\ -\omega_{a_1} & 0 & 2g(r) & 0 \\ 0 & -\omega_{a_1} & 0 & -2g(r) \end{pmatrix} \quad , \Delta t_{11} = \frac{\pi}{2\mu_B B_{m_1}} \tag{6.28}$$

$\frac{\pi}{2}$-rotation of the first spin about the y axis:

(6.29) $$H_{12}(t) = H_7(t) \quad , \Delta t_{12} = \Delta t_7$$

With the use of the Mathematica programme `CNOT-gate-distant.nb`, see App. C.10, we numerically calculated the time evolution of the system. The numerical time-evolution matrix intended to reproduce a $CNOT$-gate (up to a global $\exp[\imath\frac{3\pi}{4}]$ phase) is

(6.30)

$$U_{CN_{real}} = \exp[\imath\tfrac{3\pi}{4}]U(t) = \begin{pmatrix} 0.999+0.0572\imath & 0.0196-0.0568\imath & 0.0182+0.0212\imath & 0.0192+0.0003\imath \\ -0.0197-0.0575\imath & 0.9958-0.0592\imath & -0.0199-0.0003\imath & 0.0197+0.0174\imath \\ -0.0185-0.0008\imath & -0.0185+0.0215\imath & -0.0179+0.0585\imath & 0.9969-0.0372\imath \\ -0.0207+0.0170\imath & 0.0192-0.00004\imath & 0.9968+0.0391\imath & 0.0178+0.0593\imath \end{pmatrix}$$

We notice that the realistic time evolution affects each term of $U_{CN_{real}}$ (Eq. (6.30)) by introducing phases different from zero. This prevents the realization of a perfect $CNOT$-gate (Eq. (1.31)). However, in this case, not only is the imperfection in reproducing single-qubit rotations a source of errors, but also the small value of the amplitude of the applied microwave field. Indeed, we have runned the Mathematica programme taking as the amplitude of the microwave field a value larger of one order of magnitude, i.e. $B_m = 0.28 \times 10^{-2}T$. In this case, the source of error is smaller. However, there is an experimental limit which does not allow us to consider an amplitude larger than the chosen one ($B_m = 0.28 \times 10^{-3}T$) because of the limit on the shortest time for realizing a single-qubit rotation [78], see the related discussion in Sec 5.7.

The gate-time, i.e. the time needed to complete a $CNOT$-gate is

(6.31) $$t_{out}^{CNOT} = 5\frac{\pi}{4\mu_B B_{m_2}} + 5\frac{\pi}{4\mu_B B_{m_1}} + \frac{\pi}{2\mu_B B_{m_1}} + \frac{\pi}{8g(r)} = 2.03\mu s.$$

Even for the realization of a $CNOT$-gate the related output time acquires a value greater than in the case treated in Chap. 5, see Eq. (5.51). The order of magnitude of the gate time t_{out}^{CNOT} is determined by the time required for performing the controlled phase gate $U(t = \frac{\pi}{8g(r)})$, Eq. (6.14), which is $t = \frac{\pi}{8g(r)}$. Indeed, this transformation requires a longer time to be performed with respect to single-qubit rotations included in the $CNOT$. Since a larger separation distance between the buckyballs implies a smaller value for the dipolar coupling constant $g(r)$ and since the order of magnitude of the output time is dependent on $\frac{1}{g(r)}$, the outcome of longer operational times is explained.

From a comparison between the operational time $t_{out}^{CNOT} \simeq 2.03\mu s$ and the shortest decoherence time $T_2 \simeq 0.25ms$, we see that it could be possible to perform about $n = T_2/t_{out}^{CNOT} \simeq 10^2$ quantum operations before the system decoheres. This does not allow to meet the requirements for the application of error correcting codes. The limited number of quantum operations n depends on the value of the operational time t_{out}^{CNOT}, which, as discussed above, acquires a value too large with respect to the case treated in Chap 5.

Considering the treatment presented in Sec. 5.4, we calculated the the minimum of the quantum gate fidelity, which allows us to obtain a quantitative evaluation of the degree of agreement between the realistic and theoretical transformations. In this case we have obtained the following numerical value

$$\mathcal{F}_{CN_{real}} = 0.990944. \tag{6.32}$$

This result has been found with the use of Mathematica programme `fidelity-CNOT-gate-distant.nb`, see App. C.12. The difference between the calculated value of $\mathcal{F}$ and the ideal value 1 is less than 1%. Therefore, the realistic transformation, whose output matrix is given by Eq. (6.32), and the ideal $CNOT$-gate (Eq. (1.31)) are in very good agreement.

Finally, from the results obtained for the fidelity related to a π-gate and a $CNOT$-gate, see Eqs.(6.23) and (6.32), we can conclude that the two-buckyball system is highly reliable for performing two-qubit gates. However, since the number of allowed quantum operations before the occurrence of relaxation processes is too small ($n \simeq 10^{-2}$), the system is not suitable for the application of error correcting codes, unless the decoherence time T_2 could be reduced of two orders of magnitude.

6.4 Comments and Considerations

In this section we present comments and considerations on the possibility of realization of single-qubit rotations.

Suppose we want to perform a single-qubit rotation of the first spin. To accomplish the rotation we need a selective spin microwave pulse centered at the precession frequency of spin 1, i.e. $\omega_{p_1} = 2\omega_{0_1}$ (see Chap. 4), and characterized by a frequency bandwidth which has to cover the range of frequencies $2\omega_{0_1} \pm 4g(r)$ and not overlap the range $2\omega_{0_2} \pm 4g(r)$ (which corresponds to the range of frequencies for the excitation of the second spin).

Within the range of frequencies $2\omega_{0_1} \pm 4g(r)$, the first spin is excited, see Fig. 6.1, while the second is unaffected by the microwave pulse.

In this case, the frequency bandwidth is given by the absolute value of the difference between the upper and lower values of the range of frequencies which allow the swap of the selected spin, i.e.

$$\Delta\Omega = \mid 2\omega_{0_1} + 4g(r) - (2\omega_{0_1} - 4g(r)) \mid = 8g(r). \tag{6.33}$$

From Eq. (6.33) we see that the frequency bandwidth is only dependent on the dipole coupling constant $g(r)$. For the particular architecture considered in this chapter we obtain $\Delta\Omega = 8g(r) = 1.9MHz$. As we discussed in Sec. 5.7, since the typical time of a single-spin rotation is $32ns$, according to the bandwidth theorem $\Delta\Omega$ has a too small value. Since $\Delta\Omega$ refers to angular frequencies, here the bandwidth theorem has to be read as $\Delta\Omega\Delta t \simeq 2\pi$. In order to satisfy the bandwidth theorem we have two options

- if $t_{SQ} = 32ns$, the microwave pulse frequency bandwidth should be $\Delta\Omega = 1.96 \times 10^8 Hz$,
- if the microwave pulse frequency bandwidth is $\Delta\Omega = 1.9MHz$, the duration of a single-qubit operation should be $t_{SQ} = 3.3\mu s$.

The first option is preferable because it allows single-qubit operations in a shorter time. Therefore, we present the following comments regarding this favourable configuration.

The frequency bandwidth depends on $g(r)$. Since the time for performing a single-spin rotation is given, the bandwidth theorem allows us to give a constraint on $g(r)$ and consequently on r, the distance between the two encased particles.

According to the bandwidth theorem, since the typical time for performing single qubit rotations is $32ns$, the frequency bandwidth of the microwave pulse (see Eq. (6.33)) has to be $\Delta\Omega = 1.96 \times 10^8 Hz$. From Eq. (6.33), we see that $\Delta\Omega$ depends only on the dipolar coupling constant $g(r)$. These considerations put a constraint on $g(r)$. Therefore, according to the bandwidth theorem, the dipolar coupling constant numerical value has to be $g(r) = 2.45 \times 10^7 Hz$, which implies that the two particles are separated by a distance $r = 1.5nm$. Following [83], the distance between two C_{60} cages in a nanotube is due to Van der Waals forces and is equal to $0.3nm$, while the diameter of a C_{60} is $0.7nm$. This implies that the smallest distance between the two encased particle is $r = 1nm$. As described in Sec. 2.2.1, by attaching functional groups as spacers to $N@C_{60}$ we can achieve the desirable distance $r = 1.5nm$.

However, in order to apply the theory treated in this chapter, i.e. the dipolar Hamiltonian is diagonal in the computational basis, we need to satisfy condition (6.1). Since the calculated value for the coupling constant is $g(r) = 2.45 \times 10^7 Hz$, the difference between the resonance frequencies of the two spins has to be $\Delta\omega_p \geq 10^{10} Hz$. Since we cannot achieve such values for $\Delta\omega_p$ with the addressing scheme presented in Sec. 3.2, we need to consider other possible architectures for the addressing of the spins encased in the buckyballs. The possible alternative architectures for the single addressing of each qubit have been already discussed in Sec. 5.7. Therefore, a well designed Quantum Cellular Automaton or a more steep magnetic field gradient could allow us to set the numerical values of the physical quantities $\Delta\omega_p$ and $g(r)$ in the desirable range and subsequently enable the realization of single-qubit rotations by controlling each single spin.

Chapter 7

Conclusions

In this thesis we have studied a system composed of two endohedral fullerene molecule for the realization of quantum gates. An endohedral fullerene molecule or *buckyball* is composed of a fullerene cage which hosts an atom. The spin of the encased atom encodes a qubit. By applying static and microwave fields we were able to perform quantum gates.

In Chapter 1, we presented an introduction to quantum computation. We presented single-qubit and two-qubit quantum gates, see Secs. 1.2 and 1.3. We presented examples of quantum operations which involve complex sets of quantum gates such as multiple-qubit quantum gates, no-cloning theorem, quantum teleportation and Deutsch algorithm and we introduced DiVincenzo criteria, Secs. 1.4-1.8.

In Chapter 2, we showed the principal features which characterize endohedral fullerene molecules as promising building blocks for quantum computers. We have presented an introduction to the fullerenes' discovery, Sec. 2.1, and an overview on endohedral fullerenes' physical and chemical properties, Sec. 2.2. Among the several features, there is the ability to easily maneuver buckyballs, which could allow the building up of scalable systems, Sec. 2.2.1. Another remarkable feature is the long decoherence time $T_2 \simeq 0.25ms$, which represents an outstanding advantage in comparison with many other physical systems whose short relaxation times limit the realization of quantum computations, Sec. 2.2.2. However, the weakness of systems composed of endohedrals resides in the difficulty of the readout of the spin of the encased atom, Sec. 2.2.3. Recent experiments provide promising results which give hope for the realization of efficient devices for the detection of the encased electron spin [64, 71, 72].

In Chapter 3, we started the theoretical treatment of a system composed of two

$N@C_{60}$ molecules. We presented how the qubit can be encoded in the electron spin of the encased atom by applying static magnetic fields on the whole system, Sec. 3.1. We presented the single-qubit addressing scheme based on the realization of a static magnetic field gradient which allows each of the two spins to be subjected to different static magnetic field amplitudes, and, therefore, to be characterized by different resonance frequencies, Sec. 3.2. Each spin can be addressed by applying microwave fields tuned on to the respective resonance frequency. We introduced an overview on the entanglement by introducing the concept of concurrence, Sec. 3.3. We made calculations of the degree of entanglement acquired by the state describing our two-qubit system during the time evolution for the a time-independent case, Sec. 3.4.1, and for a time-dependent one, Sec. 3.4.2. These calculations show that in both cases the maximum degree of entanglement, which corresponds to the maximum value of concurrence, is reached in a time of the order of $10^{-8}s$. However, the time-dependent case is more convenient for creating entangled states because the maximum value of concurrence is $C(\psi(t_{max})) = 0.96$ which is larger in comparison with the related value in the time-independent case $C(\psi(t_{max})) = 0.88$. Since in the time-dependent case $C(\psi(t_{max}))$ differs from the ideal value 1 of a 4% error, the arising states are highly entangled and very reliable against spin flip transformations. Therefore we could use these states as starting states of quantum gates or consider them as elements of a quantum channel for the safe transport of quantum information.

In Chapter 4, we presented a theoretical model which explains how to realize single-qubit and two-qubit quantum gates. Considering a two buckyball system, where the qubit is encoded in the spin of the encased atom, a single-qubit gate is represented by a rotation of the respective spin, Sec. 4.1. Single-qubit gates can be realized by applying on resonance microwave fields. By making the frequency of the microwave field equal to the resonance frequency of a spin, we can perform rotations on it. On the other hand, to realize a two-qubit gate, the two buckyballs need to be coupled through a mutual interaction, Sec. 4.2. Because the mutual spin dipolar interaction is always present between the two buckyballs, the most general two-qubit gate can be realized by allowing the system to evolve freely in time (only under the action of static magnetic fields needed to encode a qubit and under the naturally present spin dipolar interaction). The first step performed in the realization of two-qubit quantum gates is the refocusing of the Hamiltonian, Sec. 4.3. The refocusing consists of a series of transformations which allows us to remove the effect of the off diagonal terms of the Hamiltonian. With the refocusing procedure, the realization of a $\frac{\pi}{4}$-phase gate is straightforward. Being able to perform single-qubit gates and controlled phase-gates, any other two-qubit gate, such π-gate and a $CNOT$-gate, Sec 4.4, can be realized.

In Chapter 5, we apply the theory described in Chapter 4 to a realistic system. We consider two buckyballs at a distance $r = 1.14nm$. Single-qubit operations can be realized by alternatively selecting the frequency of a microwave field in resonance with the Larmor precession frequency of the spin that we want to rotate, Sec. 5.1. In order to perform the desirable two-qubit gates, Sec. 5.2, we need to reproduce a set of theoretical transformations through this realistic system. To realize single-qubit and two-qubit gates, we study the realistic dynamics of system by solving a set of Schrödinger equations, Sec. 5.3. The Hamiltonian in each Schrödinger equation is constructed following the guidelines given by the theoretical model of Chap. 4. For the realization of a π-gate we considered two approaches, Secs. 5.3.1 and 5.3.2. Through numerical computations, the operational time of a π-gate is $t_{out} = 7.277ns$ through the first approach, and $t^{\pi}_{out} = 7.38ns$ through the second approach. The realization of a $CNOT$-gate, Sec. 5.3.3, is characterized by an output time $t^{CNOT}_{out} = 7.49ns$. Through a comparison between the gate time t^{CNOT}_{out} and the relaxation time T_2 (which is estimated to acquire values up to $0.25ms$), we see that before the occurrence of relaxation processes, a number of quantum of operations of the order of $n = T_2/t^{CNOT}_{out} \simeq 3 \times 10^4$ are allowed. This is a very important result in the frame of error correction. Indeed, it is believed that, in order to be able to apply error correcting codes, we should be able to perform a number of quantum operations of the order of 10^4. To check if the realistic reproduction of these quantum gates is reliable, we calculated the quantum gate fidelity, Sec. 5.4. For each gate we obtained a value of minimum fidelity $\mathcal{F}$ which differs from the ideal value $\mathcal{F} = 1$ by of the order of $10^{-2}\%$. These results show that the realistic system composed of two buckyballs is a highly reliable system for reproducing quantum gates. The small error in the numerical value of the fidelity is due to the imperfect reproduction of single-qubit rotations because of the always present mutual spin dipolar coupling. Finally, since the shortest operational time required for performing a single-qubit rotation is of the order of $t \propto 10^{-2}ns$ and the difference between the resonance frequencies of the two spins is $\Delta\nu \simeq 2MHz$, the bandwidth theorem is not satisfied, Sec. 5.7. To overcome this problem, we would need a difference between the resonance frequencies of the order of $\Delta\nu \geq 100GHz$ or an operational time for the fastest single-qubit rotation of the order of $t \geq 10^{-6}s$.

In Chapter 6, we investigated another realistic system composed of two buckyballs. In this case the two molecules are placed at a distance $r = 7nm$. This allows the difference between the angular resonance frequencies $\Delta\omega_p$ to be much greater than the dipolar coupling constant $g(r)$. This condition simplifies the theoretical treatment by omitting the off diagonal terms in the dipolar Hamiltonian, Secs. 6.1 and 6.2. Since the dipolar Hamiltonian is diagonal, in this case we do not need to perform the refocusing procedure

and the number of transformations required to reproduce a π-gate and a $CNOT$-gate is reduced with respect to the case presented in Chapter 5, Sec. 6.3. Also in this case, through the study of the dynamics of the systems, we have reproduced single-qubit and two-qubit gates with the final goal of realizing a π-gate and a $CNOT$-gate. By solving a set of Schrödinger equations dictated by the theoretical model presented in Chap. 4, we have reproduced these two-qubit quantum gates. The operational time for the reproduction of a π-gate is $t_{out}^{\pi} = 1.84\mu s$ and for a $CNOT$-gate is $t_{out}^{CNOT} = 2.03\mu s$. The difference between the calculated values of the minimum fidelity $\mathcal{F}$ and the ideal value 1 is less than 1% for both quantum gates. These results show that the two-buckyball system is highly reliable for performing quantum gates. In this case an additional source of error is the small value of the amplitude of the microwave field $B_m = 0.28mT$, which is limited by the shortest experimentally achievable operational time for the realization of a single-qubit rotation, Sec. 6.4. Finally, according to the bandwidth theorem the frequency bandwidth $\Delta\nu = 1.9MHz$ acquires a too small value. Therefore, to satisfy the bandwidth theorem we need a frequency bandwidth equal to $\Delta\Omega \geq 3.125 \times 10^7 Hz$.

In conclusion, the system presented in Chap. 5 is preferable because it allows two-quit gates in a shorter time ($t_{out} \propto 10^{-8}s$) and with a better value of minimum fidelity ($\mathcal{F} = 0.999$). Furthermore, in this case the number of operations allowed before the occurrence of relaxation processes is $n \simeq 3 \times 10^4$, which meets the requirements for applying error correcting codes. These results allow the system to be a reliable element for building quantum circuits or quantum channels for the safe transport and manipulation of quantum information. However, the time required for performing single-qubit operations is of the order of $10^{-11}s$. The possibility of realizing a single-qubit rotation in such a short time relies on the technological improvements of ESR and EPR experiments.

On the other hand, in the system presented in Chap. 6 the number of quantum operations realizable before the occurrence of decoherence processes is $n \simeq 10^2$, which does not allow the application of error correcting codes. A number of operations equal to 10^4 can be achieved if the decoherence time T_2 is increased by two orders of magnitude. In order to improve this relaxation time, we suggest to perform experimental studies of endohedral fullerenes in nanotubes. Indeed, this device would reduce the dipolar interactions between the encased spin and the randomly distributed spins in the sample. Furthermore, since a nanotube is a shield for the encased spin, it would provide further protection to it against the outer environment.

Nevertheless, in order to satisfy the bandwidth theorem, for both models we need to provide a single-qubit addressing scheme which would allow the difference between the resonance frequencies to be $\Delta\nu \geq 31.25MHz$ and $\Delta\nu \geq 31.19MHz$ for the first

and second system respectively. A convenient addressing scheme can be represented by a QCA (Quantum Cellular Automaton) with different encased particles in neighbouring fullerenes (which should be characterized by very different values of the gyromagnetic ratio g) or by a device which could realize a more steep magnetic field gradient with respect to that presented in Sec. 3.2.

Appendix A

Calculations

A.1 Single-Spin Schrödinger equation in the Rotating Frame

In this section we show the derivation of the Schrödinger equation in the rotating frame, see Eq. (4.5). If we substitute Eq. (4.3) in the Scrödinger equation (4.4), we obtain the following equation

$$\imath\frac{d}{dt}(\exp[\imath\omega_r t\sigma_z] \mid \psi\rangle^{rot}) = H\exp[\imath\omega_r t\sigma_z] \mid \psi\rangle^{rot}. \tag{A.1}$$

Solving the time derivative in the left hand side of Eq. (A.1) we obtain

$$\begin{aligned}&\imath(\imath\omega_r\sigma_z\exp[\imath\omega_r t\sigma_z] \mid \psi\rangle^{rot} + \exp[\imath\omega_r t\sigma_z]\tfrac{d}{dt} \mid \psi\rangle^{rot})\\ &= -\omega_r\sigma_z\exp[\imath\omega_r t\sigma_z] \mid \psi\rangle^{rot} + \imath\exp[\imath\omega_r t\sigma_z]\tfrac{d}{dt} \mid \psi\rangle^{rot}),\end{aligned} \tag{A.2}$$

and the complete Schrödinger can be arranged as follows

$$\begin{aligned}\imath\exp[\imath\omega_r t\sigma_z]\tfrac{d}{dt} \mid \psi\rangle^{rot} &= (-(\omega_r-\omega_r)\sigma_z - \omega_1[\cos(\omega_m t+\phi)\sigma_x\\ &\quad -\sin(\omega_m t+\phi)\sigma_y])\exp[\imath\omega_r t\sigma_z] \mid \psi\rangle^{rot}.\end{aligned} \tag{A.3}$$

In order to cancel terms $\exp[\imath\omega_r t\sigma_z]$, we need to multiply both sides of Eq. (A.3) on the left by $\exp[-\imath\omega_r t\sigma_z]$. The result of the left hand side of Eq. (A.3) is straightforward. In order to find the result of the right hand side, we need to calculate the following expressions:

$$\exp[-\imath\omega_r t\sigma_z]\sigma_x\exp[\imath\omega_r t\sigma_z], \tag{A.4}$$

and

$$\exp[-\imath\omega_r t\sigma_z]\sigma_y \exp[\imath\omega_r t\sigma_z]. \tag{A.5}$$

We start with transformation (A.4), and here it follows the calculations needed to express it in its explicit form:

$$\exp[-\imath\omega_r t\sigma_z]\sigma_x \exp[\imath\omega_r t\sigma_z] = \tag{A.6}$$

$$= (\cos(\omega_r t) - \imath \sin(\omega_r t)\sigma_z)\sigma_x(\cos(\omega_r t) + \imath \sin(\omega_r t)\sigma_z) \tag{A.7}$$

$$= (\cos^2(\omega_r t) - \sin^2(\omega_r t))\sigma_x + 2\cos(\omega_r t)\sin(\omega_r t)\sigma_y \tag{A.8}$$

$$= \cos(2\omega_r t)\sigma_x + \sin(2\omega_r t)\sigma_y, \tag{A.9}$$

where in (A.7) we used the property of exponential Pauli matrices

$$\begin{aligned} \exp[-\imath\omega_r t\sigma_z] &= \cosh(-\imath\omega_r t) + \sinh(-\imath\omega_r t)\sigma_z \\ &= \cos(-\omega_r t) + \imath \sin(-\omega_r t)\sigma_z \\ &= \cos(\omega_r t) - \imath \sin(\omega_r t)\sigma_z, \end{aligned} \tag{A.10}$$

and in (A.8) we used the following property of Pauli matrices

$$\sigma_z\sigma_x = -\sigma_x\sigma_z = \imath\sigma_y. \tag{A.11}$$

Analogously, we calculate the matrix product (A.5), as follows

$$\exp[-\imath\omega_r t\sigma_z]\sigma_y \exp[\imath\omega_r t\sigma_z] = \tag{A.12}$$

$$= (\cos(\omega_r t) - \imath \sin(\omega_r t)\sigma_z)\sigma_y(\cos(\omega_r t) + \imath \sin(\omega_r t)\sigma_z) \tag{A.13}$$

$$= (\cos^2(\omega_r t) - \sin^2(\omega_r t))\sigma_y - 2\cos(\omega_r t)\sin(\omega_r t)\sigma_x \tag{A.14}$$

$$= \cos(2\omega_r t)\sigma_y - \sin(2\omega_r t)\sigma_x, \tag{A.15}$$

where in (A.14), we used the property

$$\sigma_z\sigma_y = -\sigma_y\sigma_z = -\imath\sigma_x. \tag{A.16}$$

Therefore, considering transformations (A.6-A.9) and (A.12-A.15), the Schrödinger equation can be finally written in the form of Eq. (4.5).

A.2 Dipole-Dipole Hamiltonian in the Rotating Frame

In this section we show the calculations which lead to Eq. (4.25). In order to calculate the explicit expression of transformation (4.24), we need to evaluate the following matrix

products

(A.17) $$\exp[-\imath\omega_{0_1}t\sigma_{z_1}]\exp[-\imath\omega_{0_2}t\sigma_{z_2}]\sigma_{x_1}\sigma_{x_2}\exp[\imath\omega_{0_1}t\sigma_{z_1}]\exp[\imath\omega_{0_2}t\sigma_{z_2}],$$

and

(A.18) $$\exp[-\imath\omega_{0_1}t\sigma_{z_1}]\exp[-\imath\omega_{0_2}t\sigma_{z_2}]\sigma_{y_1}\sigma_{y_2}\exp[\imath\omega_{0_1}t\sigma_{z_1}]\exp[\imath\omega_{0_2}t\sigma_{z_2}].$$

From (A.6-A.9), transformation (A.17) becomes

(A.19) $$(\cos(2\omega_{0_1}t)\sigma_{x_1}+\sin(2\omega_{0_1}t)\sigma_{y_1})(\cos(2\omega_{0_2}t)\sigma_{x_2}+\sin(2\omega_{0_2}t)\sigma_{y_2}),$$

and from (A.12-A.15), we obtain the following expression for (A.18)

(A.20) $$(\cos(2\omega_{0_1}t)\sigma_{y_1}-\sin(2\omega_{0_1}t)\sigma_{x_1})(\cos(2\omega_{0_2}t)\sigma_{y_2}-\sin(2\omega_{0_2}t)\sigma_{x_2}).$$

Summing terms (A.19) and (A.20), we obtain

(A.21)
$$\begin{aligned}&\exp[-\imath\omega_{0_1}t\sigma_{z_1}]\exp[-\imath\omega_{0_2}t\sigma_{z_2}](\sigma_{x_1}\sigma_{x_2}+\sigma_{y_1}\sigma_{y_2})\exp[-\imath\omega_{0_1}t\sigma_{z_1}]\exp[-\imath\omega_{0_2}t\sigma_{z_2}]=\\&=(\cos(2\omega_{0_1}t)\cos(2\omega_{0_2}t)+\sin(2\omega_{0_1}t)\sin(2\omega_{0_2}t))(\sigma_{x_1}\sigma_{x_2}+\sigma_{y_1}\sigma_{y_2})\\&=\cos[(2\omega_{0_1}-2\omega_{0_2})t](\sigma_{x_1}\sigma_{x_2}+\sigma_{y_1}\sigma_{y_2}).\end{aligned}$$

Substituting the previous transformation into (4.13), Eq. (4.25) is proved.

A.3 Refocusing of the Dipole-Dipole Hamiltonian

We show the calculations which allow us to refocus H_{DD} of Eq.(4.13).

Considering matrices $\sigma_{x_1}\sigma_{x_2}$, $\sigma_{y_1}\sigma_{y_2}$ and $\sigma_{z_1}\sigma_{z_2}$, and considering their commutator

(A.22) $$[\sigma_{j_1}\sigma_{j_2},\sigma_{k_1}\sigma_{k_2}],$$

with $i_1, j_1 = x_1, y_1, z_1$ and $i_2, j_2 = x_2, y_2, z_2$. Pauli matrices properties can be condensed into the form

(A.23) $$\sigma_j\sigma_k=-\sigma_k\sigma_j+\delta_{jk}I=\imath\sum_l\epsilon_{jkl}\sigma_l+\delta_{jk}I,$$

where ϵ_{jkl} is antisymmetric with respect to the interchange of any two of its indexes. It is equal to $\epsilon_{jkl}=0$ if the indexes j,k,l are not all different, $\epsilon=1$ if j,k,l is an even

permutation of x, y, z, and $\epsilon_{jkl} = -1$ if j, k, l is an odd permutation of x, y, z. Therefore, commutator in Eq. (A.22) can be evaluated as follows

$$\begin{aligned}
&[\sigma_{j_1}\sigma_{j_2}, \sigma_{k_1}\sigma_{k_2}] = \sigma_{j_1}\sigma_{j_2}\sigma_{k_1}\sigma_{k_2} - \sigma_{k_1}\sigma_{k_2}\sigma_{j_1}\sigma_{j_2} \\
&= \sigma_{j_1}\sigma_{j_2}\sigma_{k_1}\sigma_{k_2} - [(-\sigma_{j_1}\sigma_{k_1})(-\sigma_{j_2}\sigma_{k_2}) = \\
&= \sigma_{j_1}\sigma_{j_2}\sigma_{k_1}\sigma_{k_2} - \sigma_{j_1}\sigma_{j_2}\sigma_{k_1}\sigma_{k_2} = 0.
\end{aligned} \tag{A.24}$$

This shows that matrices $\sigma_{x_1}\sigma_{x_2}$, $\sigma_{y_1}\sigma_{y_2}$ and $\sigma_{z_1}\sigma_{z_2}$ all commute with each other, therefore we can write

$$\exp[-\imath H_{DD}t] = \exp[-\imath g(r)\sigma_{x_1}\sigma_{x_2}t]\exp[-\imath g(r)\sigma_{y_1}\sigma_{y_2}t]\exp[2\imath g(r)\sigma_{z_1}\sigma_{z_2}t], \tag{A.25}$$

from which we obtain

$$\begin{aligned}
&\exp[-\imath\tfrac{\pi}{2}\sigma_{z_2}]\exp[-\imath H_{DD}t]\exp[\imath\tfrac{\pi}{2}\sigma_{z_2}] = \\
&= \exp[-\imath\tfrac{\pi}{2}\sigma_{z_2}]\exp[-\imath g(r)\sigma_{x_1}\sigma_{x_2}t]\exp[\imath\tfrac{\pi}{2}\sigma_{z_2}] \\
&\quad \exp[-\imath\tfrac{\pi}{2}\sigma_{z_2}]\exp[-\imath g(r)\sigma_{y_1}\sigma_{y_2}t]\exp[\imath\tfrac{\pi}{2}\sigma_{z_2}] \\
&\quad \exp[-\imath\tfrac{\pi}{2}\sigma_{z_2}]\exp[2\imath g(r)\sigma_{z_1}\sigma_{z_2}t]\exp[\imath\tfrac{\pi}{2}\sigma_{z_2}].
\end{aligned} \tag{A.26}$$

Since by virtue of the properties of Pauli matrices, see Eqs. (A.10), (A.11) and (A.16), we can write

$$\exp[-\imath g(r)\sigma_{x_1}\sigma_{x_2}t] = \cos[g(r)t] - \imath\sin[g(r)t]\sigma_{x_1}\sigma_{x_2}, \tag{A.27}$$

we obtain

$$\begin{aligned}
&\exp[-\imath\tfrac{\pi}{2}\sigma_{z_2}]\exp[-\imath g(r)\sigma_{x_1}\sigma_{x_2}t]\exp[\imath\tfrac{\pi}{2}\sigma_{z_2}] \\
&= \exp[-\imath\tfrac{\pi}{2}\sigma_{z_2}](\cos[g(r)t] - \imath\sin[g(r)t]\sigma_{x_1}\sigma_{x_2})\exp[\imath\tfrac{\pi}{2}\sigma_{z_2}] \\
&= (\cos[g(r)t] + \imath\sin[g(r)t]\sigma_{x_1}\sigma_{x_2}) = \exp[\imath g(r)\sigma_{x_1}\sigma_{x_2}t],
\end{aligned} \tag{A.28}$$

from which we can see that this transformation allows us to cancel $\exp[-\imath g(r)\sigma_{x_1}\sigma_{x_2}t]$. Since the same holds for $\exp[-\imath g(r)\sigma_{y_1}\sigma_{y_2}t]$, the only term which survives in Eq. (A.26) is $\exp[2\imath g(r)\sigma_{z_1}\sigma_{z_2}t]$. Finally, we show the result of the complete transformation (4.31):

$$\begin{aligned}
U(t) &= \exp[-\imath H_{DD}t]\exp[-\imath\tfrac{\pi}{2}\sigma_{z_2}]\exp[-\imath H_{DD}t]\exp[\imath\tfrac{\pi}{2}\sigma_{z_2}] \\
&= \exp[4\imath g(r)\sigma_{z_1}\sigma_{z_2}t].
\end{aligned} \tag{A.29}$$

A.4 Series of Transformations which Realize a CNOT-gate

We show the explicit matrix products in Eq. (4.42), which lead to the $CNOT$-gate.

First, we show the explicit matrix product of Eq. (4.41)

$$
\begin{aligned}
CNOT = & \imath \begin{pmatrix} -\imath & 0 \\ 0 & \imath \end{pmatrix}_1 \tfrac{1}{\sqrt{2}} \begin{pmatrix} 1 & 1 \\ -1 & 1 \end{pmatrix}_2 \begin{pmatrix} 1 & 0 & 0 & 0 \\ 0 & 1 & 0 & 0 \\ 0 & 0 & 1 & 0 \\ 0 & 0 & 0 & -1 \end{pmatrix} \tfrac{1}{\sqrt{2}} \begin{pmatrix} 1 & -1 \\ 1 & 1 \end{pmatrix}_2 \\
= & \tfrac{1}{2} \begin{pmatrix} 1 & 1 & 0 & 0 \\ -1 & 1 & 0 & 0 \\ 0 & 0 & -1 & -1 \\ 0 & 0 & 1 & -1 \end{pmatrix} \begin{pmatrix} 1 & 0 & 0 & 0 \\ 0 & 1 & 0 & 0 \\ 0 & 0 & 1 & 0 \\ 0 & 0 & 0 & -1 \end{pmatrix} \begin{pmatrix} 1 & -1 & 0 & 0 \\ 1 & 1 & 0 & 0 \\ 0 & 0 & 1 & -1 \\ 0 & 0 & 1 & 1 \end{pmatrix} \qquad \text{(A.30)} \\
= & \begin{pmatrix} 1 & 0 & 0 & 0 \\ 0 & 1 & 0 & 0 \\ 0 & 0 & 0 & 1 \\ 0 & 0 & 1 & 0 \end{pmatrix}.
\end{aligned}
$$

In order to show the equivalence between Eq. (4.41) and Eq. (4.42), we need to focus on the matrix product

$$
\begin{aligned}
M &= \exp[-\imath\tfrac{\pi}{2}\sigma_{z_1}] \exp[\imath\tfrac{\pi}{4}\sigma_{y_2}] \exp[-\imath\tfrac{\pi}{4}\sigma_{z_1}] \exp[-\imath\tfrac{\pi}{4}\sigma_{z_2}] && \text{(A.31)} \\
&= \underbrace{\exp[-\imath\frac{\pi}{2}\sigma_{z_1}] \exp[-\imath\frac{\pi}{4}\sigma_{z_1}]}_{\exp[-\imath\frac{3\pi}{4}\sigma_{z_1}]} \exp[\imath\tfrac{\pi}{4}\sigma_{y_2}] \exp[-\imath\tfrac{\pi}{4}\sigma_{z_2}] && \text{(A.32)} \\
&= \underbrace{\exp[-\imath\frac{3\pi}{4}\sigma_{z_1}]}_{=M_1} \underbrace{\exp[\imath\frac{\pi}{4}\sigma_{y_2}] \exp[-\imath\frac{\pi}{4}\sigma_{z_2}]}_{=M_2}, && \text{(A.33)}
\end{aligned}
$$

where in line (A.32) matrices $\exp[\imath\frac{\pi}{4}\sigma_{y_2}]$ and $\exp[-\imath\frac{\pi}{4}\sigma_{z_1}]$ have been swapped because they commute, since they act on different Hilbert spaces. Considering the following ma-

trix product in line (A.33)

$$M_2 = \exp[\imath\tfrac{\pi}{4}\sigma_{y_2}]\exp[-\imath\tfrac{\pi}{4}\sigma_{z_2}] \tag{A.34}$$

$$= (\tfrac{1}{\sqrt{2}} + \tfrac{\imath}{\sqrt{2}}\sigma_{y_2})(\tfrac{1}{\sqrt{2}} - \tfrac{\imath}{\sqrt{2}}\sigma_{z_2}) \tag{A.35}$$

$$= \tfrac{1}{2} + \underbrace{\frac{\imath}{2}\sigma_{y_2}}_{\frac{1}{2}\sigma_{z_2}\sigma_{x_2}} - \tfrac{\imath}{2}\sigma_{z_2} + \underbrace{\frac{1}{2}\sigma_{y_2}\sigma_{z_2}}_{\frac{\imath}{2}\sigma_{x_2}} \tag{A.36}$$

$$= (\tfrac{1}{\sqrt{2}} - \tfrac{\imath}{\sqrt{2}}\sigma_{z_2})(\tfrac{1}{\sqrt{2}} + \tfrac{\imath}{\sqrt{2}}\sigma_{x_2}) \tag{A.37}$$

$$= \exp[-\imath\tfrac{\pi}{4}\sigma_{z_2}]\exp[\imath\tfrac{\pi}{4}\sigma_{x_2}], \tag{A.38}$$

where in line (A.36) we used properties (A.23) of Pauli matrices. Substituting in Eq. (A.33) the result obtained in line (A.38) for M_2, gives

$$M = M_1 \otimes M_2 = \exp[-\imath\frac{3\pi}{4}\sigma_{z_1}]\exp[-\imath\frac{\pi}{4}\sigma_{z_2}]\exp[\imath\frac{\pi}{4}\sigma_{x_2}], \tag{A.39}$$

and, since $\imath\sqrt{\imath} = \exp[\imath\frac{\pi}{2}]\exp[\imath\frac{\pi}{4}] = \exp[\imath\frac{3\pi}{4}]$, the equivalence between Eq. (4.41) and Eq. (4.42) is verified.

A.5 Realistic Unitary Transformation U

We show the derivation of matrix U, see Sec. 5.4.

Matrix U represents the realistic unitary transformation which acts on the two-buckyball system in order to reproduce a $CNOT$-gate. We present the procedure which allows us to obtain matrix U, starting from the set of Scrödinger equations (5.20-5.27,5.37-5.42,5.45-5.49). The sequence of these Schrödinger equations can be incorporated in only one expression given by

$$\imath\frac{d}{dt} \mid \psi(t)\rangle = U \mid \psi(t)\rangle, \tag{A.40}$$

which is simply the Schrödinger equation of a system described by a wavefunction $\mid \psi(t)\rangle$ and subjected to the unitary transformation U.

We numerically solved the presented set of Schrödinger equations with the use of the Mathematica programme `CNOT.nb`. Choosing a set of initial conditions for coefficients c_α, see Eq. (5.57), the programme allows us to calculate the time evolved coefficients $c_\alpha(t_{out})$, see Eq. (5.69). If we choose the computational basis states as input states,

running the programme for each of these states, the action of the programme provides the following results

(A.41)

$$
\begin{aligned}
&|\psi\rangle = |00\rangle \Rightarrow |\psi\rangle_{out} = c_{11}(t_{out})\,|00\rangle + c_{21}(t_{out})\,|01\rangle + c_{31}(t_{out})\,|10\rangle + c_{41}(t_{out})\,|11\rangle \\
&|\psi\rangle = |01\rangle \Rightarrow |\psi\rangle_{out} = c_{12}(t_{out})\,|00\rangle + c_{22}(t_{out})\,|01\rangle + c_{32}(t_{out})\,|10\rangle + c_{42}(t_{out})\,|11\rangle \\
&|\psi\rangle = |10\rangle \Rightarrow |\psi\rangle_{out} = c_{13}(t_{out})\,|00\rangle + c_{23}(t_{out})\,|01\rangle + c_{33}(t_{out})\,|10\rangle + c_{43}(t_{out})\,|11\rangle \\
&|\psi\rangle = |11\rangle \Rightarrow |\psi\rangle_{out} = c_{14}(t_{out})\,|00\rangle + c_{24}(t_{out})\,|01\rangle + c_{34}(t_{out})\,|10\rangle + c_{44}(t_{out})\,|11\rangle
\end{aligned}
$$

from which matrix U can be reconstructed as follows

(A.42)

$$
U = \begin{pmatrix}
c_{11}(t_{out}) & c_{12}(t_{out}) & c_{13}(t_{out}) & c_{14}(t_{out}) \\
c_{21}(t_{out}) & c_{22}(t_{out}) & c_{23}(t_{out}) & c_{24}(t_{out}) \\
c_{31}(t_{out}) & c_{32}(t_{out}) & c_{33}(t_{out}) & c_{34}(t_{out}) \\
c_{41}(t_{out}) & c_{42}(t_{out}) & c_{43}(t_{out}) & c_{44}(t_{out})
\end{pmatrix}.
$$

Appendix B

Schrödinger equations

B.1 Realization of a $\frac{\pi}{4}$-phase gate

The following set of Schrödinger equations allows to reproduce the refocusing of H_{DD}, Eq. (4.31), which leads to the realization of a $\frac{\pi}{4}$-phase gate, Eq.(4.34). Each of the following sets of differential equations is obtained by substituting the Hamiltonians (5.20-5.27) into the Schrödinger equation, Eq. (5.1).

$-\frac{\pi}{2}$-rotation of the second qubit about the y axis, $\exp[\imath\frac{\pi}{4}\sigma_{y_2}]$:

$$\left.\begin{aligned}
\dot{c}_1(t) &= -\imath(-2g(r)c_1(t) - \imath\omega_{a_2}c_2(t)) \\
\dot{c}_2(t) &= -\imath(\imath\omega_{a_2}c_1(t) + 2g(r)c_2(t) + 2g(r)l(t)c_3(t)) \\
\dot{c}_3(t) &= -\imath(2g(r)l(t)c_2(t) + 2g(r)c_3(t) - \imath\omega_{a_2}c_4(t)) \\
\dot{c}_4(t) &= -\imath(\imath\omega_{a_2}c_3(t) - 2g(r)c_4(t))
\end{aligned}\right\} \Delta t_1 = \frac{\pi}{4\mu_B B_{m_2}} \tag{B.1}$$

π-rotation of the second qubit about the x axis, $\exp[-\imath\frac{\pi}{2}\sigma_{x_2}]$:

$$\left.\begin{aligned}
\dot{c}_1(t) &= -\imath(-2g(r)c_1(t) + \omega_{a_2}c_2(t)) \\
\dot{c}_2(t) &= -\imath(\omega_{a_2}c_1(t) + 2g(r)c_2(t) + 2g(r)l(t)c_3(t)) \\
\dot{c}_3(t) &= -\imath(2g(r)l(t)c_2(t) + 2g(r)c_3(t) + \omega_{a_2}c_4(t)) \\
\dot{c}_4(t) &= -\imath(\omega_{a_2}c_3(t) - 2g(r)c_4(t))
\end{aligned}\right\} \Delta t_2 = \frac{\pi}{2\mu_B B_{m_2}} \tag{B.2}$$

$\frac{\pi}{2}$-rotation of the second qubit about the y axis, $\exp[-\imath\frac{\pi}{4}\sigma_{y_2}]$:

$$\left.\begin{aligned}
\dot{c}_1(t) &= -\imath(-2g(r)c_1(t) + \imath\omega_{a_2}c_2(t)) \\
\dot{c}_2(t) &= -\imath(-\imath\omega_{a_2}c_1(t) + 2g(r)c_2(t) + 2g(r)l(t)c_3(t)) \\
\dot{c}_3(t) &= -\imath(2g(r)l(t)c_2(t) + 2g(r)c_3(t) + \imath\omega_{a_2}c_4(t)) \\
\dot{c}_4(t) &= -\imath(-\imath\omega_{a_2}c_3(t) - 2g(r)c_4(t))
\end{aligned}\right\} \Delta t_3 = \frac{\pi}{4\mu_B B_{m_2}} \tag{B.3}$$

Evolution when the system is subjected to Hamiltonian H_{DD}^{rot}, which is intended to reproduce transformation $U_a(t)$

$$\left.\begin{aligned}
\dot{c}_1(t) &= -\imath(-2g(r)c_1(t)) \\
\dot{c}_2(t) &= -\imath(2g(r)c_2(t) + 2g(r)l(t)c_3(t)) \\
\dot{c}_3(t) &= -\imath(2g(r)l(t)c_2(t) + 2g(r)c_3(t)) \\
\dot{c}_4(t) &= -\imath(-2g(r)c_4(t))
\end{aligned}\right\} \Delta t_4 = \frac{\pi}{16g(r)} \tag{B.4}$$

$-\frac{\pi}{2}$-rotation of the second qubit about the y axis, $\exp[\imath\frac{\pi}{4}\sigma_{y_2}]$:

$$\left.\begin{aligned}
\dot{c}_1(t) &= -\imath(-2g(r)c_1(t) - \imath\omega_{a_2}c_2(t)) \\
\dot{c}_2(t) &= -\imath(\imath\omega_{a_2}c_1(t) + 2g(r)c_2(t) + 2g(r)l(t)c_3(t)) \\
\dot{c}_3(t) &= -\imath(2g(r)l(t)c_2(t) + 2g(r)c_3(t) - \imath\omega_{a_2}c_4(t)) \\
\dot{c}_4(t) &= -\imath(\imath\omega_{a_2}c_3(t) - 2g(r)c_4(t))
\end{aligned}\right\} \Delta t_5 = \frac{\pi}{4\mu_B B_{m_2}} \tag{B.5}$$

$-\pi$-rotation of the second qubit about the x axis, $\exp[\imath\frac{\pi}{2}\sigma_{x_2}]$:

$$\left.\begin{aligned}
\dot{c}_1(t) &= -\imath(-2g(r)c_1(t) - \omega_{a_2}c_2(t)) \\
\dot{c}_2(t) &= -\imath(-\omega_{a_2}c_1(t) + 2g(r)c_2(t) + 2g(r)l(t)c_3(t)) \\
\dot{c}_3(t) &= -\imath(2g(r)l(t)c_2(t) + 2g(r)c_3(t) - \omega_{a_2}c_4(t)) \\
\dot{c}_4(t) &= -\imath(-\omega_{a_2}c_3(t) - 2g(r)c_4(t))
\end{aligned}\right\} \Delta t_6 = \frac{\pi}{2\mu_B B_{m_2}} \tag{B.6}$$

$\frac{\pi}{2}$-rotation of the second qubit about the y axis, $\exp[-\imath\frac{\pi}{4}\sigma_{y_2}]$:

$$\left.\begin{aligned}
\dot{c}_1(t) &= -\imath(-2g(r)c_1(t) + \imath\omega_{a_2}c_2(t)) \\
\dot{c}_2(t) &= -\imath(-\imath\omega_{a_2}c_1(t) + 2g(r)c_2(t) + 2g(r)l(t)c_3(t)) \\
\dot{c}_3(t) &= -\imath(2g(r)l(t)c_2(t) + 2g(r)c_3(t) + \imath\omega_{a_2}c_4(t)) \\
\dot{c}_4(t) &= -\imath(-\imath\omega_{a_2}c_3(t) - 2g(r)c_4(t))
\end{aligned}\right\} \Delta t_7 = \frac{\pi}{4\mu_B B_{m_2}} \tag{B.7}$$

Evolution when the system is subjected to Hamiltonian H_{DD}^{rot}, which is intended to reproduce transformation $U_b(t)$

$$\left.\begin{aligned}
\dot{c}_1(t) &= -\imath(-2g(r)c_1(t)) \\
\dot{c}_2(t) &= -\imath(2g(r)c_2(t) + 2g(r)l(t)c_3(t)) \\
\dot{c}_3(t) &= -\imath(2g(r)l(t)c_2(t) + 2g(r)c_3(t)) \\
\dot{c}_4(t) &= -\imath(-2g(r)c_4(t))
\end{aligned}\right\} \Delta t_8 = \frac{\pi}{16g(r)} \tag{B.8}$$

B.2 Realization of a π-gate

We present the set of Schrödinger equations obtained by substituting the Hamiltonians (5.37-5.42). The solution of these sets of differential equations, in addition to the solution of Eqs. (B.1-B.8), are intended to reproduce a π-gate, which is defined by Eq. (4.35).

$-\frac{\pi}{2}$-rotation about the y axis on the second qubit, $\exp[\imath\frac{\pi}{4}\sigma_{y_2}]$:

$$\left.\begin{aligned}
\dot{c}_1(t) &= -\imath(-2g(r)c_1(t) - \imath\omega_{a_2}c_2(t)) \\
\dot{c}_2(t) &= -\imath(\imath\omega_{a_2}c_1(t) + 2g(r)c_2(t) + 2g(r)l(t)c_3(t)) \\
\dot{c}_3(t) &= -\imath(2g(r)l(t)c_2(t) + 2g(r)c_3(t) - \imath\omega_{a_2}c_4(t)) \\
\dot{c}_4(t) &= -\imath(\imath\omega_{a_2}c_3(t) - 2g(r)c_4(t))
\end{aligned}\right\} \Delta t_9 = \frac{\pi}{4\mu_B B_{m_2}} \tag{B.9}$$

$-\frac{\pi}{2}$-rotation on the second qubit about the x axis, $\exp[\imath\frac{\pi}{4}\sigma_{x_2}]$:

$$\left.\begin{aligned}
\dot{c}_1(t) &= -\imath(-2g(r)c_1(t) - \omega_{a_2}c_2(t)) \\
\dot{c}_2(t) &= -\imath(-\omega_{a_2}c_1(t) + 2g(r)c_2(t) + 2g(r)l(t)c_3(t)) \\
\dot{c}_3(t) &= -\imath(2g(r)l(t)c_2(t) + 2g(r)c_3(t) - \omega_{a_2}c_4(t)) \\
\dot{c}_4(t) &= -\imath(-\omega_{a_2}c_3(t) - 2g(r)c_4(t))
\end{aligned}\right\} \Delta t_{10} = \frac{\pi}{4\mu_B B_{m_2}} \tag{B.10}$$

$\frac{\pi}{2}$-rotation on the second qubit about the y axis, $\exp[-\imath\frac{\pi}{4}\sigma_{y_2}]$:

$$\left.\begin{aligned}
\dot{c}_1(t) &= -\imath(-2g(r)c_1(t) + \imath\omega_{a_2}c_2(t)) \\
\dot{c}_2(t) &= -\imath(-\imath\omega_{a_2}c_1(t) + 2g(r)c_2(t) + 2g(r)l(t)c_3(t)) \\
\dot{c}_3(t) &= -\imath(2g(r)l(t)c_2(t) + 2g(r)c_3(t) + \imath\omega_{a_2}c_4(t)) \\
\dot{c}_4(t) &= -\imath(-\imath\omega_{a_2}c_3(t) - 2g(r)c_4(t))
\end{aligned}\right\} \Delta t_{11} = \frac{\pi}{4\mu_B B_{m_2}} \tag{B.11}$$

$-\frac{\pi}{2}$-rotation about the y axis on the first qubit, $\exp[\imath\frac{\pi}{4}\sigma_{y_1}]$

$$\left.\begin{aligned}
\dot{c}_1(t) &= -\imath(-2g(r)c_1(t) - \imath\omega_{a_1}c_3(t)) \\
\dot{c}_2(t) &= -\imath(2g(r)c_2(t) + 2g(r)l(t)c_3(t) - \imath\omega_{a_1}c_4(t)+) \\
\dot{c}_3(t) &= -\imath(\imath\omega_{a_1}c_1(t) + 2g(r)l(t)c_2(t) + 2g(r)c_3(t)) \\
\dot{c}_4(t) &= -\imath(\imath\omega_{a_1}c_2(t) - 2g(r)c_4(t))
\end{aligned}\right\} \Delta t_{12} = \frac{\pi}{4\mu_B B_{m_1}} \tag{B.12}$$

$-\frac{\pi}{2}$-rotation on the first qubit about the x axis, $\exp[\imath\frac{\pi}{4}\sigma_{x_1}]$:

$$\left.\begin{aligned}
\dot{c}_1(t) &= -\imath(-2g(r)c_1(t) - \omega_{a_1}c_3(t)) \\
\dot{c}_2(t) &= -\imath(2g(r)c_2(t) + 2g(r)l(t)c_3(t) + \omega_{a_1}c_4(t)) \\
\dot{c}_3(t) &= -\imath(\omega_{a_1}c_1(t) + 2g(r)l(t)c_2(t) + 2g(r)c_3(t)) \\
\dot{c}_4(t) &= -\imath(-\omega_{a_1}c_2(t) - 2g(r)c_4(t))
\end{aligned}\right\} \Delta t_{13} = \frac{\pi}{4\mu_B B_{m_1}} \tag{B.13}$$

$\frac{\pi}{2}$-rotation on the first qubit about the y axis, $\exp[-\imath\frac{\pi}{4}\sigma_{y_1}]$:

$$\left.\begin{aligned}
\dot{c}_1(t) &= -\imath(-2g(r)c_1(t) + \imath\omega_{a_1}c_3(t)) \\
\dot{c}_2(t) &= -\imath(2g(r)c_2(t) + 2g(r)l(t)c_3(t) + \imath\omega_{a_1}c_4(t)) \\
\dot{c}_3(t) &= -\imath(-\imath\omega_{a_1}c_1(t) + 2g(r)l(t)c_2(t) + 2g(r)c_3(t)) \\
\dot{c}_4(t) &= -\imath(-\imath\omega_{a_1}c_2(t) - 2g(r)c_4(t))
\end{aligned}\right\} \Delta t_{14} = \frac{\pi}{4\mu_B B_{m_1}} \tag{B.14}$$

B.3 Realization of a $CNOT$-gate

In this section we present the last sets of Schrödinger equations for the realization of a $CNOT$-gate. The solution of the following differential equations, together with the solution of Eqs. (B.1-B.8) and of Eqs. (B.9-B.14), performs the transformations included in Eq. (4.42). These differential equations are obtained by considering the Hamiltonians (5.45-5.49).

The Schrödinger equation, whose solution allows to reproduce a $\frac{\pi}{2}$ rotation of the second qubit about the y axis, is given by the following:

$$\left.\begin{aligned}
\dot{c}_1(t) &= -\imath(-2g(r)c_1(t) + \imath\omega_{a_2}c_2(t)) \\
\dot{c}_2(t) &= -\imath(-\imath\omega_{a_2}c_1(t) + 2g(r)c_2(t) + 2g(r)l(t)c_3(t)) \\
\dot{c}_3(t) &= -\imath(2g(r)l(t)c_2(t) + 2g(r)c_3(t) + \imath\omega_{a_2}c_4(t)) \\
\dot{c}_4(t) &= -\imath(-\imath\omega_{a_2}c_3(t) - 2g(r)c_4(t)).
\end{aligned}\right\} \Delta t_{15} = \frac{\pi}{4\mu_B B_{m_2}} \tag{B.15}$$

After the transformation represented by G_π (Eq. (4.41)) we find a $-\frac{\pi}{2}$ rotation about the y axis of the second qubit. This transformation can be reproduced with all the same choices made for the realization of a $\frac{\pi}{2}$ rotation about the y axis, with a different choice of $\phi = -\frac{\pi}{2}$. The resulting Scrödinger equation gives the following set of differential equations:

$$\left.\begin{aligned}
\dot{c}_1(t) &= -\imath(-2g(r)c_1(t) - \imath\omega_{a_2}c_2(t)) \\
\dot{c}_2(t) &= -\imath(\imath\omega_{a_2}c_1(t) + 2g(r)c_2(t) + 2g(r)l(t)c_3(t)) \\
\dot{c}_3(t) &= -\imath(2g(r)l(t)c_2(t) + 2g(r)c_3(t) - \imath\omega_{a_2}c_4(t)) \\
\dot{c}_4(t) &= -\imath(\imath\omega_{a_2}c_3(t) - 2g(r)c_4(t))
\end{aligned}\right\} \Delta t_{16} = \frac{\pi}{4\mu_B B_{m_2}} \tag{B.16}$$

In order to complete the procedure which allows us to perform a $CNOT$-gate up to a global phase $\exp[\imath\frac{\pi}{2}]$, we need to reproduce the last transformation in Eq. (6.24) which is represented by a π rotation about the z axis on the first qubit. The set of Scrhödinger equations which represent a π-rotation about the z axis of the first qubit is the following:

$-\frac{\pi}{2}$-rotation about the y axis:

$$\left.\begin{aligned}
\dot{c}_1(t) &= -\imath(-2g(r)c_1(t) - \imath\omega_{a_1}c_3(t)) \\
\dot{c}_2(t) &= -\imath(2g(r)c_2(t) + 2g(r)l(t)c_3(t) - \imath\omega_{a_1}c_4(t)+) \\
\dot{c}_3(t) &= -\imath(\imath\omega_{a_1}c_1(t) + 2g(r)l(t)c_2(t) + 2g(r)c_3(t)) \\
\dot{c}_4(t) &= -\imath(\imath\omega_{a_1}c_2(t) - 2g(r)c_4(t))
\end{aligned}\right\} \Delta t_{17} = \frac{\pi}{4\mu_B B_{m_1}} \tag{B.17}$$

$-\pi$-rotation about the x axis:

$$\left.\begin{aligned}
\dot{c}_1(t) &= -\imath(-2g(r)c_1(t) - \omega_{a_1}c_3(t)) \\
\dot{c}_2(t) &= -\imath(2g(r)c_2(t) + 2g(r)l(t)c_3(t) + \omega_{a_1}c_4(t)) \\
\dot{c}_3(t) &= -\imath(\omega_{a_1}c_1(t) + 2g(r)l(t)c_2(t) + 2g(r)c_3(t)) \\
\dot{c}_4(t) &= -\imath(-\omega_{a_1}c_2(t) - 2g(r)c_4(t))
\end{aligned}\right\} \Delta t_{18} = \frac{\pi}{2\mu_B B_{m_1}} \tag{B.18}$$

$\frac{\pi}{2}$-rotation about the y axis:

$$\left.\begin{aligned}
\dot{c}_1(t) &= -\imath(-2g(r)c_1(t) + \imath\omega_{a_1}c_3(t)) \\
\dot{c}_2(t) &= -\imath(2g(r)c_2(t) + 2g(r)l(t)c_3(t) + \imath\omega_{a_1}c_4(t)) \\
\dot{c}_3(t) &= -\imath(-\imath\omega_{a_1}c_1(t) + 2g(r)l(t)c_2(t) + 2g(r)c_3(t)) \\
\dot{c}_4(t) &= -\imath(-\imath\omega_{a_1}c_2(t) - 2g(r)c_4(t))
\end{aligned}\right\} \Delta t_{19} = \frac{\pi}{4\mu_B B_{m_1}} \tag{B.19}$$

Appendix C

Mathematica programmes

C.1 concurrence-time-independent.nb

$\text{mo} = 9.10939 * 10^{-31};$

$\text{lo} = 1.88973 * 10^{10};$

$\text{to} = 4.13414 * 10^{16};$

$\text{Vo} = 0.0367493;$

$\text{mb} = 9.27402 * 10^{-24};$

$\text{no} = 0.000669176;$

$\text{q} = 1.60218 * 10^{-19};$

$\text{h} = 1.05459 * 10^{-34};$

$\text{teso} = 4.25438 * 10^{-6};$

$\omega_1 = 1.75986\,10^{10}/\text{to};$

$\omega_2 = 1.75772\,10^{10}/\text{to};$

$\nu_1 = 1;$

$\nu_2 = \omega_2/\omega_1;$

$r = 1.14 * 10^{-9} * (\text{lo});$

$\mu = 1/2;$

$n = \text{no}/(4 * \pi);$

$\text{gr} = \mu 2 * n/(r3);$

$B_1 = \left(1000 * 10^{-4} + 0.0000608\right) * \text{teso};$

$B_2 = \left(1000 * 10^{-4} - 0.0000608\right) * \text{teso};$

$\mathrm{m1} = -\mu(B_1 + B_2);$
$\mathrm{m2} = -\mu(B_1 - B_2);$
$G = \omega_1;$

solution1 =
NDSolve[
$\{y'[t] == -\frac{1}{G}((\mathrm{gr} + \mathrm{m1}) * y[t] - 3 * \mathrm{gr} * p[t]),$
$x'[t] == -\frac{1}{G}((-\mathrm{gr} + \mathrm{m2}) * x[t] - \mathrm{gr} * z[t]),$
$z'[t] == -\frac{1}{G}((-\mathrm{gr} - \mathrm{m2}) * z[t] - \mathrm{gr} * x[t]),$
$p'[t] == -\frac{1}{G} * ((\mathrm{gr} - \mathrm{m1}) * p[t] - 3 * \mathrm{gr} * y[t]),$
$y[0] == 1/3, x[0] == \mathrm{Sqrt}[7/2]/3, z[0] == 1/3, p[0] == \mathrm{Sqrt}[7/2]/3\},$
$\{y[t], x[t], z[t], p[t]\}, \{t, 0, 10000\}, \mathrm{MaxSteps} \rightarrow 1000000]$
$c =$
Plot[
Evaluate[
$2 * \mathrm{Abs}[(\mathrm{Conjugate}[x[t]] * \mathrm{Conjugate}[z[t]]) - (\mathrm{Conjugate}[y[t]] * \mathrm{Conjugate}[p[t]])]/$
$(\mathrm{Abs}[y[t]]2 + \mathrm{Abs}[x[t]]2 + \mathrm{Abs}[z[t]]2 + \mathrm{Abs}[p[t]]2)/.\mathrm{solution1}], \{t, 0, 200\},$
$\mathrm{PlotRange} \rightarrow \{\{0, 173\}, \{0, 1\}\}, \mathrm{FrameTicks} \rightarrow \mathrm{Automatic},$
$\mathrm{FrameLabel} \rightarrow \{\text{"time (atomic units)"}, "C(\psi)",$
$\mathrm{None}, \mathrm{None}\}, \mathrm{Frame} \rightarrow \mathrm{True}]$

C.2 concurrence-time-dependent.nb

$\mathrm{mo} = 9.10939 * 10^{-31};$
$\mathrm{lo} = 1.88973 * 10^{10};$
$\mathrm{to} = 4.13414 * 10^{16};$
$\mathrm{Vo} = 0.0367493;$

$$\text{mb} = 9.27402 * 10^{-24};$$
$$\text{no} = 0.000669176;$$
$$\text{q} = 1.60218 * 10^{-19};$$
$$\text{h} = 1.05459 * 10^{-34};$$
$$\text{teso} = 4.25438 * 10^{-6};$$
$$\omega_1 = 1.75986\,10^{10}/\text{to};$$
$$\omega_2 = 1.75772\,10^{10}/\text{to};$$
$$\nu_1 = 1;$$
$$\nu_2 = \omega_2/\omega_1;$$
$$r = 1.14 * 10^{-9} * (\text{lo});$$
$$\mu = 1/2;$$
$$n = \text{no}/(4 * \pi);$$
$$\text{gr} = \mu 2 * n/(r3);$$
$$B_1 = \left(1000 * 10^{-4} + 0.0000608\right) * \text{teso};$$
$$B_2 = \left(1000 * 10^{-4} - 0.0000608\right) * \text{teso};$$
$$\text{B11} = 3 * 10^{-4} * \text{teso};$$
$$\text{B12} = 3 * 10^{-4} * \text{teso};;$$
$$\text{m1} = -\mu(B_1 + B_2);$$
$$\text{m2} = -\mu(B_1 - B_2);$$
$$G = \omega_1;$$

$$\text{solution1} =$$
$$\text{NDSolve}[$$
$$\{y'[t] ==$$
$$-\tfrac{\imath}{G}((\text{gr} + \text{m1}) * y[t]$$
$$-\mu * \text{B12} * (\cos[\nu_2 * t + \gamma/\omega_1] - \imath * \cos[\nu_2 * t + \gamma/\omega_1]) * x[t] -$$
$$\mu * \text{B11} * (\cos[\nu_1 * t + \gamma/\omega_1] - \imath * \cos[\nu_1 * t + \gamma/\omega_1]) * z[t]$$
$$-3 * \text{gr} * p[t]),$$
$$x'[t] == -\tfrac{\imath}{G}((-\text{gr} + \text{m2}) * x[t] -$$
$$\mu * \text{B12} * (\cos[\nu_2 * t + \gamma/\omega_1] + \imath * \cos[\nu_2 * t + \gamma/\omega_1]) * y[t]$$
$$-\text{gr} * z[t] -$$
$$\mu * \text{B11} * (\cos[\nu_1 * t + \gamma/\omega_1] - \imath * \cos[\nu_1 * t + \gamma/\omega_1]) * p[t]),$$

$z'[t] == -\frac{\imath}{G}((-\text{gr} - \text{m2}) * z[t] -$
$\mu * \text{B11} * (\cos[\nu_1 * t + \gamma/\omega_1] + \imath * \cos[\nu_1 * t + \gamma/\omega_1]) * y[t]$
$-\text{gr} * x[t] -$
$\mu * \text{B12} * (\cos[\nu_2 * t + \gamma/\omega_1] - \imath * \cos[\nu_2 * t + \gamma/\omega_1]) * p[t]),$
$p'[t] == -\frac{\imath}{G} * ((\text{gr} - \text{m1}) * p[t] -$
$\mu * \text{B11} * (\cos[\nu_1 * t + \gamma/\omega_1] + \imath * \cos[\nu_1 * t + \gamma/\omega_1]) * x[t]$
$-3 * \text{gr} * y[t] -$
$\mu * \text{B12} * (\cos[\nu_2 * t + \gamma/\omega_1] + \imath * \cos[\nu_2 * t + \gamma/\omega_1]) * z[t]),$
$y[0] == 1/3, x[0] == \text{Sqrt}[7/2]/3, z[0] == 1/3, p[0] == \text{Sqrt}[7/2]/3\},$
$\{y[t], x[t], z[t], p[t]\}, \{t, 0, 10000\},$
$\text{MaxSteps} \rightarrow 1000000]$
$c =$
Plot[
Evaluate[
$2 * \text{Abs}[(\text{Conjugate}[x[t]] * \text{Conjugate}[z[t]]) - (\text{Conjugate}[y[t]] * \text{Conjugate}[p[t]])]/$
$(\text{Abs}[y[t]]2 + \text{Abs}[x[t]]2 + \text{Abs}[z[t]]2 + \text{Abs}[p[t]]2)/.\text{solution1}], \{t, 0, 200\},$
$\text{PlotRange} \rightarrow \{\{0, 173\}, \{0, 1\}\}, \text{FrameTicks} \rightarrow \text{Automatic},$
$\text{FrameLabel} \rightarrow \{"time(atomicunits)", "C(\psi)",$
$\text{None}, \text{None}\}, \text{Frame} \rightarrow \text{True}]$

C.3 Phase-gate.nb

$\text{mo} = 9.10939 * 10^{-31};$
$\text{lo} = 1.88973 * 10^{10};$
$\text{to} = 4.13414 * 10^{16};$
$\text{Vo} = 0.0367493;$
$\text{mb} = 9.27402 * 10^{-24};$
$\text{no} = 0.000669176;$
$\text{q} = 1.60218 * 10^{-19};$

$$\mathrm{h} = 1.05459 * 10^{-34};$$
$$\mathrm{teso} = 4.25438 * 10^{-6};$$
$$\mathrm{r} = 1.14 * 10^{-9} * (\mathrm{lo});$$
$$\mu = 1/2;$$
$$n = \mathrm{no}/(4 * \pi);$$
$$\mathrm{gr} = \mu 2 * n/(r3);$$
$$\mathrm{B01} = (0.3 + 0.0000304) * \mathrm{teso};$$
$$\mathrm{B02} = (0.3 - 0.0000304) * \mathrm{teso};$$
$$\mathrm{B1} = 0.5 * \mathrm{teso};$$
$$\mathrm{BM} = 0.5 * \mathrm{teso};$$
$$\mathrm{BT} = \{\mathrm{BM}, \mathrm{BM}, \mathrm{BM}, 0, \mathrm{BM}, \mathrm{BM}, \mathrm{BM}, 0\};$$
$$\mathrm{BN} = \{0, 0, 0, 0, 0, 0, 0, 0\};$$
$$\mathrm{time} = \{0, \pi/(4 * \mu * \mathrm{BM}) * G, \pi/(2 * \mu * \mathrm{BM}) * G,$$
$$\pi/(4 * \mu * \mathrm{BM}) * G, \pi/(16 * \mathrm{gr}) * G, \pi/(4 * \mu * \mathrm{BM}) * G,$$
$$\pi/(2 * \mu * \mathrm{BM}) * G, \pi/(4 * \mu * \mathrm{BM}) * G, \pi/(4 * \mu * \mathrm{BM}) * G,$$
$$\pi/(4 * \mu * \mathrm{BM}) * G, \pi/(4 * \mu * \mathrm{BM}) * G, \pi/(4 * \mu * \mathrm{BM}) * G,$$
$$\pi/(4 * \mu * \mathrm{B1}) * G, \pi/(4 * \mu * \mathrm{B1}) * G\};$$
$$\mathrm{tintb} = \{\pi/(4 * \mu * \mathrm{BM}) * G, \pi/(2 * \mu * \mathrm{BM}) * G,$$
$$\pi/(4 * \mu * \mathrm{BM}) * G, \pi/(16 * \mathrm{gr}) * G, \pi/(4 * \mu * \mathrm{BM}) * G,$$
$$\pi/(2 * \mu * \mathrm{BM}) * G, \pi/(4 * \mu * \mathrm{BM}) * G, \pi/(16 * \mathrm{gr}) * G,$$
$$\pi/(4 * \mu * \mathrm{BM}) * G, \pi/(4 * \mu * \mathrm{BM}) * G, \pi/(4 * \mu * \mathrm{BM}) * G,$$
$$\pi/(4 * \mu * \mathrm{B1}) * G, \pi/(4 * \mu * \mathrm{B1}) * G, \pi/(4 * \mu * \mathrm{B1}) * G, \pi/(4 * \mu * \mathrm{BM}) * G,$$
$$\pi/(4 * \mu * \mathrm{B1}) * G, \pi/(2 * \mu * \mathrm{B1}) * G, \pi/(4 * \mu * \mathrm{B1}) * G\};$$
$$\phi = \{-\pi/2, \pi, \pi/2, \pi/2, -\pi/2, 0, \pi/2, \pi/2, -\pi/2, -\pi/2, 0, \pi/2\};$$
$$\alpha = (2 * \mathrm{mb} * \mathrm{B01}/\mathrm{teso}/h)/\mathrm{to};$$
$$\beta = (2 * \mathrm{mb} * \mathrm{B02}/\mathrm{teso}/h)/\mathrm{to};$$
$$G = \alpha;$$
$$\omega 1 = \alpha/\alpha;$$
$$\omega 2 = \beta/\alpha;$$

```
For[b1 = {0, a1, a1, a1, a1, a1, a1, a1};
b2 = {0, a2, a2, a2, a2, a2, a2, a2};
b3 = {1, a3, a3, a3, a3, a3, a3, a3};
b4 = {0, a4, a4, a4, a4, a4, a4, a4};
ta = 0; tb = 0; i = 1, i < 9,
φ[[i]];
BT[[i]];
BN[[i]];
tintb[[i]];
tb+ = tintb[[i]];
n12[t_] = −μ * BN[[i]](cos[φ[[i]]] + I * sin[φ[[i]]]);
n11[t_] = −μ * BN[[i]](cos[φ[[i]]] − I * sin[φ[[i]]]);
n22[t_] = −μ * BT[[i]](cos[φ[[i]]] + I * sin[φ[[i]]]);
n21[t_] = −μ * BT[[i]](cos[φ[[i]]] − I * sin[φ[[i]]]);
solution1 = NDSolve[{
y'[t] ==
−i/G((−2 * gr) * y[t] + n22[t_] * x[t] + n12[t_] * z[t]),
x'[t] ==
−i/G(n21[t_] * y[t] + (2 * gr) * x[t] + 2 * gr * cos[(ω1 − ω2) * t] * z[t] + n12[t_] * p[t]),
z'[t] ==
−i/G(n11[t_] * y[t] + 2 * gr * cos[(ω1 − ω2) * t] * x[t] + (2 * gr) * z[t] + n22[t_] * p[t]),
p'[t] ==
−i/G(n11[t_] * x[t] + n21[t_] * z[t] − (2 * gr) * p[t]),
y[0] == b1[[i]], x[0] == b2[[i]], z[0] == b3[[i]],
p[0] == b4[[i]]}, {y[t], x[t], z[t], p[t]},
{t, 0, tintb[[i]]}, MaxSteps → 1000000];
a11 = y[t]/.solution1/.t → tintb[[i]];
a21 = x[t]/.solution1/.t → tintb[[i]];
a31 = z[t]/.solution1/.t → tintb[[i]];
a41 = p[t]/.solution1/.t− > tintb[[i]];
```

a1 = a11[[1]];
a2 = a21[[1]];
a3 = a31[[1]];
a4 = a41[[1]];
$i++$]
a1a = a1;
a2a = a2;
a3a = a3;
a4a = a4;
a1a
a2a
a3a
a4a

C.4 Pi-gate.nb

mo = $9.10939 * 10^{-31}$;
lo = $1.88973 * 10^{10}$;
to = $4.13414 * 10^{16}$;
Vo = 0.0367493;
mb = $9.27402 * 10^{-24}$;
no = 0.000669176;
q = $1.60218 * 10^{-19}$;
h = $1.05459 * 10^{-34}$;
teso = $4.25438 * 10^{-6}$;
r = $1.14 * 10^{-9} * (lo)$;
$\mu = 1/2$;
$n = no/(4 * \pi)$;
gr = $\mu 2 * n/(r3)$;

B01 = (0.3 + 0.0000304) * teso;
B02 = (0.3 − 0.0000304) * teso;
B1 = 0.5 * teso;
BM = 0.5 * teso;
BT = {BM, BM, BM, 0, BM, BM, BM, 0, BM, BM, BM, 0, 0, 0};
BN = {0, 0, 0, 0, 0, 0, 0, 0, 0, 0, 0, B1, B1, B1};
tintb = {π/(4 * μ * BM) * G, π/(2 * μ * BM) * G,
π/(4 * μ * BM) * G, π/(16 * gr) * G, π/(4 * μ * BM) * G,
π/(2 * μ * BM) * G, π/(4 * μ * BM) * G, π/(16 * gr) * G,
π/(4 * μ * BM) * G, π/(4 * μ * BM) * G, π/(4 * μ * BM) * G,
π/(4 * μ * B1) * G, π/(4 * μ * B1) * G, π/(4 * μ * B1) * G};
ϕ = {$-\pi/2, \pi, \pi/2, \pi/2, -\pi/2, 0, \pi/2, \pi/2,$
$-\pi/2, 0, \pi/2, -\pi/2, 0, \pi/2$};
α = (2 * mb * B01/teso/h)/to;
β = (2 * mb * B02/teso/h)/to;
$G = \alpha$;
$\omega 1 = \alpha/\alpha$;
$\omega 2 = \beta/\alpha$;
For[b1 = {0, a1, a1, a1, a1, a1, a1, a1, a1, a1, a1, a1, a1, a1};
b2 = {0, a2, a2, a2, a2, a2, a2, a2, a2, a2, a2, a2, a2, a2};
b3 = {1, a3, a3, a3, a3, a3, a3, a3, a3, a3, a3, a3, a3, a3};
b4 = {0, a4, a4, a4, a4, a4, a4, a4, a4, a4, a4, a4, a4, a4};
ta = 0; tb = 0; $i = 1, i < 15$,
ϕ[[i]];
BT[[i]];
BN[[i]];
tintb[[i]];
tb+ = tintb[[i]];
n12[t_] = $-\mu$ * BN[[i]](cos[ϕ[[i]]] + I * sin[ϕ[[i]]]);
n11[t_] = $-\mu$ * BN[[i]](cos[ϕ[[i]]] − I * sin[ϕ[[i]]]);
n22[t_] = $-\mu$ * BT[[i]](cos[ϕ[[i]]] + I * sin[ϕ[[i]]]);
n21[t_] = $-\mu$ * BT[[i]](cos[ϕ[[i]]] − I * sin[ϕ[[i]]]);

```
solution1 = NDSolve[{
y'[t] ==
-i/G((-2 * gr) * y[t] + n22[t_] * x[t] + n12[t_] * z[t]),
x'[t] ==
-i/G(n21[t_] * y[t] + (2 * gr) * x[t] + 2 * gr * cos[(ω1 - ω2) * t] * z[t] + n12[t_] * p[t]),
z'[t] ==
-i/G(n11[t_] * y[t] + 2 * gr * cos[(ω1 - ω2) * t] * x[t] + (2 * gr) * z[t] + n22[t_] * p[t]),
p'[t] ==
-i/G(n11[t_] * x[t] + n21[t_] * z[t] - (2 * gr) * p[t]),
y[0] == b1[[i]], x[0] == b2[[i]], z[0] == b3[[i]],
p[0] == b4[[i]]}, {y[t], x[t], z[t], p[t]},
{t, 0, tintb[[i]]}, MaxSteps → 1000000];
a11 = y[t]/.solution1/.t → tintb[[i]];
a21 = x[t]/.solution1/.t → tintb[[i]];
a31 = z[t]/.solution1/.t → tintb[[i]];
a41 = p[t]/.solution1/.t− > tintb[[i]];
a1 = a11[[1]];
a2 = a21[[1]];
a3 = a31[[1]];
a4 = a41[[1]];
i + +]
a1a = a1;
a2a = a2;
a3a = a3;
a4a = a4;
a1a
a2a
a3a
a4a
```

C.5 CNOT-gate.nb

$mo = 9.10939 * 10^{-31};$

$lo = 1.88973 * 10^{10};$

$to = 4.13414 * 10^{16};$

$Vo = 0.0367493;$

$mb = 9.27402 * 10^{-24};$

$no = 0.000669176;$

$q = 1.60218 * 10^{-19};$

$h = 1.05459 * 10^{-34};$

$teso = 4.25438 * 10^{-6};$

$r = 1.14 * 10^{-9} * (lo);$

$\mu = 1/2;$

$n = no/(4 * \pi);$

$gr = \mu 2 * n/(r3);$

$B01 = (0.3 + 0.0000304) * teso;$

$B02 = (0.3 - 0.0000304) * teso;$

$B1 = 0.5 * teso;$

$BM = 0.5 * teso;$

$BT = \{BM, BM, BM, BM, 0, BM, BM, BM, 0, BM, BM, BM, 0, 0, 0, BM, 0, 0, 0\};$

$BN = \{0, 0, 0, 0, 0, 0, 0, 0, 0, 0, 0, 0, 0, B1, B1, B1, 0, B1, B1, B1\};$

$tintb = \{\pi/(4 * \mu * BM) * G, \pi/(4 * \mu * BM) * G, \pi/(2 * \mu * BM) * G,$

$\pi/(4 * \mu * BM) * G, \pi/(16 * gr) * G, \pi/(4 * \mu * BM) * G,$

$\pi/(2 * \mu * BM) * G, \pi/(4 * \mu * BM) * G, \pi/(16 * gr) * G,$

$\pi/(4 * \mu * BM) * G, \pi/(4 * \mu * BM) * G, \};$

$\phi = \{\pi/2, -\pi/2, \pi, \pi/2, \pi/2, -\pi/2, 0, \pi/2, \pi/2,$

$-\pi/2, 0, \pi/2, -\pi/2, 0, \pi/2, -\pi/2, -\pi/2, 0, \pi/2\};$

$\alpha = (2 * mb * B01/teso/h)/to;$

$\beta = (2 * mb * B02/teso/h)/to;$

$G = \alpha;$

$\omega 1 = \alpha/\alpha;$

$\omega 2 = \beta/\alpha;$

```
For[b1 = {0, a1, a1, a1, a1, a1, a1, a1, a1, a1, a1, a1, a1, a1, a1};
b2 = {0, a2, a2, a2, a2, a2, a2, a2, a2, a2, a2, a2, a2, a2, a2};
b3 = {1, a3, a3, a3, a3, a3, a3, a3, a3, a3, a3, a3, a3, a3, a3};
b4 = {0, a4, a4, a4, a4, a4, a4, a4, a4, a4, a4, a4, a4, a4, a4};
ta = 0; tb = 0; i = 1, i < 20,
ϕ[[i]];
BT[[i]];
BN[[i]];
tintb[[i]];
tb+ = tintb[[i]];
n12[t_] = −μ * BN[[i]](cos[ϕ[[i]]] + I * sin[ϕ[[i]]]);
n11[t_] = −μ * BN[[i]](cos[ϕ[[i]]] − I * sin[ϕ[[i]]]);
n22[t_] = −μ * BT[[i]](cos[ϕ[[i]]] + I * sin[ϕ[[i]]]);
n21[t_] = −μ * BT[[i]](cos[ϕ[[i]]] − I * sin[ϕ[[i]]]);
solution1 = NDSolve[{
y'[t] ==
−ι/G((−2 * gr) * y[t] + n22[t_] * x[t] + n12[t_] * z[t]),
x'[t] ==
−ι/G(n21[t_] * y[t] + (2 * gr) * x[t] + 2 * gr * cos[(ω1 − ω2) * t] * z[t] + n12[t_] * p[t]),
z'[t] ==
−ι/G(n11[t_] * y[t] + 2 * gr * cos[(ω1 − ω2) * t] * x[t] + (2 * gr) * z[t] + n22[t_] * p[t]),
p'[t] ==
−ι/G(n11[t_] * x[t] + n21[t_] * z[t] − (2 * gr) * p[t]),
y[0] == b1[[i]], x[0] == b2[[i]], z[0] == b3[[i]],
p[0] == b4[[i]]}, {y[t], x[t], z[t], p[t]},
{t, 0, tintb[[i]]}, MaxSteps → 1000000];
a11 = y[t]/.solution1/.t → tintb[[i]];
a21 = x[t]/.solution1/.t → tintb[[i]];
a31 = z[t]/.solution1/.t → tintb[[i]];
a41 = p[t]/.solution1/.t− > tintb[[i]];
a1 = a11[[1]];
a2 = a21[[1]];
a3 = a31[[1]];
a4 = a41[[1]];
i + +]
```

```
a1a = a1;
a2a = a2;
a3a = a3;
a4a = a4;
a1a
a2a
a3a
a4a
```

C.6 fidelity-phase-gate.nb

$B = \{\{0.703528 + 0.710625i, 0.00284812 + 0.00176065i, -0.00225219 + 0.00620788i,$
$0.00177297 + 0.00175457i\},$
$\{-0.00283919 + 0.00178207i, 0.704164 - 0.71001i, 0.00148651 - 0.00152784i,$
$-0.00229008 - 0.00428019i\},$
$\{0.00227697 + 0.00619767i, -0.00148485 + 0.00154229i, 0.702892 - 0.71124i,$
$-0.0052997 + 0.00178061i\},$
$\{-0.00177293 - 0.00175158i, 0.00227543 - 0.00428633i, 0.0053118 + 0.00175131i,$
$0.703528 + 0.710625i\}\};$
$a = \text{Array}[F, 998];$

```
For[j = 1, j < 1000,
s1 = Random[];
s2 = Random[];
s3 = Random[];
s11 = s1 * 2 * π;
s12 = s2 * 2 * π;
s13 = s3 * 2 * π;
c0 = cos[s11] * sin[s12] * sin[s13];
c1 = sin[s11] * sin[s12] * sin[s13];
c2 = cos[s12] * sin[s13];
```

c3 = cos[s13];
B2 = Conjugate[Transpose[B]];
s = {{c0}, {c1}, {c2}, {c3}};
s1 = {c0, c1, c2, c3};
id = {{exp[$I * \pi/4$] * c0}, {exp[$-I * \pi/4$] * c1},
{exp[$-I * \pi/4$] * c2}, {exp[$I * \pi/4$] * c3}};
id1 = {exp[$-I * \pi/4$] * c0, exp[$I * \pi/4$] * c1,
exp[$I * \pi/4$] * c2, exp[$-I * \pi/4$] * c3};
$F[j-1]$ = Re[(id1.B.s) * (s1.B2.id)];
$j++$]
fm = Flatten[a];

min[fm]0.99989

C.7 fidelity-pi-gate.nb

B = {{0.714082 − 0.699934i, 0.00692515 − 0.00128067i, 0.0113218 + 0.000654491i,
0.000364076 − 0.000393688i},
{−0.00123931 + 0.0068975i, 0.700573 − 0.713499i, −0.00485227 − 0.00143465i,
0.00282855 − 0.00580356i},
{0.00069303 + 0.0113412i, −0.00156419 − 0.00477428i, 0.699282 − 0.71473i,
−0.000216576 + 0.003386i},
{0.000402374 − 0.000347015i, 0.00580285 − 0.00280803i, −0.00340598 + 0.000200908i,
−0.714165 + 0.699939i}};
a = Array[F, 998];

For[$j = 1, j < 1000$,
s1 = Random[];
s2 = Random[];
s3 = Random[];

s11 = s1 * 2 * π;
s12 = s2 * 2 * π;
s13 = s3 * 2 * π;
c0 = cos[s11] * sin[s12] * sin[s13];
c1 = sin[s11] * sin[s12] * sin[s13];
c2 = cos[s12] * sin[s13];
c3 = cos[s13];
B2 = Conjugate[Transpose[B]];
s = {{c0}, {c1}, {c2}, {c3}};
s1 = {c0, c1, c2, c3};
id = {{c0}, {c1}, {c2}, {−c3}};
id1 = {c0, c1, c2, −c3};
F[j − 1] = Re[(id1.B.s) * (s1.B2.id)];
j + +]

fm = Flatten[a];

min[fm]

0.999673

C.8 fidelity-CNOT-gate.nb

$B = \{\{-0.700368 - 0.713657i, -0.0103758 + 0.00212941i, -0.00505261 - 0.00505082i, -0.00375702 - 0.000852106i\},$
$\{-0.00213618 + 0.0103302i, -0.713016 - 0.700913i, -0.00347813 + 0.0102535i, 0.000736186 - 0.0100269i\},$
$\{0.000733605 + 0.00373919i, 0.00999176 - 0.000949307i, 0.005046 - 0.00879934i, -0.710656 - 0.703384i\},$
$\{0.00503255 + 0.0051884i, -0.0101818 + 0.00360701i, -0.703959 - 0.710049i, 0.00872855 - 0.00510289i\}\};$

```
a = Array[F, 9998];

For[j = 1, j < 10000,
s1 = Random[];
s2 = Random[];
s3 = Random[];
s11 = s1 * 2 * π;
s12 = s2 * 2 * π;
s13 = s3 * 2 * π;
c0 = cos[s11] * sin[s12] * sin[s13];
c1 = sin[s11] * sin[s12] * sin[s13];
c2 = cos[s12] * sin[s13];
c3 = cos[s13];
B2 = Conjugate[Transpose[B]];
s = {{c0}, {c1}, {c2}, {c3}};
s1 = {c0, c1, c2, c3};
id = {{c0}, {c1}, {c3}, {c2}};
id1 = {c0, c1, c3, c2};
F[j - 1] = Re[(id1.B.s) * (s1.B2.id)];
j++]

fm = Flatten[a];

min[fm]
0.999536
```

C.9 Pi-gate-distant.nb

```
mo = 9.10939 * 10^-31;
lo = 1.88973 * 10^10;
to = 4.13414 * 10^16;
```

$$\text{Vo} = 0.0367493;$$
$$\text{mb} = 9.27402 * 10^{-24};$$
$$\text{no} = 0.000669176;$$
$$\text{q} = 1.60218 * 10^{-19};$$
$$\text{h} = 1.05459 * 10^{-34};$$
$$\text{teso} = 4.25438 * 10^{-6};$$
$$\text{r} = 7 * 10^{-9} * (\text{lo});$$
$$\mu = 1/2;$$
$$n = \text{no}/(4 * \pi);$$
$$\text{gr} = \mu 2 * n/(r3);$$
$$\text{B01} = \left(0.3 + 2.67 * 10^{-4}\right) * \text{teso};$$
$$\text{B02} = \left(0.3 - 2.67 * 10^{-4}\right) * \text{teso};$$
$$\text{B1} = 0.28 * 10^{-3} * \text{teso};$$
$$\text{BM} = 0.28 * 10^{-3} * \text{teso};$$
$$\text{BT} = \{0, B1, B1, B1, 0, 0, 0\};$$
$$\text{BN} = \{0, 0, 0, 0, \text{BM}, \text{BM}, \text{BM}\};$$
$$\text{tintb} = \{\pi/(8 * \text{gr}) * G, \pi/(4 * \mu * \text{BM}) * G,$$
$$\pi/(4 * \mu * \text{BM}) * G, \pi/(4 * \mu * \text{BM}) * G, \pi/(4 * \mu * \text{BM}) * G,$$
$$\pi/(4 * \mu * \text{B1}) * G, \pi/(4 * \mu * \text{B1}) * G\};$$
$$\phi = \{-\pi/2, -\pi/2, 0, \pi/2, -\pi/2, 0, \pi/2\};$$
$$\alpha = (2 * \text{mb} * \text{B01}/\text{teso}/h)/\text{to};$$
$$\beta = (2 * \text{mb} * \text{B02}/\text{teso}/h)/\text{to};$$
$$G = \alpha;$$
$$\omega 1 = \alpha/\alpha;$$
$$\omega 2 = \beta/\alpha;$$
$$\text{For}[\text{b1} = \{1, \text{a1}, \text{a1}, \text{a1}, \text{a1}, \text{a1}, \text{a1}\};$$
$$\text{b2} = \{0, \text{a2}, \text{a2}, \text{a2}, \text{a2}, \text{a2}, \text{a2}\};$$
$$\text{b3} = \{0, \text{a3}, \text{a3}, \text{a3}, \text{a3}, \text{a3}, \text{a3}\};$$
$$\text{b4} = \{0, \text{a4}, \text{a4}, \text{a4}, \text{a4}, \text{a4}, \text{a4}\};$$

```
ta = 0; tb = 0; i = 1, i < 8,
ϕ[[i]];
BT[[i]];
BN[[i]];
tintb[[i]];
n12[t_] = −μ * BN[[i]](cos[ϕ[[i]]] + ι * sin[ϕ[[i]]]);
n11[t_] = −μ * BN[[i]](cos[ϕ[[i]]] − ι * sin[ϕ[[i]]]);
n22[t_] = −μ * BT[[i]](cos[ϕ[[i]]] + ι * sin[ϕ[[i]]]);
n21[t_] = −μ * BT[[i]](cos[ϕ[[i]]] − ι * sin[ϕ[[i]]]);
Print[solution1 = NDSolve[{
y'[t] == −ι/G((−2 * gr) * y[t] + n22[t_] * x[t] + n12[t_] * z[t]),
x'[t] == −ι/G(n21[t_] * y[t] + (2 * gr) * x[t] + n12[t_] * p[t]),
z'[t] == −ι/G(n11[t_] * y[t] + (2 * gr) * z[t] + n22[t_] * p[t]),
p'[t] == −ι/G(n11[t_] * x[t] + n21[t_] * z[t] − (2 * gr) * p[t]),
y[0] == b1[[i]], x[0] == b2[[i]], z[0] == b3[[i]],
p[0] == b4[[i]]}, {y[t], x[t], z[t], p[t]},
{t, 0, tintb[[i]]}, MaxSteps → 1000000]];
a11 = y[t]/.solution1/.t → tintb[[i]];
a21 = x[t]/.solution1/.t → tintb[[i]];
a31 = z[t]/.solution1/.t → tintb[[i]];
a41 = p[t]/.solution1/.t− > tintb[[i]];
a1 = a11[[1]];
a2 = a21[[1]];
a3 = a31[[1]];
a4 = a41[[1]];
i + +]

a1a = a1;
a2a = a2;
a3a = a3;
a4a = a4;
```

a1a

a2a

a3a

a4a

C.10 CNOT-gate-distant.nb

$\text{mo} = 9.10939 * 10^{-31};$

$\text{lo} = 1.88973 * 10^{10};$

$\text{to} = 4.13414 * 10^{16};$

$\text{Vo} = 0.0367493;$

$\text{mb} = 9.27402 * 10^{-24};$

$\text{no} = 0.000669176;$

$\text{q} = 1.60218 * 10^{-19};$

$\text{h} = 1.05459 * 10^{-34};$

$\text{teso} = 4.25438 * 10^{-6};$

$\text{r} = 7 * 10^{-9} * (\text{lo});$

$\mu = 1/2;$

$n = \text{no}/(4 * \pi);$

$\text{gr} = \mu 2 * n/(r3);$

$\text{B01} = \left(0.3 + 2.67 * 10^{-4}\right) * \text{teso};$

$\text{B02} = \left(0.3 - 2.67 * 10^{-4}\right) * \text{teso};$

$\text{B1} = 0.28 * 10^{-3} * \text{teso};$

$\text{BM} = 0.28 * 10^{-3} * \text{teso};$

$\text{BT} = \{B1, 0, B1, B1, B1, 0, 0, 0, B1, 0, 0, 0\};$

$\text{BN} = \{0, 0, 0, 0, 0, \text{BM}, \text{BM}, \text{BM}, 0, \text{BM}, \text{BM}, \text{BM}\};$

$\text{tintb} = \{\pi/(4 * \mu * \text{BM}) * G, \pi/(8 * \text{gr}) * G,$

$\pi/(4 * \mu * \text{BM}) * G, \pi/(4 * \mu * \text{BM}) * G, \pi/(4 * \mu * \text{BM}) * G,$

$\pi/(4 * \mu * \text{BM}) * G, \pi/(4 * \mu * \text{B1}) * G, \pi/(4 * \mu * \text{B1}) * G,$

$\pi/(4 * \mu * \text{B1}) * G, \pi/(4 * \mu * \text{BM}) * G, \pi/(2 * \mu * \text{B1}) * G,$

$\pi/(4 * \mu * \text{B1}) * G\};$

$\phi = \{\pi/2, -\pi/2, -\pi/2, 0, \pi/2, -\pi/2, 0, \pi/2, -\pi/2, -\pi/2, 0, \pi/2\};$
$\alpha = (2 * \text{mb} * \text{B01}/\text{teso}/h)/\text{to};$
$\beta = (2 * \text{mb} * \text{B02}/\text{teso}/h)/\text{to};$
$G = \alpha;$
$\omega 1 = \alpha/\alpha;$
$\omega 2 = \beta/\alpha;$
For[b1 = {1, a1, a1, a1, a1, a1, a1, a1, a1, a1, a1, a1};
b2 = {0, a2, a2, a2, a2, a2, a2, a2, a2, a2, a2, a2};
b3 = {0, a3, a3, a3, a3, a3, a3, a3, a3, a3, a3, a3};
b4 = {0, a4, a4, a4, a4, a4, a4, a4, a4, a4, a4, a4}; ta = 0; tb = 0; $i = 1, i < 13,$
$\phi[[i]];$
BT[[i]];
BN[[i]];
tintb[[i]];
n12[t_] = $-\mu * \text{BN}[[i]](\cos[\phi[[i]]] + \imath * \sin[\phi[[i]]]);$
n11[t_] = $-\mu * \text{BN}[[i]](\cos[\phi[[i]]] - \imath * \sin[\phi[[i]]]);$
n22[t_] = $-\mu * \text{BT}[[i]](\cos[\phi[[i]]] + \imath * \sin[\phi[[i]]]);$
n21[t_] = $-\mu * \text{BT}[[i]](\cos[\phi[[i]]] - \imath * \sin[\phi[[i]]]);$
Print[solution1 = NDSolve[{
$y'[t] == -\imath/G((-2 * \text{gr}) * y[t] + \text{n22[t\_]} * x[t] + \text{n12[t\_]} * z[t]),$
$x'[t] == -\imath/G(\text{n21[t\_]} * y[t] + (2 * \text{gr}) * x[t] + \text{n12[t\_]} * p[t]),$
$z'[t] == -\imath/G(\text{n11[t\_]} * y[t] + (2 * \text{gr}) * z[t] + \text{n22[t\_]} * p[t]),$
$p'[t] == -\imath/G(\text{n11[t\_]} * x[t] + \text{n21[t\_]} * z[t] - (2 * \text{gr}) * p[t]),$
$y[0] == \text{b1}[[i]], x[0] == \text{b2}[[i]], z[0] == \text{b3}[[i]],$
$p[0] == \text{b4}[[i]]\}, \{y[t], x[t], z[t], p[t]\},$
$\{t, 0, \text{tintb}[[i]]\}, \text{MaxSteps} \rightarrow 1000000]];$
a11 = $y[t]/.\text{solution1}/.t \rightarrow \text{tintb}[[i]];$
a21 = $x[t]/.\text{solution1}/.t \rightarrow \text{tintb}[[i]];$
a31 = $z[t]/.\text{solution1}/.t \rightarrow \text{tintb}[[i]];$
a41 = $p[t]/.\text{solution1}/.t- > \text{tintb}[[i]];$
a1 = a11[[1]];
a2 = a21[[1]];
a3 = a31[[1]];
a4 = a41[[1]];

$i++]$

a1a = a1;

a2a = a2;

a3a = a3;

a4a = a4;

a1a

a2a

a3a

a4a

C.11 fidelity-pi-gate-distant.nb

B5 = {{0.732885 − 0.679252i, 0.0273477 + 0.000519169i, 0.0273474 − 0.000537343i, 0.000527238 + 0.000527238i},
{0.000537387 + 0.0273474i, 0.678765 − 0.733339i, −0.000525058 + 0.000525058i, 0.0272343 + 0.000535122i},
{−0.000519125 + 0.0273477i, −0.000529428 + 0.000529428i, 0.678765 − 0.733339i, 0.0272345 − 0.00051702i},
{0.000527238 + 0.000527238i, −0.000516979 − 0.0272345i, 0.000535163 − 0.0272343i, −0.733794 + 0.678279i}};

a = Array[F, 98];

For[$j = 1, j < 100$,

s1 = Random[];

s2 = Random[];

s3 = Random[];

s11 = s1 * 2 * π;

s12 = s2 * 2 * π;

s13 = s3 * 2 * π;

c0 = cos[s11] * sin[s12] * sin[s13];

c1 = sin[s11] * sin[s12] * sin[s13];

c2 = cos[s12] * sin[s13];

c3 = cos[s13];
B6 = Conjugate[Transpose[B5]];
s = {{c0}, {c1}, {c2}, {c3}};
s1 = {c0, c1, c2, c3};
id = {{c0}, {c1}, {c2}, {−c3}};
id1 = {c0, c1, c2, −c3};
$F[j-1]$ = Re[Sqrt[(id1.B5.s) * (s1.B6.id)]];
$j++$]
fm = Flatten[a];
min[fm]

C.12 fidelity-CNOT-gate-distant.nb

B3 = {{−0.663803 − 0.744719i, −0.0540428 + 0.0262495i, 0.00210103 − 0.0278197i,
−0.0133703 − 0.0138546i},
{−0.0266872 + 0.0546016i, −0.746046 − 0.662294i, 0.0138532 + 0.0143693i,
−0.00162589 − 0.0262202i},
{0.0125269 + 0.0136849i, 0.0282937 − 0.00208078i, 0.054004 − 0.0287346i,
−0.73116 − 0.678612i},
{0.0267219 + 0.00263023i, −0.01359 − 0.0135228i, −0.67715 − 0.732495i,
0.029359 − 0.0544827i}};
a = Array[F, 98];
For[$j = 1, j < 100$,
s1 = Random[];
s2 = Random[];
s3 = Random[];
s11 = s1 * 2 * π;
s12 = s2 * 2 * π;
s13 = s3 * 2 * π;

```
c0 = cos[s11] * sin[s12] * sin[s13];
c1 = sin[s11] * sin[s12] * sin[s13];
c2 = cos[s12] * sin[s13];
c3 = cos[s13];
B4 = Conjugate[Transpose[B3]];
s = {{c0}, {c1}, {c2}, {c3}};
s1 = {c0, c1, c2, c3};
id = {{c0}, {c1}, {c3}, {c2}};
id1 = {c0, c1, c3, c2};
F[j - 1] = Re[(id1.B3.s) * (s1.B4.id)];
j++]

fm = Flatten[a];

min[fm]
```

Bibliography

[1] J.I. Cirac and P. Zoller, Phys. Rev. Lett. **74**, 4091 (1995).

[2] A. Steane, Appl. Phys. B **64**, 623 (1997)

[3] M. Sasura and V. Buzek, Journ. of Mod. Opt. **49**, 1593 (2002).

[4] T. Calarco, J. I. Cirac and P. Zoller, Phys. Rev. A **63**, 062304 (2001).

[5] T. Pellizzari, S. A. Gardiner, J. I. Chirac and P. Zoller, Phys. Rev. Lett. **75**, 3788 (1995).

[6] S. J. van Enk, J. I. Cirac and P. Zoller, Phys. Rev. Lett. **79**, 5178 (1997).

[7] A. Rauschenbeutel, G. Nogues, S. Osnaghi, P. Bertet, M. Brune, J. M. Raimond and S. Haroche, Phys. Rev. Lett. **83**, 5166 (1999).

[8] L. M. Duan, A. Kuzmich and H. J. Kimble, Phys. Rev. A **67**, 032305 (2003).

[9] N. A. Gershenfeld and I. L. Chuang, Science **275**, 350 (1997).

[10] F. Schmidt-Kaler, H. Haffner, M. Riebe, S. Gulde, G.P.T. Lancaster, T. Deutschle, C. Becher, C. Roos, J. Eschner and R. Blatt, Nature **422**, 408 (2003).

[11] D. Leibfried, B. Demarco, V. Meyer, D. Lucas, M. Barrett, J. Britton, W. M. Itano, B. Jelenkovich, C. Langer, T. Rosenband et al., Nature **422**, 412 (2003).

[12] M. A. Nielsen and I. L. Chuang, *Quantum Computation and Quantum Information* (Cambridge University Press, 2000).

[13] A. Steane, Rep. Progr. Phys. **61**, 117 (1998).

[14] A. Ekert, P. Hayden, H. Inamori, e-print `quant-ph/0011013`.

[15] V. Barone, *Notes on quantum Computation*, Universita' del Piemonte Orientale, unpublished notes (2002).

[16] B. Schumacher, Phys. Rev. A **51**, 2738 (1995).

[17] D. Dieks, Phys. Lett. A **92**, 271 (1982).

[18] W.K. Zurek, W. H. Zurek, Nature **299**, 802 (1982).

[19] D. Bouwmeester, A. Ekert, A. Zeilinger, *The Physics of Quantum Information: Quantum Cryptography, Quantum Teleportation, Quantum Computation* (Spinger-Verlag Berlin and Heidelberg GmbH & co, May 2001).

[20] D. Deutsch, Proc. Roy. Soc. London A **400**, 97 (1982).

[21] R. Cleve,A. Ekert, C. Macchiavello, M. Mosca, Proc. R. Soc. Lond. A **454**, 339 (1998).

[22] L. M. K. Vandersypen, I. L. Chuang, Rev. Mod. Phys. **74**, 1037 (2005).

[23] M. D. Bowdrey, D. K. Oi, A. J. Short, K. Banaszek, J. A.Jones, Phys. Lett. A 294, 258 (2002).

[24] E. R. Knill, R. Laflamme, W. H. Zurek, Science **279**, 342 (1998).

[25] E. R. Knill, R. Laflamme, W. H. Zurek, Proc. Roy. Soc. London A **454**, 365 (1998).

[26] A. Steane, Phys. Rev. A **68**, 042322 (2003)

[27] D. Bouwmeester, A. Ekert, A. Zeilinger, *The Physics of Quantum Information*(Springer, 2000).

[28] D.P.DiVincenzo, *Science* **270**,255 (1995).

[29] H. W. Kroto, J. R. Heath, S. C. O'Brien, R. F. Curl and R. E. Smalley, Nature **318**, 162 (1985).

[30] H. O. Pierson *Handbook of Carbon, Graphite, Diamond and Fullerenes* (Noyes Publications, 1993).

[31] R. E. Smalley, Acc. Chem. Res. **25** 98 (1992).

[32] R. F. Curl and R. E. Smalley, Scientific American, 54-63 (1991).

[33] W. Krätschmer, L. D. Lamb, K. Fostiropolous, D. R. Huffman, Nature **347**, 354 (1990).

[34] M. Arndt, O. Nairz, J. Vos-Andreae, C. Keller, G. van der Zouw, A. Zeilinger, Nature **401**, 680 (1999).

[35] R. Tellgmann,N. Krawez, S. H. Lin, I.V. Hertel, E. E. B. Campbell, Nature **382**, 407 (1996).

[36] R. Shimshi, R. J. Cross, M. Saunders, J. Am. Chem. Soc. **119**, 1163 (1997).

[37] T. Almeida Murphy, T. Pawlik, A. Weidinger, M. Höhne, R. Alcala, J. M. Spaeth, Phys. Rev. Lett. **77**, 1075 (1996).

[38] C. Knapp, K. P. Dinse,B. Pietzak, M. Waiblinger, A. Weidinger, Chem. Phys. Lett **272**, 433 (1997).

[39] H. Mauser, N. van Eikema Hommes, T. Clark, A. Hirsch, B. Pietzak, A. Weidinger, L. Dunsch, Angew. Chem. **109**, 2858 (1997); Angew. Chem. Int. Ed. **36**, 2835 (1997).

[40] B. Pietzak, M. Waiblinger, T. Almeida Murphy, A. Weidinger, M. Höhne, E. Dietel, A. Hirsch, Carbon **36**, 613 (1998).

[41] B. Pietzak, M. Waiblinger, T. Almeida Murphy, A. Weidinger, M. Höhne, E. Dietel, A. Hirsch, Chem. Phys. Lett **279**, 259 (1997).

[42] A. Weidinger, M. Waiblinger, B.Pietzak, T. Almeida Murphy, Appl. Phys. A **66**, 287 (1998).

[43] J. C. Greer, Chem. Phys. Lett. **326**, 567 (2000).

[44] W. Harneit, Phys. Rev. A **65**, 032322 (2002).

[45] M. Waiblinger, B. Goedde, K. Lips, W. Harneit, P. Jakes, A. Weidinger and K. P. Dinse, AIP Conf. Proc. **544**, 195 (2000).

[46] S. C. Benjamin, A. Ardavan, G. A. Briggs, D. A. Britz, D. Gunlycke, J. Jefferson, M. A. G. Jones, D. F. Leigh, B. W. Lovett, A. N. Khlobystov, J. J. L. Morton, K. Porfyrakis, M. R. Sambrook, A. M. Tyryshkin, e-print arXiv:quant-ph/0511198 (2005).

[47] C. T. White, T. N. Todorov, Nature **393**, 240 (1998).

[48] J. Lee, H. Kim, S. J. Kahng, G. Kim, Y. W. Son, J. Ihm, H. Kato, Z. W. Wang, T. Okazaki, H. Shinohara, Y. Kuk, Nature **415**, 1005 (2002).

[49] A. Horsfield, Phys. Rev. B **56**, 6594 (1997).

[50] S. Lloyd, Science **261**, 1569 (1993).

[51] S. C. Benjamin, Phys. Rev. Lett. **88**, 017994 (2002).

[52] S. Knorr, A. Grupp, M. Mehring, M. Waiblinger and A. Weidinger, AIP Conf. Proc. **544**, 191 (2000).

[53] S. Knorr, A. Grupp, M. Mehring, M. Waiblinger and A. Weidinger, AIP Conf. Proc. **591**, 105 (2001).

[54] A. N. Khlobystov, D. A. Britz, A. Ardavan and G. A. D. Briggs, Phys. Rev. Lett. **92**, 245507 (2004).

[55] J. J. L. Morton, A. M. Tyryshkin, A. Ardavan, K. Porfyrakis, S. A. Lyon, G. A. Briggs, J. Chem. Phys. **124**, 014508 (2006).

[56] J. R. Klauder, P. W. Anderson, Phys. Rev. **125**, 912 (1962).

[57] W. B. Mims, Phys. Rev. **168**, 370 (1968).

[58] K. M. Salikhov, S. A. Dzuba, A. M. Raitsimring, J. Mag. Res. **42**, 255 (1981).

[59] C. Knapp, N. Weiden, K. Kass, K. P. Dinse, B. Pietzak, M. Waiblinger, A. Weidinger, Mol. Phys. **95**, 999 (1988).

[60] A. Steane, Phys. Rev. A **68**, 042322 (2003).

[61] C. I. Pakes, P. W. Josephs-Frans, R. P. Reed, S. G. Corner, M. S. Colclough, IEEE Trans. Instrum. Meas. **50**, 310 (2001).

[62] D. Rugar, R. Budakian, H. J. Mamin, B. W. Chui, Nature **430** 329 (2004).

[63] C. Durkan, M. E. Welland, Appl. Phys. Lett. **80**, 458 (2002).

[64] S. C. Benjamin, A. Ardavan, G. A. D. Briggs, D. A. Britz, D. Gunlycke, J. Jefferson, M. A. G. Jones, D. F. Leigh, B. W. Lovett, A. N. Khlobystov, S. A. Lyon, J. J. L. Morton, K. Porfyrakis, M. R. Sambrook, A. M. Tyryshkin, J. Phys: Condens. Matter **18**, S867 (2006).

[65] H. Park, J. Park, A. K. L. Lim, E. H. Anderson, A. P. Alivastos, P. L. McEuen, Nature **407**, 57 (2000).

[66] F. Elste, C. Timm, Phys. Rev. B **71**, 155403 (2005).

[67] K. M. Lee, L. S. Dang, G. D. Watkins, Phys. Rev. B **32**, 2273 (1985).

[68] M. Kroutvar, Y. Ducommun, D. Heiss, M. Bichler, D. Schuh, G. Abstreiter, J. J. Finley, Nature **432**, 81 (2004).

[69] F. T. Charnock, T. A. Kennedy, Phys. Rev. B **64**, 41201 (2001).

[70] J. Twamley, Phys. Rev. A **67**, 052318 (2003).

[71] S. Stevenson et al. Nature **401**, 55 (1999).

[72] M. Jones *et al.*, preprint.

[73] M. S. Garelli, F. V. Kusmartsev, Eur. Phys. J. B **48**, 199 (2005).

[74] M.S. Garelli,F. V. Kusmartsev, Proc. SPIE **6264**, 62640A (2006).

[75] W. Harneit, C. Meyer, A. Weidinger, D. Suter and J. Twamley, Phy. Stat. Sol **233**, 453 (2002).

[76] M. Feng and J. Twamley, Phys. Rev. A **57**, 120 (1998).

[77] D. Suter and K. Lim, Phys. Rev. A. **65**, 052309 (2002).

[78] J. J. L. Morton, A. M. Tyryshkin, A. Ardavan, K. Porfyrakis, S. A. Lyon, G. A. Briggs, Phys. Rev. A **71**, 012332 (2005).

[79] S. Groth, P. Krüger, S. Wildermuth, R. Folman, T. Fernholz, D. Mahalu, I. Bar-Joseph and J. Schmiedmayer, Appl. Phys. Lett. **85**, 2980 (2004).

[80] W. K. Wootters, Phys. Rev. Lett. **80**, 2245 (1998).

[81] C. H. Bennett, D. P. DiVincenzo, J. A. Smolin and W. K. Wootters, Phys. Rev. A. **54**, 3824 (1996).

[82] J. J. Sakurai, *Modern Quantum Mechanics* (San Fu Tuan, 1994).

[83] www.nanotech.org/?path=Research/Fullerenes/Peapods/Peapod/sAssembly

[84] `www.emsl.pnl.gov/capabs/instruments/instrument_pages/1079.shtml`.